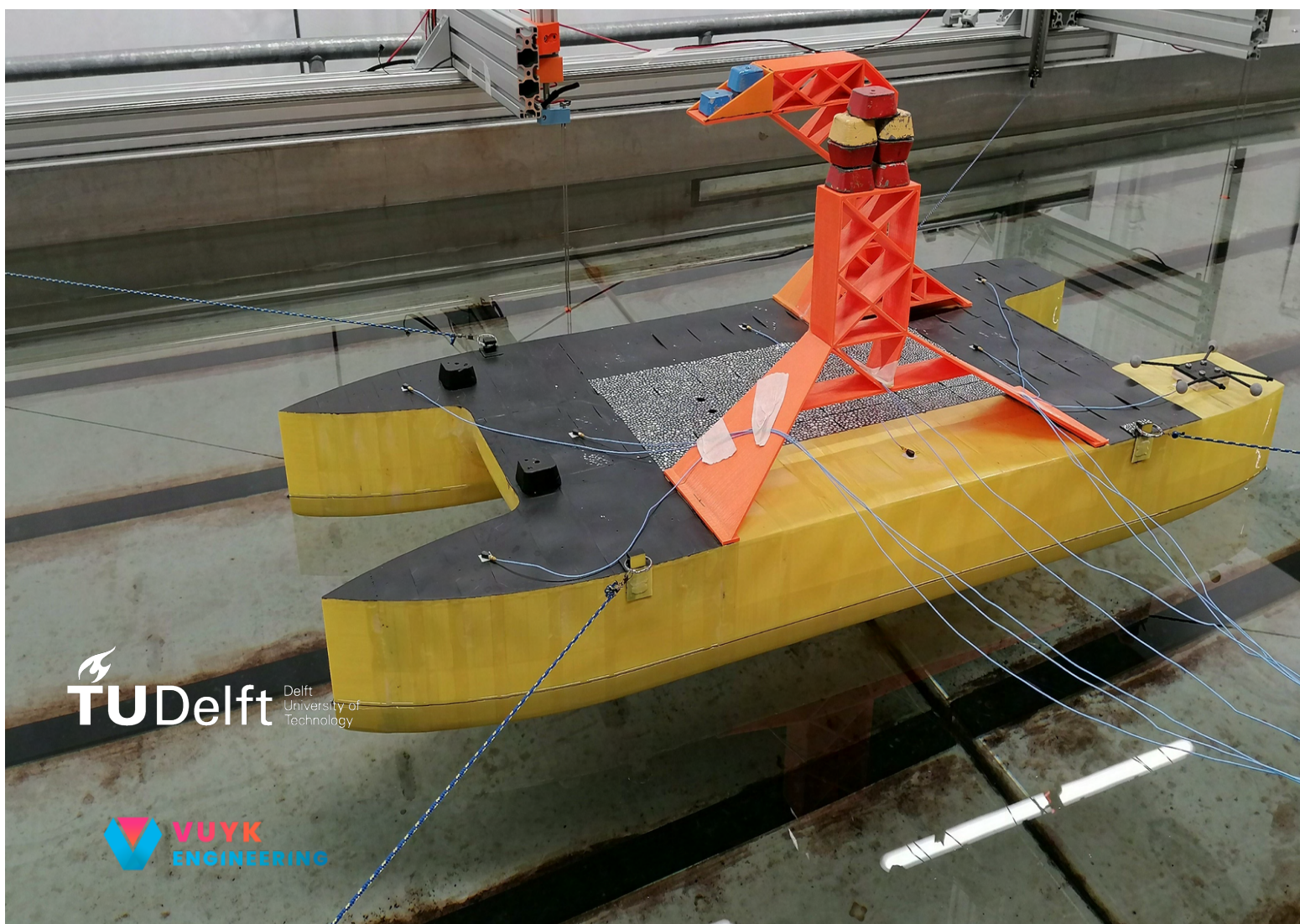


Experimental Investigation of Wet-Deck Slamming on Fully Elastic Catamaran Model

Michail Katsouros



Experimental Investigation of Wet-Deck Slamming on Fully Elastic Catamaran Model

Michail Katsouros

A Thesis submitted for the degree of
Master of Science

Offshore and Dredging Engineering
Delft University of Technology

September 2024

Company Daily Supervisor:

Ir.M. Verdult

Thesis Exam Committee:

Chair: Dr.H.C. Seyffert

Staff Member:Dr.A. Grammatikopoulos

Staff Member:Dr.H. den Besten

Company Member:Ir.M. Verdult

Abstract

The current demands of the Offshore and Maritime industry have lead to the design and production of larger vessels of complex geometries. These vessels are subjected to unique loading conditions that have not been investigated extensively. Such a case is presented in wet deck slamming of large catamaran vessels. These vessels have been designed and produced to conduct offshore platform installation operations and are expected to operate in severe conditions where wet deck submergence becomes a threat.

Wet deck slamming is a water entry impact phenomenon that can induce extreme loads when a part of the floating structure pierces the water surface during severe waves. This event can trigger a transient dynamic response at both local and global levels. The event has multiple influencing factors that can contribute to the severity and probability of occurrence.

Although the examination of slamming started over a century ago, the criteria concerning the incident definition, identification and prediction are applied from different perspectives. Modern methods identify slamming events based on the structural responses, while the statistical analysis considers correlation between the events, as opposed to older approaches treating the incidents as independent.

Progress in understanding slamming is achieved through full-scale measurements, experimental tests, and numerical simulations. Each method presents unique advantages and drawbacks, and all three are used for knowledge development but also verification and validation. As numerical capabilities increase, it is also important for the experimental method to evolve and explore new ways of representation of the complex events.

This project aims to investigate wet deck slamming using a rarely used form of model that could closely mimic real life responses. This research can enhance the experimental method capabilities and serve as stepping stone for further evolution of similar research. The experimental test runs for the needs of the project were conducted in the Ship and Hydromechanics laboratory facilities of TU Delft.

Acknowledgments

This thesis is the product of many people's hard work, and it is important to recognize and credit everyone's contributions. The unique model at the heart of this study was designed and produced by Anabel Keser as part of her own MSc thesis [1]. The results of her work were not only noteworthy but also inspired both my supervisors and me to further explore the possibilities it presents. I am grateful to Anabel for making herself available throughout my thesis, providing valuable insights and advice.

I would like to express my sincere gratitude to all my supervisors for their unwavering support. Their guidance and recommendations were instrumental in shaping the direction of my research. Michiel, my daily supervisor, was especially helpful in overcoming obstacles as they arose and in assisting me in developing a sound plan of approach through our discussions. Apostolos and Harleigh also provided tremendous support throughout this journey. Their efficient communication, eagerness to help, and enthusiasm for the project gave me a significant boost in motivation. I am also grateful to both the University and Vuyk for providing an excellent environment to work on my project and for trusting me with such a challenging research endeavor.

A significant advantage of working on this project was its multifaceted nature, which required the help and insight of many individuals. I am grateful to both establishments for their support and for making resources available to me. I would also like to thank Anna Boon and Hanna Pot for generously sharing their knowledge from their own research, which was beneficial to my work.

I also wish to thank the technicians who were indispensable during the experimental process. Jasper den Ouden and Sedat Tokgoz, in particular, offered invaluable assistance in preparing the model and setting up the experiments, sharing their expertise at every step. Sebastian Schreier, as a laboratory supervisor, guided me through the most challenging phases of testing and helped me establish a framework for the experimental process I followed. Finally, I would like to thank all the staff members present during my testing for their patience with the noise from the wave generator.

Contents

1	Introduction	1
1.1	Overview	1
1.2	Background	2
1.2.1	Twin-Hull Vessels	2
1.2.2	Slamming Research	2
1.3	Current Framework	3
1.4	Project Objectives	3
1.5	Methodology	4
2	Numerical Analysis	5
2.1	Introduction	5
2.2	RAO calculation	6
2.3	Wet Modal Analysis	7
2.3.1	Mathematical model	7
2.3.2	Methodology	8
2.3.3	Results	9
3	Experimental Set Up	13
3.1	Introduction	13
3.2	Model preparation	13
3.3	Oscillation tests	14
3.4	Waves and Current Conditions	15
3.4.1	Wave Generation	16
3.5	Mooring system	16
3.6	Motion tracking system	17
3.7	Stereo DIC	17
3.7.1	High-Speed Cameras	17
3.7.2	Speckle pattern	18
3.8	Accelerometers	19
3.9	Complete tank set up	20
3.10	Limitations	21
4	Modal Analysis	22
4.1	Impact Hammer Tests	22
4.1.1	Test process	22
4.1.2	Impact Hammer Results	23
4.1.3	Comparison of experimental and numerical results	25
4.2	DIC measurements	27
4.2.1	DIC Modal Results	28
4.2.2	Conclusions	32
5	Monochromatic Regular Wave Runs	33
5.1	Introduction	33
5.2	Results & Comparison to Numericals	33
5.3	Conclusion	34

6	Bichromatic Wave Impact Runs	35
6.1	Introduction	35
6.2	Slamming Identification	36
6.2.1	Threshold values for slamming identification	37
6.2.2	Empirical Mode Decomposition	37
6.2.3	Whipping Criterion	37
6.2.4	Slamming identification results for run 5_74	38
6.2.5	Slamming identification results for run 5_75	42
6.2.6	Slamming identification results for run 5_76	44
6.2.7	Slamming identification results for run 5_77	46
6.2.8	Comparison between whipping criterion and EMD	48
6.3	Analysis in the time domain	49
6.3.1	Green Water	49
6.3.2	Run 5_74	50
6.3.3	Run 5_75	55
6.3.4	Run 5_76	60
6.3.5	Run 5_77	65
6.3.6	Conclusions	70
7	Conclusions	71
7.1	Experimental Setup Possible Improvements	72
A	Intrinsic Mode Functions	75
B	Slamming Identification Full Signals	82

List of Tables

2.1	Dry and Wet natural frequencies	10
2.2	Structural generalised dry mass matrix (kg)	10
2.3	Generalised total mass matrix, including hydrodynamic added mass (kg)	11
3.1	Results from Oscillation tests	15
3.2	Sensor Placement	20
4.1	Comparison of numerical and experimental modal characteristics	25
6.1	Test Runs without Added Pretension	35
6.2	Test Runs with Added Pretension	36
6.3	First mode frequencies of the model deck plates (clamped-clamped)	37

List of Figures

2.1	Vertical R.A.O. calculated by AQWA: <i>a</i>)Heave, <i>b</i>)Roll, <i>c</i>)Pitch	6
2.2	Wet Natural frequency values for different radiation $\omega(rad/s)$	9
2.3	Relative error of wet natural frequencies for different radiation $\omega(rad/s)$	10
2.4	Calculated Dry shape $f_d = 21.65Hz$	12
2.5	Calculated Dry shape $f_d = 23.69Hz$	12
2.6	Calculated Dry shape $f_d = 39.86Hz$	12
2.7	Calculated Dry shape $f_d = 44.14Hz$	12
2.8	Calculated Wet shape $f_w = 17.42Hz$	12
2.9	Calculated Wet shape $f_w = 22.09Hz$	12
2.10	Calculated Wet shape $f_w = 36.58Hz$	12
2.11	Calculated Wet shape $f_w = 38.79Hz$	12
2.12	Dry and wet flexible mode shapes.	12
3.1	Prepared model	13
3.2	Empty cradle set up for oscillation tests	14
3.3	Cradle-model system set up for oscillation tests	14
3.6	Manually applied speckle pattern	19
3.7	Completed measurement set up.	20
3.8	Model Instrumentation	20
3.9	Epoxy treatment to cover hull delamination	21
4.1	Frequency Response Function from SIMO impact hammer tests	23
4.2	Phase of the transfer function from SIMO impact hammer tests	24
4.3	Coherence for the SIMO impact hammer tests	24
4.4	Mode Indicator Function for the SIMO impact hammer tests	25
4.5	Comparison of calculated and measured mode shapes	26
4.6	Evaluated surface usnig istra4D software.	27
4.7	Data points used for the modal analysis.	28
4.8	Total z displacement (mm) for hammer impact.	28
4.9	Frequency dependency of total vertical displacement.	29
4.10	Flexible motion z displacement (mm) for hammer impact.	29
4.11	Frequency dependency of flexible vertical displacement	30
4.12	Comparison between DIC and Accelerometer measured shapes	31
5.1	R.A.O. measured and compared to AQWA estimation, initial configuration	33
5.2	R.A.O. measured and compared to AQWA estimation, final configuration	34
6.1	Intrinsic Mode Functions in frequency domain run of 5_74	38
6.2	Intrinsic Mode Functions in time domain run of 5_74	39
6.3	EMD process for reconstruction of signal for run 5_74	40
6.4	Slamming events identified by the EMD of run 5_74	41
6.5	Slamming events identified by the whipping criterion of run 5_74	41
6.6	Reconstruction of signal of run 5_75	42
6.7	Slamming events identified by the EMD of run 5_75	43
6.8	Slamming events identified by the whipping criterion of run 5_75	43
6.9	EMD process for reconstruction of signal for run 5_76	44
6.10	Slamming events identified by the EMD of run 5_76	45

6.11	Slamming events identified by the whipping criterion of run 5_76	45
6.12	EMD process for reconstruction of signal for run 5_77	46
6.13	Slamming events identified by the EMD of run 5_77	47
6.14	Slamming events identified by the whipping criterion (run 5_77)	47
6.15	Side by side comparison of green water runs	49
6.16	Acceleration recordings of run 5_74.	50
6.17	Scalogram of run 5_74.	51
6.18	Zoomed in responses of slamming	52
6.19	Zoomed in hydroelastic responses of slamming	53
6.20	ODS for maximum hydroelastic response in run 5_74	54
6.21	Fast Fourier Transform of investigated slam in run 5_74	54
6.22	Acceleration recordings	55
6.23	Scalogram of run 5_75.	56
6.24	Zoomed in responses of slamming	57
6.25	Hydroelastic responses of slamming	58
6.26	ODS for maximum hydroelastic response in run 5_75.	59
6.27	Fast Fourier Transform of investigated slam in run 5_75	59
6.28	Acceleration recordings on the highest hydroelastic response recorded.	60
6.29	Scalogram for run 5_76	61
6.30	Zoomed in responses of slamming	62
6.31	Band pass filtered signal for Hydroelastic frequency range 10-41Hz	63
6.32	ODS for maximum hydroelastic response in run 5_76	64
6.33	Fast Fourier Transform of investigated slam in run 5_76	64
6.34	Acceleration recordings of run 5_77.	65
6.35	Scalogram of run 5_77.	66
6.36	Zoomed in responses of slamming	67
6.37	Zoomed in hydroelastic responses of slamming	68
6.38	ODS for maximum hydroelastic response in run 5_77	69
6.39	Fast Fourier Transform of investigated slam in run 5_77	69
A.1	Intrinsic Mode Functions in frequency domain of run 5_75	76
A.2	Intrinsic Mode Functions in time domain of run 5_75	77
A.3	Intrinsic Mode Functions in frequency domain of run 5_76	78
A.4	Intrinsic Mode Functions in time domain of run 5_76	79
A.5	Intrinsic Mode Functions in frequency domain of run 5_77	80
A.6	Intrinsic Mode Functions in time domain of run 5_77	81
B.1	Reconstructed signal of run 5_74	82
B.2	Slamming identification EMD 5_74	83
B.3	Slamming identification Dessi 5_74	84
B.4	Reconstructed signal of run 5_75	85
B.5	Slamming identification EMD 5_75	86
B.6	Slamming identification Dessi 5_75	87
B.7	Reconstructed signal of run 5_76	88
B.8	Slamming identification EMD 5_76	89
B.9	Slamming identification Dessi 5_76	90
B.10	Reconstructed signal of run 5_77	91
B.11	Slamming identification EMD 5_77	92
B.12	Slamming identification Dessi 5_77	93

Nomenclature

χ	Displacement Amplitude	F_r	Radiation Force
δ	Mode Shapes	f_w	Wet Natural Frequency
ω	Angular Frequency	<i>FEA</i>	Finite Element Analysis
Φ	Radiation Potential	<i>FFT</i>	Fast Fourier Transform
ρ	Water Density	<i>FRF</i>	Frequency Response Function
v	Displacement Vector	<i>IE</i>	Instantaneous Energy
<i>A</i>	Generalised Hydrodynamic Added Mass Matrix	<i>IMF</i>	Intrinsic Mode Function
<i>BEM</i>	Boundary Element Method	K^{Str}	Generalised Dry Structural Stiffness Matrix
<i>C</i>	Generalised Hydrostatic Stiffness Matrix	K^{Tot}	Generalised Total Stiffness Matrix
<i>CSD</i>	Cumulative Spectral Density	K_s	Structural Stiffness Matrix
<i>DIC</i>	Digital Image Correlation	M^{Str}	Generalised Dry Structural Mass Matrix
<i>EMA</i>	Experimental Modal Analysis	M^{Tot}	Generalised Total Mass Matrix
<i>EMD</i>	Empirical Mode Decomposition	M_s	Structural Mass Matrix
f_d	Dry Natural Frequency	<i>MIF</i>	Mode Indicator Function
f_n	Natural Frequency	n_j	Panel j Normal Vector
		<i>OMA</i>	Operational Modal Analysis
		p_{ij}	Participation Factor of Dry Modes i to Wet Mode j
		<i>RAO</i>	Response Amplitude Operator
		<i>SIMO</i>	Single Input Multiple Output
		<i>VCoG</i>	Vertical Centre of Gravity
		<i>W</i>	Eigenvector Matrix
		w_i	Mode i Eigenvector

Chapter 1

Introduction

1.1 Overview

Offshore structures and ships are subject to extreme conditions. The operability and lifespan of these structures are compromised by stochastic cyclic wave loads, affecting both ultimate and fatigue strength. Extreme wave phenomena such as slamming and green water can introduce loads dangerous to the integrity of the vessel and the well-being of the crew. Slamming, in particular, raises concerns due to the dynamic transient responses it induces, known as whipping.

Understanding these phenomena has been a primary objective for many researchers. Recent advancements in numerical methods have improved our ability to accurately represent fluid and structural domains. These methods now incorporate the influence of structural deformations induced by flow loading and their subsequent effects on the incident flow, enabling more accurate fluid-structure interaction modeling.

Experimental research works in parallel with numerical studies, investigating these phenomena and their effects on floating structures on both local and global scales. Flexible models are often used, consisting of rigid segments connected by flexible backbones or joints, mimicking actual ship stiffness. While fully elastic models offer a more realistic representation of the vessel's structural characteristics, they are less commonly used due to the challenges in manufacturing.

Despite these challenges, fully elastic models provide a faithful representation of stiffness distribution and can manifest torsional and non-symmetric modal behavior. They offer continuous measurements of deformations and loads, presenting high-accuracy data for validating numerical models. Advances in additive manufacturing have made the construction of fully elastic models more feasible, though further progress is needed in model calibration and experimental instrumentation.

This study aims to explore the capabilities of a fully elastic model in capturing meaningful measurements and investigating slamming and whipping in a twin hull crane vessel. These objectives are interconnected, as accurately representing slamming and whipping responses depends on the model's capabilities and the performance of the chosen experimental settings.

For this project, a model fabricated and calibrated by Anabel Keser is utilised. A detailed description of the experimental process is presented, the resulting measurements are analysed and conclusions are drawn.

1.2 Background

1.2.1 Twin-Hull Vessels

Twin-Hull vessels are becoming popular in the offshore industry, as they provide increased deck surface while maintaining slender hull shapes and transverse stability. The slender hull geometry results in reduced restoring forces during vertical motion oscillations. Additionally, twin hull interaction also serves in the increase of the wave height under the cross-deck structure. These design characteristics make twin hull vessels prone to slamming and green water.

Twin hull geometry induces unique loading to the vessels. The cross-deck structure connecting the two side-hulls results in additional bending and torsional moments that are not present in mono-hulls. Namely, the differential pitch rotation of the side-hulls results in a connecting moment, the differential roll rotation results in splitting moments and the torsional moment is augmented by the wide deck surface.

The hydrodynamic behaviour of these vessels and the unique global loads induced need to be considered in the design phase and proper measures taken to ensure structural and operational integrity.

1.2.2 Slamming Research

Slamming is a wave impact phenomenon that can compromise the strength of a floating structure. Slamming can be described by a sharp impulse load often followed by a transient dynamic response known as whipping. The response of the structure can be local, global or both. The event is connected to extreme vertical vessel motions and severe sea states. In mono-hulls bottom and bow-flare slamming occurs, but when a twin-hull vessel is considered wet deck slamming can happen, when the bottom of the cross deck surface submerges into the water surface.

Especially in wet deck slamming, many nonlinear effects are involved, mainly concerning the free surface, the hull interactions and the fluid-structure interaction. Many works are dedicated in describing the physics of slamming using numerical and experimental simulations as well as full scale measurements.

Given the critical nature of slamming induced responses, many researchers have worked on further understanding slamming phenomena. Full-scale testing is costly and time-consuming. Numerical methods, while advanced, still struggle with the statistical analysis of slamming due to computational power limits. As a result, experimental data remains essential for verifying numerical models.

The most common experimental approaches are drop tests and model tests, both of which provide valuable insights. Drop tests cover mostly local effects of slamming, while wave impact tests are meaningful for an all round investigation of the phenomenon. Depending on each case different modelling choices are made. Considering how the experimental approach seeks to improve in accuracy and efficiency, alternative modelling methods should be considered.

Experimental State of the Art

The widespread use of segmented models has led to significant research findings. Ramos used a scaled four-segment model connected to a flexible bar to investigate slam induced stresses of a container ship [2]. The segmented model was able to capture the vibratory responses to slamming loads. Only the vertical bending moments and shear forces were measured. Dessi developed the whipping identification criterion using a segmented model [3], [4].

Multihull vessels have also been investigated experimentally, with emphasis on high-speed wave piercing catamaran vessels [5],[6], [7], [8], [9],[10], [11]. The models used are comprised of rigid segments, the wet deck surface geometry entails a centerbow element, operating speeds are much higher and the vessel size is much smaller compared to that of a large crane twin-hull vessel. Forward speed, deadrise angle, wet deck geometry and relative vertical velocity are shown to influence the slamming physics of each vessel significantly. It becomes apparent that separate research is necessary to investigate wet deck slamming for the current vessel in question.

As the size and complexity of the vessels increase, so do the dynamic response non linearities. For a more advanced analysis of the vessel response, many have tried to use more sophisticated models to capture torsional and

asymmetric phenomena [3]. The oversimplified segmented models of uniform flexibility only allow for Froude scaling and offer limited insight in the transient responses due to slamming[12].

As more advanced manufacturing techniques have emerged in recent years, it could be fruitful to consider such new techniques to address the manufacturing of fully elastic vessels. In recent works, additive manufacturing has been used to construct accurate fully elastic models, Grammatikopoulos and Keser have manufactured such models and have tested their modal responses [1], [13], demonstrating their prospects as a new way of modelling.

The special properties of these newly developed models, such as the continuous flexibility of their hull, the increased structural detail and their fragility, must be treated with new measuring methodologies. While usually, strain gauges and force transducers are used to measure strains and loads directly on the flexible backbones of the segmented vessels, more refined techniques are necessary now. To investigate the capabilities of fully elastic models in wave impact tests, an experimental methodology to measure impact induced responses needs to be developed considering the distinctive features of these models. In the current project, such an experimental set up will be attempted to fully exploit the model capabilities.

1.3 Current Framework

Modern vessel designs demonstrate unique load cases and dynamic responses due to their particular geometry. A twin-hull crane vessel constitutes such a case. The vessel's dynamic responses also refer to asymmetric modes caused by torsion and differential responses of the side-hulls. It was previously mentioned that such cases are poorly presented by conventional experimental models.

The alternative of fully elastic models to investigate complex fluid-structure interaction phenomena has shown good prospects as a modeling method, but has not been extensively investigated. In her work, Keser [14] showed a fully elastic model could indeed exhibit the expected advantages of a continuous flexible model using modal tests and presented the opportunity for further research of the matter. The model itself has not yet been tested in experimental slamming conditions.

Fully elastic models are not usually chosen for the experimental process. A robust set up for such models, that tackles the challenges posed by their unique nature while also harnessing their full potential is not established.

1.4 Project Objectives

Considering the gap in experimental approaches to wet deck slamming with fully elastic models, this study builds on Keser's fully elastic model by extending its application to wave impact testing, focusing specifically on wet deck slamming in twin-hull vessels. The main objectives of the current work are:

- Calculate the model hydrodynamic behaviour and modal characteristics in water and verify the results with experimental measurements.
- Apply instrumentation capable of providing meaningful measurements for slamming and whipping.
- Perform wave tests that can induce slamming for various sea states.
- Collect the measurement data and analyse them so conclusions regarding the model slamming behaviour can be drawn.
- Investigate the best method to identify slamming and whipping based on the criteria established in literature and the capabilities of the set up.
- Conduct individual slamming analysis in the time domain to investigate the response of the model in critical events, using the data from different sensors.
- Reflect on the measurement methods and the choices made to build the current set up, and provide insight on the improvement of the set up for future works with similar models.

1.5 Methodology

The method of approach followed in this project consists of three distinct parts :

- **Numerical Analysis:** It is important to ensure the design of the model corresponds to the actual fabricated model behaviour. This is achieved in two steps:
 - **Hydrodynamic Verification:** The vertical motion Response Amplitude Operators are calculated using commercial software AQWA-LINE.
 - **Modal Characteristics:** Numerical dry analysis is corrected by including the hydrodynamic added mass. The modal characteristics are computed for the floating model.
- **Experimental Process:** The investigation of the model capabilities and the physics of wet deck slamming is achieved through the experimental method.
 - **Model Preparation:** The model is adjusted for the scheduled experimental runs, measurement instrumentation is installed.
 - **Experimental set-up:** The equipment is calibrated, the data acquisition system settings are adjusted and the measurements are synchronised. An analytical description of the steps taken is presented.
 - **Tests for numerical verification:** Tests are conducted for verification of the calculated RAOs with low amplitude mono-chromatic waves and modal characteristics through hammer SIMO tests in still water.
 - **Wave Impact Tests:** Tests meant to induce wet deck slamming, bi-chromatic waves are used for less monotonous excitation, different wave frequency combinations, wave heights and current speeds are used.
- **Data Analysis & Conclusions:** The findings of the project are processed and conclusions are drawn regarding the measured quantities and suggestions on possible improvements of the experimental set up for future works are given.

Chapter 2

Numerical Analysis

2.1 Introduction

The scaled model is designed to represent a reference model. During the design and production, certain decisions were made to ensure the resemblance of the produced model to the reference vessel.

Such decisions are the introduction of point lead masses inside the model to satisfy the sound scaling of the mass. The positioning of the lead masses was determined based on the modal behavior of the model with respect to the reference vessel. To ensure a watertight hull, resin coating was applied to the model. This has led to added stiffness of the produced model compared to the numerical model.

These decisions, combined with any small discrepancies that have occurred at the construction of the physical model have influenced its behaviour. It is imperative that the properties of the physical model match the numerical estimations regarding the design of the scaled model as well as the full scale reference vessel. To that end, a comparison between the numerical and experimental behaviour of the model is conducted, to verify the model suitability for further investigation of the slamming phenomena.

Motion tracking was used to measure the RAOs in the experimental set up. The measured RAOs of the physical model were compared to the computed RAOs of the reference vessel. The numerical RAOs were computed using the radiation diffraction potential BEM software AQWA. The software includes certain functions that can account for numerical discrepancies that could occur for complex geometries such as multi-hulls. The irregular frequencies as well as the hydrodynamic interaction of the side-hulls are accounted for, ensuring a sound numerical analysis for the appropriate frequency range.

Furthermore, the dynamic behaviour of the physical model needs to be representative of the reference model. The unique nature of the model do not allow for conventional hammer tests in the air, given that the common support systems used in these processes could damage the model and more elastic supports like bicycle rubbers introduce too much stiffness to the model, resulting in mode shapes that do not correspond to free-free support conditions. In this project, emphasis was given to the modal analysis of the model in the water, rather than in vacuo. The numerical values of the mode shapes and natural frequencies were calculated from a 3D structural modal analysis. The modal mass and stiffness elements were extracted from the model and were used to conduct a wet modal analysis. The wet mode shapes are derived from the solution of radiation problem, including the effects of the hydrodynamic mass and the hydrostatic stiffness.

2.2 RAO calculation

As previously stated, the hydrodynamic behaviour of the model needs to be verified. Using the commercial radiation diffraction software AQWA, the free floating RAOs were calculated. The estimation of RAOs could pose various issues if the scaled model dimensions were used. The wave amplitude used for the estimation of the RAOs as well as the numerical functions used by the software to account for the side-hull hydrodynamic interaction and irregular frequencies of the model are not designed for such small structures. As such, the actual dimensions of the reference vessel were used, while the structural characteristics such as the weight, location of the center of gravity and the inertia components were measured from the actual model and were also up-scaled to match the reference vessel size.

A virtual lid was established during the calculations to mitigate the overestimation of the standing waves that formed between the side-hulls due to their hydrodynamic interaction. The lid introduces additional damping in a specified region of the free water surface to mitigate the standing wave amplitudes that are produced due to the close proximity of the side-hulls of the catamaran structure. Various damping values were tested and it was found that a value of 0.2 yields the best results based on the calculation of the hydrodynamic quantities. For lower values negative added mass was found in some frequencies. Additionally, the internal lid function was used to account for potential numerical errors that may occur during the solution of the boundary value problem.

Having set up the problem for the desired conditions of forward speed and wave heading 180 degrees with respect to the vessel, the AQWA-LINE suite was run to obtain the free floating RAOs and hydrodynamic coefficients. In addition to the free floating Response Amplitude Operators (RAOs). The numerical analysis serves as the means by which the hydrodynamic response of the model is verified using experimental measurements.

The information regarding the model center of gravity and moments of inertia were taken from measurements using an oscillation test set-up. The tests were conducted in the workshop of the Ship and Hydromechanics Laboratory. A specially crafted cradle was used to insert the model and conduct heeling and oscillation tests, where the exact location of the center of gravity of the model and the inertia moments would be measured. Using the measured data regarding the structural characteristics of the model, the RAOs were calculated for the upscaled model design as presented below.

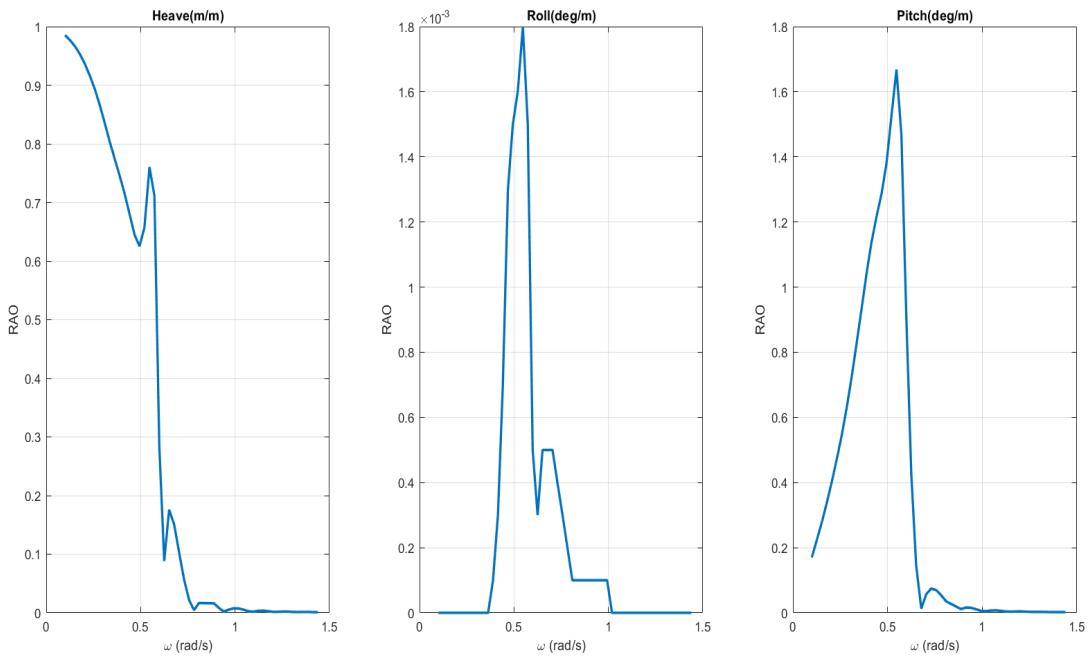


Figure 2.1: Vertical R.A.O. calculated by AQWA: a) Heave, b) Roll, c) Pitch

2.3 Wet Modal Analysis

In order to validate the model properties and ensure the dynamic behaviour of the constructed model is well described by the design, the added mass contribution should be considered when solving the modal analysis eigenvalue problem. The hydrodynamic added mass adds coupling terms in the diagonal generalised mass matrix that is produced from a structural modal analysis. The non-diagonal terms that are introduced, indicate a coupling of the dry modes of the structure, changing the natural frequencies and mode shapes of the model.

2.3.1 Mathematical model

The equation of motion for a free vibration of the structure in absence of any surrounding fluid is as follows.

$$[M_s]\{\ddot{v}\} + [K_s]\{v\} = \{0\}$$

Where:

- $[M_s]$ is the structural mass matrix,
- $[K_s]$ is the structural stiffness matrix,
- v is the structure displacement vector,
- $v = xe^{i\omega t}$, with x being the displacement amplitude and ω being the angular frequency.

To solve the eigenvalue problem, the equation becomes

$$\{-\omega^2[M_s] + [K_s]\}\{\delta\} = \{0\}$$

With ω and $\{\delta\}$ the dry natural frequencies and mode shapes respectively. The mode shapes are expressed as vector of displacements of the nodes of the structure in the x,y and z directions.

Based on the results of the dry modal analysis, the generalised modal mass and stiffness diagonal matrices can be formulated, defined as:

$$\begin{aligned} [M_{ij}] &= \{\delta_j^T\}[M_s]\{\delta_i\} \\ [K_{ij}] &= \{\delta_j^T\}[K_s]\{\delta_i\} \end{aligned}$$

With $i,j=1\dots 10$, the investigated modes of the analysis. Incorporating the generalised matrices will result in a more computationally efficient analysis. When considering the forcing of the surrounding fluid and the contribution of the hydrodynamic added mass, the equation takes the form:

$$[M_{ij} + A_{ij}]\{\ddot{v}\} + [K_{ij} + C_{ij}]\{v\} = \{0\}$$

Where:

- $[A_{ij}]$ is the generalised hydrodynamic added mass
- $[C_{ij}]$ is the generalised hydrostatic stiffness

The contribution of added mass can be calculated using potential theory, solving the radiation potential around the structure. Since potential theory is adopted, the fluid flow is considered inviscid, irrotational and incompressible. The added mass component is defined as the in-phase component of the radiation force, calculated based on the following formula:

$$Fr_{ij} = \iint_{S_0} \left(\rho \frac{\partial}{\partial t} (\det(\Phi_j) \mathbf{n}_i) dS \right) = A_{ij} \ddot{\zeta} + B_{ij} \dot{\zeta}$$

In the present project, numerical package capytaine was used to solve the radiation problem. Usually, in this methodology, the radiation problem is solved for each dry natural frequency. As the model's natural frequencies are very high, the actual mesh requirements to solve the radiation potential for those cases grow exponentially. It is chosen instead, to keep the mesh density to a reasonable size of 1cm and conduct a convergence analysis for lower omega frequencies. The convergence study shows that the wet natural frequency values converge after a certain omega frequency is reached. In other words, the wet natural frequencies can be estimated adequately even if lower frequencies are used for the radiation problem solution, since the added mass doesn't increase much after a certain frequency. The description of the exact methodology used is presented in the following chapter.

2.3.2 Methodology

The wet natural frequencies and mode shapes are calculated using the dry modal analysis results, as they are given by the FEA software ANSYS Mechanical. The dry modal analysis yields the dry natural frequencies, the modal mass and stiffness matrices and the mode shapes in form of displacement vectors for each node of the structural mesh. The first ten modes are extracted, including the six rigid body modes and the first four flexible modes. Using these quantities, the groundwork for the wet analysis has been laid.

As mentioned earlier, the capytaine radiation-diffraction solver is used. Capytaine is a python library, based on Nemoh's core routines, used to analyse marine structures in the frequency domain. The key functions that make the program suitable for the wet mode analysis is the capability to calculate the hydrodynamic coefficients of a structure as well as its capability of defining flexible mode shapes manually. Capytaine is well documented and provides a good tool for hydrodynamic analysis. It is a BEM method, using potential theory, while it also offers options for the import and manipulation of meshes.

Since the structural and hydrodynamic parts of the simulation are solved in separate programs, it is important to consider the different conventions followed by each software. The most important difference between the solvers, is the location of the coordinate system origin point with respect to the mesh, while ANSYS defines the coordinate system origin to be at the aft and bottom of the mesh, Capytaine considers the origin of the coordinate system to be at the mean water level plane, aligning with the center of gravity of the structure. The necessary transformations of the mesh were conducted to ensure the model's mesh is located in the appropriate position for each analysis. Furthermore, only the submerged part of the mesh is needed for the calculation of the hydrodynamic added mass, hence the part of the structure above the waterline is omitted.

After the dry modal analysis is concluded, the mode shapes of each investigated flexible mode is extracted as a displacement vector for each node of the mesh in the form: $\delta = [x_N^{dry}, y_N^{dry}, z_N^{dry}]$

The mode shapes can be inserted in capytaine to define the flexible degrees of freedom for the radiation potential analysis. Since capytaine defines the degrees of freedom based on displacement vectors at the center of the mesh facets and not the nodes, it is necessary to map the mesh nodes and displacements and define the displacements at the facet centers based on the displacements at the nodes of each facet.

Later, linear interpolation is used to transfer the facet center displacements from the structural mesh to the hydrodynamic mesh. The model is split in sections, and an average displacement is found for a specific longitudinal position for each side-hull. These average displacements of each section are assigned to a virtual point at the centerline of each side-hull. In short, each section of the model has two virtual points with an average displacement of the section for each sidehull. Based on the longitudinal location of the facet centers of the hydrodynamic mesh and which side-hull they belong to, an appropriate displacement is assigned via linear interpolation. The number of sections is determined based on the face size of the hydrodynamic mesh, and chosen to have as close a number of sections as the number of facets of the hydrodynamic mesh. In the current project, one hundred sections were defined, closely aligning with the mesh size of one centimeter, increasing the accuracy of the linear interpolation of displacements for each facet.

After the displacements have been assigned to the hydrodynamic mesh, the custom flexible degrees of freedom are defined in capytaine and then attributed to the floating body. The radiation problem is defined for one of the flexible natural frequencies of the model in rad/s and the depth of the flume tank, as well as the location of the center of gravity with respect to the origin point of the coordinate system. The radiation problem is solved and the hydrodynamic added mass and hydrostatic stiffness generalised matrices are extracted.

Now that the first approximation of the influence of water has been computed, it is time to form the total mass and stiffness generalised matrices as follows:

$$[M_{ij}^{Tot0}] = [M_{ij}^{str0}] + [A_{ij}^0(\omega^n)], [K_{ij}^{Tot0}] = [K_{ij}^{str0}] + [C_{ij}^0(\omega^n)]$$

The first approximations of the total mass and stiffness of the system are now used to calculate the first approximations of the wet natural frequencies and the new wet modes by solving the eigenvalue problem for the total quantities.

$$\{-(\omega^{wet0})^2[M_{ij}^{Tot0}] + [K_{ij}^{Tot0}]\}\{W^0\} = \{0\}$$

where W^0 represents the $i \times i$ eigenvector matrix, of eigenvectors $w_j^0 = [ix1]$ containing the contribution factors of each dry mode shape $i=1...10$ to the resulting wet mode shape j . The wet mode shapes are calculated as : $w_j^0 = \sum_{i=1}^10 p_{ij}^0 [x_i^{dry}, y_i^{dry}, z_i^{dry}]$.

After the first approximations of the wet quantities have been computed, the radiation problem is solved once again, this time for the wet natural frequency ω^{wet0} , to extract the new value for the hydrodynamic added masses. The degrees of freedom of the flexible modes are updated with the new wet mode shapes and the hydrostatic stiffness is calculated once more. Once the new values are available, the total system matrices are updated and the eigenvalue problem is solved again. This iterative process should last until the consecutive natural frequencies reach a convergence in the order of $\epsilon = 10^{-6}$.

The above process should be followed for all the flexible mode natural frequencies, until the desired wet mode shapes and natural frequencies are found. As mentioned earlier, the model natural frequencies are very high, mandating the use of extremely small mesh size. Instead of using an excessively dense mesh that would skyrocket the computational time of the analysis, a convergence analysis takes place. The analysis shows that the added mass values reach a point where they do not alter significantly with the increase of the omega frequency of the radiation problem, meaning the hydrodynamic added mass calculation can be valid for lower frequency values.

2.3.3 Results

The radiation problem is solved for various frequencies, the results of the convergence study are presented in the following figure, showing the flexible wet natural frequency values converge after a certain omega frequency for the radiation problem.

As the process above was followed for all four flexible modes, the following results were extracted.

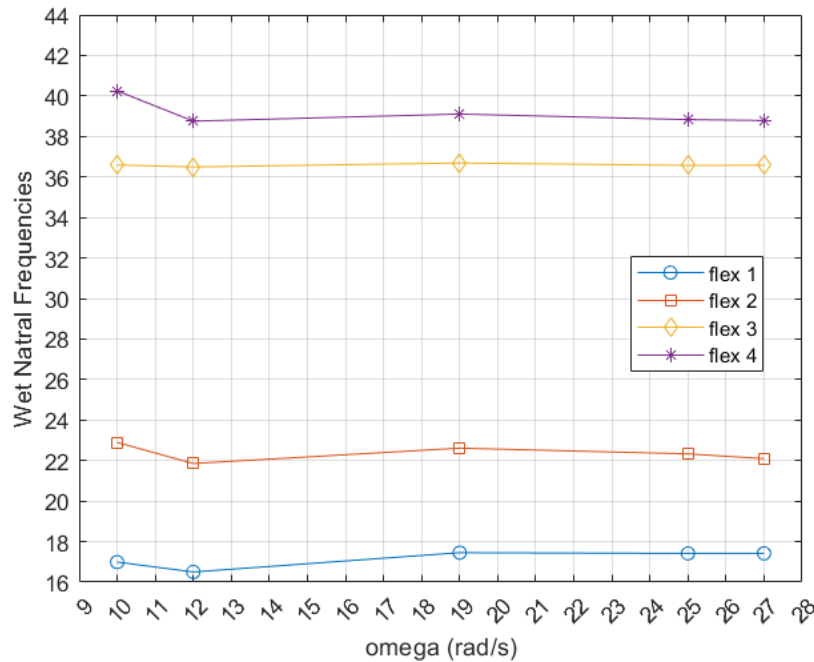


Figure 2.2: Wet Natural frequency values for different radiation $\omega(rad/s)$.

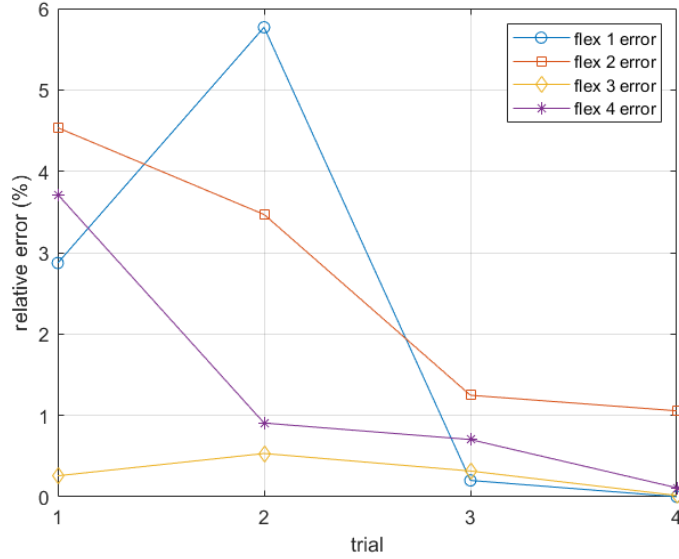


Figure 2.3: Relative error of wet natural frequencies for different radiation $\omega(rad/s)$.

As can be seen at figure 2.2, the values of the wet natural frequencies are not changing significantly after an ω value of $19 rad/s$. Figure 2.3 shows that the relative error of the calculated wet natural frequencies reaches values below 1 percent for flexible modes one, two and four, while mode three reaches a relative error value of 1.2 percent when using the ω values of 25 and $27 rad/s$. The process is considered converged, as all quantities seem to have reached a stable value. The findings of this computational process will be further validated with the experimental hammer test set up. Using an ω frequency of $27 rad/s$, the following results are found.

Flexible Mode	Dry (Hz)	Wet (Hz)
1	21.65	17.42
2	23.69	22.09
3	39.86	36.58
4	44.14	38.79

Table 2.1: Dry and Wet natural frequencies

It can be seen that the calculated wet natural frequencies are significantly lower than the respective dry frequencies. Such a result is expected, as the increase of mass in the system is more substantial than the hydrostatic stiffness of the water, as such the system wet natural frequencies are lower.

14.29	0	0	0	0	0	0	0	0	0
0	4.987	0	0	0	0	0	0	0	0
0	0	4.986	0	0	0	0	0	0	0
0	0	0	3.738	0	0	0	0	0	0
0	0	0	0	7.368	0	0	0	0	0
0	0	0	0	0	4.009	0	0	0	0
0	0	0	0	0	0	5.098	0	0	0
0	0	0	0	0	0	0	4.035	0	0
0	0	0	0	0	0	0	0	5.39	0
0	0	0	0	0	0	0	0	0	2.979

Table 2.2: Structural generalised dry mass matrix (kg)

14.4375	-8.17e-05	0.367	-9.29e-06	0.247	-0.00017	0.00217	-0.0748	0.00691	0.0443
0.000131	5.802	0.000409	0.00354	0.00019	0.1692	-0.0623	-0.0683	0.169	-0.0849
0.3659	6.76e-05	21.944	-0.000139	0.342	-0.000144	0.667	-3.893	0.197	-0.396
-1.051e-05	0.0172	-0.00015	4.24	2.16e-05	0.00917	0.1187	0.215	-0.652	0.273
0.244	8e-07	0.34	1.55e-05	8.43	-5.12e-05	-0.0286	-0.0642	-0.065	-0.0561
-9.735e-05	0.161	-0.00022	0.0101	-1.345e-05	4.091	-0.049	0.00497	0.0383	-0.0292
0.00352	-0.0485	0.67	0.12	-0.0265	-0.0607	7.298	-1.3	-0.446	0.334
-0.0738	-0.0683	-3.89	0.215	-0.063	0.01061	-1.302	5.946	-0.174	0.0285
0.00831	0.15	0.2	-0.656	-0.063	0.0434	-0.449	-0.174	6.557	-0.0498
0.0432	-0.0764	-0.396	0.274	-0.0569	-0.0315	0.334	0.0267	-0.0496	3.908

Table 2.3: Generalised total mass matrix, including hydrodynamic added mass (kg)

From the structural and total generalised matrices, it can be seen how the surrounding water influences the dynamic characteristics of the model. All the terms on the main diagonal are increased. It can be seen that the heave hydrodynamic added mass is greatly increasing the heaving mass of the system, while the off-diagonal terms showcase the coupling between the different modes. The off-diagonal terms showcase a behavior close to a symmetric matrix, although the values do not completely align with such a case.

The corresponding wet mode shapes are presented bellow, in comparison to the calculated dry mode shapes. The differences in the pattern are not significant, even though the magnitude of the relative deformations changes, as a result of the contribution of the other dry mode shapes.

The results present a good estimation of the expected values, in the following chapters, the calculated results are compared to the measured quantities and further conclusions are made with regards to the model's structural and dynamic behaviour compared to its intended design.

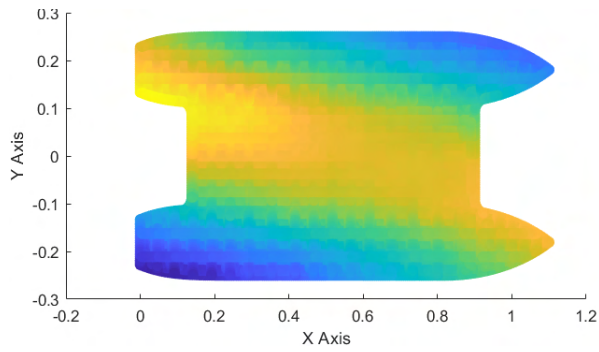


Figure 2.4: Calculated Dry shape $f_d = 21.65Hz$

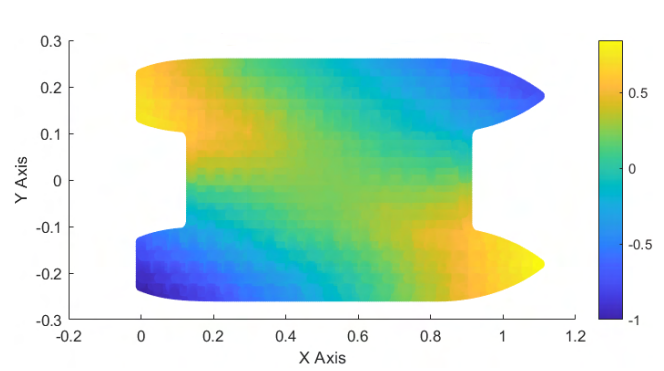


Figure 2.8: Calculated Wet shape $f_w = 17.42Hz$

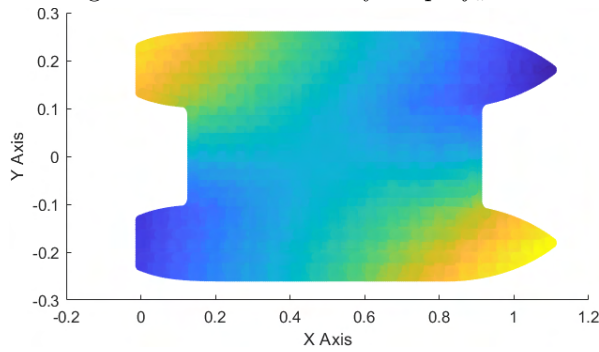


Figure 2.5: Calculated Dry shape $f_d = 23.69Hz$

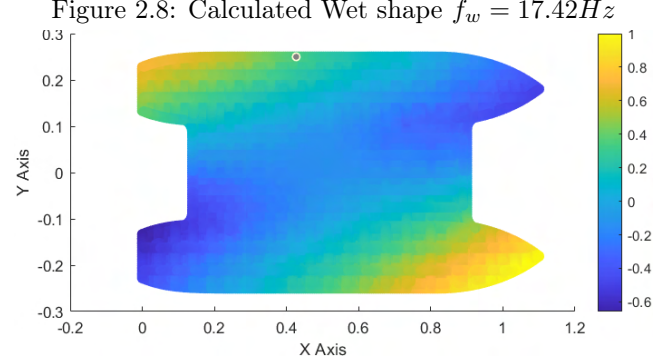


Figure 2.9: Calculated Wet shape $f_w = 22.09Hz$

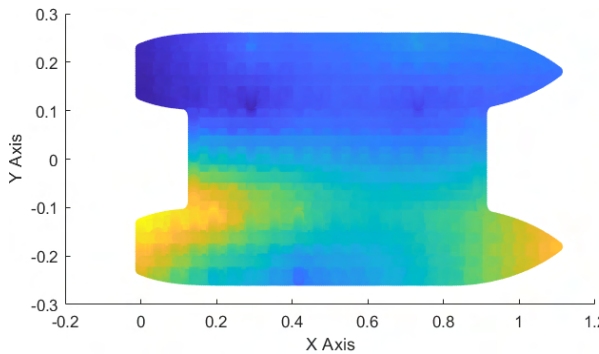


Figure 2.6: Calculated Dry shape $f_d = 39.86Hz$

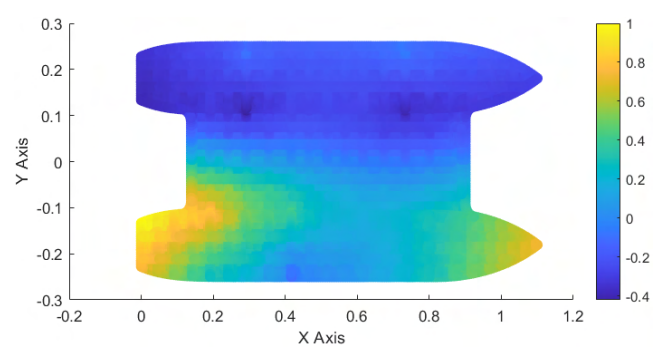


Figure 2.10: Calculated Wet shape $f_w = 36.58Hz$

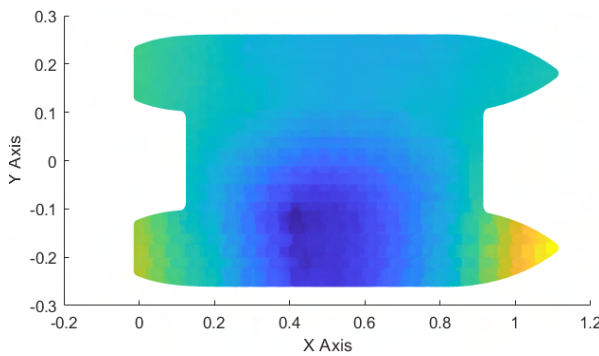


Figure 2.7: Calculated Dry shape $f_d = 44.14Hz$

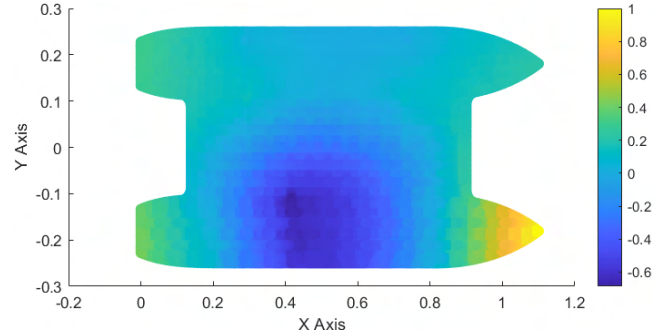


Figure 2.11: Calculated Wet shape $f_w = 38.79Hz$

Figure 2.12: Dry and wet flexible mode shapes.

Chapter 3

Experimental Set Up

3.1 Introduction

In this chapter the set up of the experimental tests will be presented. The measurement systems will be introduced and the calibration, synchronisation and triggering settings will be described in detail. Every procedure to design, measure and build the experimental environment will be reported, while the choices made, the existing set up limitations and the possible effects they can have to the experimental results will be discussed in length.

3.2 Model preparation

The model has been previously prepared for slamming experiments with DIC. A sheet of paper is placed on the deck to represent a speckle pattern that would be used for DIC measurements. This project has decided to use a different method of speckle pattern application. It is necessary to remove the previous speckle pattern and prepare the model for the new test runs. Initially, the paper sheet is removed and the black surface on the deck is sand papered. The deck is painted black except for the places where the crane and cargo structures, as well as the motion tracking marker have been placed. The result of the model preparation can be seen in the following image.



Figure 3.1: Prepared model

3.3 Oscillation tests

The existing model has been constructed based on designs and numerical calculations so that it can have a representative dynamic behaviour. As in every actual model, there is some divergence between the designed and manufactured product. Small errors in dimensions, material properties and location of the existing lead masses are inevitable. The accumulation of these small errors can lead to behaviour that diverges from the desired numerical estimations. One of those differences between the numerical and actual design is the coating of resin applied on the model to ensure watertight conditions. This additional material changes the stiffness of the structure as well as its weight, in ways that are not accounted for in the numerical analyses so far. The thickness of the coating is unknown so a quantified estimation is hard. In order to account for the actual model properties and approach its behaviour as close to reality as possible, oscillation tests are necessary to evaluate the structure's exact position of the center of gravity as well as the moments of inertia of the model. The information that occurs from these tests can be input in the hydrodynamic analysis to calculate the hydrodynamic behaviour of the produced model.

The oscillation tests were conducted in the workshop of the Ship and Hydromechanics laboratory. A custom cradle was used to perform the model, the tests were first conducted with an empty cradle to calculate the center of gravity and the moments of inertia. The oscillation tests were performed for the roll, pitch and yaw rotational degrees of freedom. The first step of the process was to place known weights to the system and measure the angles acquired by the cradle. The next step entailed the measurement of the periods for the completion of ten oscillations of the cradle. Each measurement took place three times and the average of each measurement time was used in the calculations of the results to minimise the measurement error. After the structural characteristics were estimated, the model was placed inside the cradle and the process was repeated for the cradle-model system. The structural characteristics were estimated for the total system. Finally, using the empty cradle quantities, the model's center of mass location and moments of inertia were found.

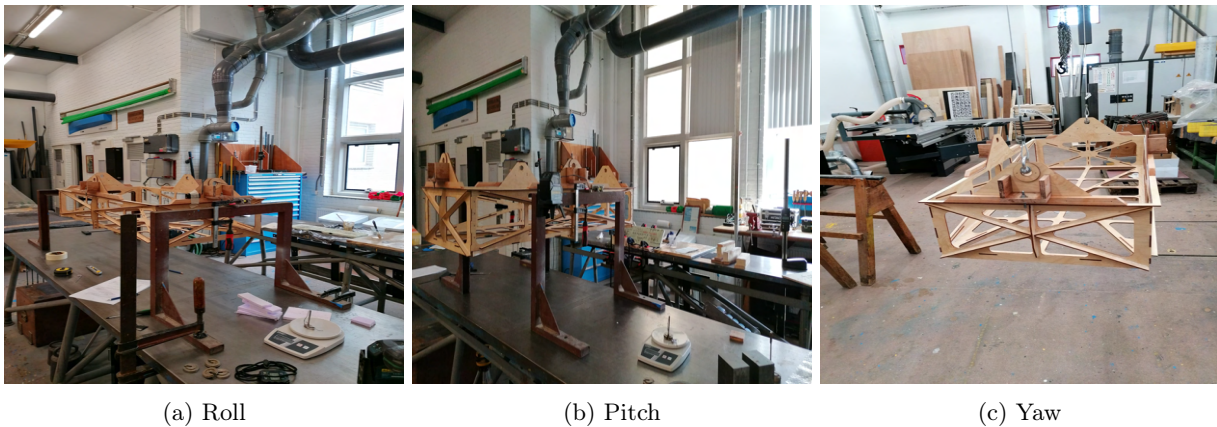


Figure 3.2: Empty cradle set up for oscillation tests

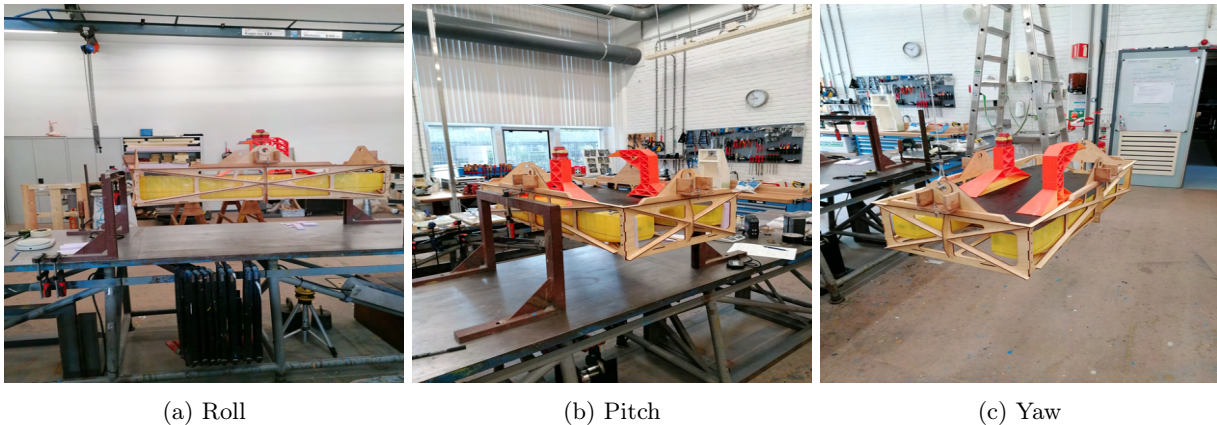


Figure 3.3: Cradle-model system set up for oscillation tests

The results from the oscillation tests are presented in the following table:

Measurement	Roll	Pitch	Yaw
V CoG (m)	0.128	0.131	-
Moment of Inertia (kgm^2)	0.65	1.47	1.65

Table 3.1: Results from Oscillation tests

The results above are used as input for the calculation of the hydrodynamic behaviour of the model. It is worth noting that the yaw test configuration does not yield the vertical position of the center of gravity. The set up for this degree of freedom included the suspension of the cradle and the system from the ceiling, using ropes to facilitate the rotation of the bodies about the vertical axis.

3.4 Waves and Current Conditions

The model is tested in the flume tank, a facility designed for long-term runs capable of generating both currents and waves. The test runs involve currents to simulate the model's forward speed and waves to induce wet deck slamming. The maximum current speed that can be produced is 0.4 m/s, which can impact the actual amplitude of the produced waves. Therefore, it is important to take measurements during testing. Wave probes are used to measure the actual generated wave elevation at three locations: in front of the model, next to it, and behind it.

Two current speeds are simulated: 0.1 m/s and 0.2 m/s. According to the Doppler effect, the encounter frequency at which the model experiences the waves changes in accordance with the current speed, mimicking the effects of the model moving against the waves.

The model is tested under two types of waves: monochromatic regular waves of low amplitude and bichromatic waves of varying frequencies and amplitudes. The monochromatic wave conditions are used to determine the vessel's Response Amplitude Operators (RAOs) and compare them to the numerically computed responses. By verifying the experimental and numerical approaches of the hydrodynamic behaviour of the model, it is ensured the produced model is following the expected responses and there are no functional issues.

Bichromatic regular waves are used to excite the model in two distinct frequencies providing more realistic wave conditions than the monochromatic waves while still maintaining a degree of repeatability. These wave conditions offer useful information on slamming behaviour. By testing frequencies close to the model's high vertical motion response frequencies and adjusting the amplitude of the components, multiple slamming events can occur. In contrast, a monochromatic wave component quickly reaches a steady state and the variety of the different slamming events is limited. With bichromatic waves, multiple wave amplitudes are tested in a single run. The model responses are less predictable than in case of a single component leading to higher variability of the vertical velocity. Consequently, a wider range of parameters are tested and their contribution to slamming occurrence and severity can be assessed.

Irregular seas would also provide valuable insights into the phenomenon, as they approach realistic waves the closest and can be used for extensive statistical analyses of the phenomenon. The flume tank has the ability to create irregular waves, given the appropriate signal. For the present study, it was considered that the investigation of regular monochromatic and bichromatic waves would be sufficient to investigate the parameters related to slamming and the model's overall behaviour. The finite availability of the tank facility, combined with the considerable time required to tune the waves and the substantial amount of data collected from each test run, presented challenges. Hence irregular seas were not tested.

3.4.1 Wave Generation

The wave generation equipment of the tank consists of a flap wave maker, connected to the computer from where the motion of the flap is controlled. Two programmes are used for the motion control of the flap, the automation program that controls the flap motion system controls and the program that receives a signal input file in voltage that is sent to the control system of the flap to dictate the motion signal.

The control system program adjusts the positioning of the flap and the motion parameters such as scaling of the voltage to represent movement in centimeters. Once the flap is positioned in the zero position, and the setting to read input signal is chosen, the flap is ready to move according to the voltage signal. Every signal needs to include a rump-up and rump-down at the beginning and the end respectively, to allow for the flap to adjust its motion smoothly.

The wave conditions were first tested in absence of the model. The relation between input signal amplitude and resulting wave amplitude differ based on the desired wave frequency and current speed. Some indication for the required signal amplitude is given by known polynomials that compute the motion amplitude based on the wave period and wave amplitude. These polynomials were empirically formulated based on measurements in the flume tank in the past. In any case, further testing was necessary to determine the signal amplitude for each case, as the empirical relations were not always accurate. Once the wave conditions were tested, the model was put inside the tank to verify that slamming phenomena would occur for these conditions.

3.5 Mooring system

The experimental set up includes the use of mooring lines to keep the model from drifting away. The mooring line system is composed of four vertical springs, supported by vertical rods at the edges of the flume tank. The springs are attached to inelastic ropes, connected to wheels at the level of the floating model's deck and are connected to the metal rings connected to it. That way the spring stiffness will not affect the vertical motions of the model.

It is intended for the model to be tested under forward speed conditions. In the flume tank facilities, the forward speed is simulated as a current speed. The maximum current speed that can be produced is $0.4m/s$. The mean horizontal offset of the model is expected to be caused by the current drag force and the wave mean drift forces. Therefore, the mooring system is designed to withstand these forces and result in small offset of the model. The tests refer to a free floating model, hence the rest of the wave induced motions should not be heavily affected by the system. Soft spring systems like moored floating structures can have significant horizontal oscillatory responses due to resonance of the moored system to the low frequency component of the incident waves. To account for this case, it is ensured that the moored system natural surge period is well below than the low frequency component of the expected waves to be tested. This consideration can only be valid for the regular and bichromatic wave cases that are intended to be tested, for the irregular seas, the low wave frequency component is not known.

The stiffness of the springs to be used is measured by suspending the springs and applying known weight at their free ends. The deformation of the spring is measured in three different measurements and an average is taken for all measurements. Many weights are used in order to be able to capture the most realistic stiffness relation of the spring, as it is a on-linear one. From the measurements, the stiffness is found to follow the formula below:

$$K = 233.63x^{-0.604}$$

,where x in mm

Using the above formula for the spring stiffness and the geometric characteristics of the moored system as it is designed, the mean offset is calculated for the estimated current drag and mean wave drift forces. The offset is found to not be significant and therefore the adequacy of the measured mooring springs is verified. The horizontal offset of the model needs to be small, since it is intended for high speed cameras to record the top deck of the model to capture the in and out of plane deformations due to slamming. It is therefore important for the model to remain within the field of view of the two cameras.

3.6 Motion tracking system

The rigid body motions of the model are recorded by a series of cameras located at the ceiling around the tank to capture the model from different angles. These cameras are directed to record the motions of the tracking marker placed at the model, and calculate the location and angle of the model for the six rigid body motions, video data can also be extracted. The cameras are calibrated and set to the ground plane where the deck of the structure is.

3.7 Stereo DIC

DIC, also known as Digital Image Correlation, is a measurement method that can capture the horizontal displacements and strains occurring at the top deck surface of the model. When more than one camera is used, the method is called stereo-DIC and can evaluate the vertical motions as well. In the current project, two high speed cameras are used, hence stereo DIC is applied. For the sake of simplicity the measurement will be referred to simply as DIC from this point on.

The methodology followed makes use of a speckled pattern applied on the investigated surface. The pattern must be random, high contrast is needed so usually, white and black are used for the background and the speckles. The size of the speckles depends on the available field of view and the camera resolution, as a rule of thumb a speckle should take approximately 3 to 7 pixels of the camera recording. The speckle motions are captured by high-speed cameras that record the full field deformations. The recordings are later evaluated in specialised software that discretizes the measured field of view into facets. The displacements and strains are calculated for each facet, resulting in a continuous representation of the surface response.

The method accuracy depends on the speckle pattern quality as well as the sampling frequency and available field of view. In the current project, the sampling frequency (camera frame rate) is chosen as 125 Hz. Based on the Nyquist frequency, responses up to 62 Hz can be captured, well above the investigated global responses. The analytical description of the DIC set up is given below.

3.7.1 High-Speed Cameras

The deck deformations will be estimated using stereo-DIC. For this method, two cameras are needed. The current set up makes use of two high speed Photron SA-Z cameras, placed on top of the model in such a way that the center of the deck is captured by both devices. A frame is built and installed on the ceiling above the flume tank, the frame needs to be able to keep the cameras in a stable position. The field of view of the cameras is defined by the available distance between them and the recording target, as well as the lenses used. In the current case, lenses of focal length equal to 80 mm were used, in a distance of 1,5 m between the cameras and the model. These conditions provide for a field of view of approximately 350 mm.

The cameras can record in a very high frame rate, resulting in a heavy data load. It is important that the cameras do not record for the whole test duration but only during the slamming events. As such a trigger needs to be applied so that the recording of the cameras is limited to instances of interest. It is decided that the trigger will be sent from the acceleration sensors that are placed in the model deck, once the acceleration reaches a high value, a signal is sent to the cameras to initiate the recording. The cameras also need to be supplied by power and be connected to the DAQ system and main computer. To achieve that, network cables and trigger cables are used to connect the high-speed cameras to the necessary outlets.

Other than the positioning and connectivity of the cameras, a calibration needs to be conducted, both for the camera visibility but also for the DIC software to be used, Istra4D. A target is used for calibration, placed in the position of interest and translated and rotated around this position to define the space of the expected deformations to be recorded.



(a) High speed cameras configuration

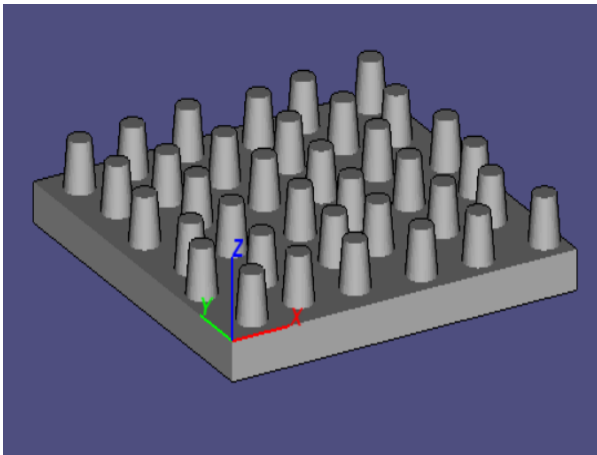


(b) Calibration of DIC software

3.7.2 Speckle pattern

The speckle pattern to be applied will define the deformations of the deck, based on the displacements of the speckles recorded by the high-speed cameras. The pattern needs to have well defined speckles with contrast, clear shape and random positioning. The size of the speckles are also important, capturing between three to seven pixels. In the current case, the optimum speckle size is found to be approximately 1,2 mm. As it has been found that applying a paper sheet with a printed pattern on top of the deck is not efficient, different application methods are investigated.

Initially, a stamp is considered. However, the material of the vessel is hard, meaning a rubber stamp needs to be used. A 3D-printed stamp has been proven hard to manufacture, especially for a speckle size of 1.2 mm. A regular PLA stamp was printed and tested in a hard material, proving the initial concerns that a hard material will result in poor quality of speckles. The printed stamp is presented below:



(a) Design of stamp



(b) Speckle stamp out of PLA

Other approaches such as the use of a stencil or spray painting were also considered. Due to the non-flat surface of the deck of the model and the concerns about the paint spreading further than intended, combine with the hardship of repairing a bad quality outcome in the deck, it was decided to apply the pattern manually. It is recognised that manual application of the pattern is not ideal as parameters like the randomness of the patter, the speckle size and the percentage of coverage are harder to control. Another major drawback to this method is the amount of time that need to be spent to apply the pattern. Nonetheless, the manual application took place and resulted in the following pattern at the middle of the model's deck:

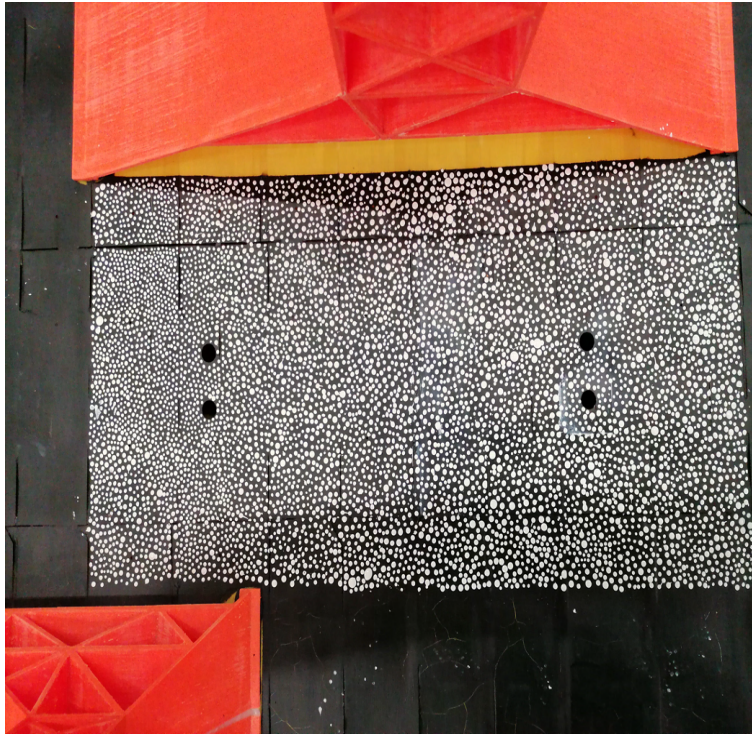


Figure 3.6: Manually applied speckle pattern

It is evident that the quality of the pattern is not uniform throughout the application field, with the quality decreasing at the fore of the model, with more large speckles. Some of the drawbacks discussed earlier can be seen in the image above. Nevertheless, the unique nature of the deck necessitates to first apply the pattern in this way to evaluate whether or not it is prudent to consider different application methods. The other possible scenarios of application would be the use of a small rubber stamp, not 3D-printed but manufactured by a designated specialist or the use of a laser cut plastic stencil to use as a spray painting pattern. Both methods were dismissed due to time limitations and uncertainty of efficiency. At the conclusions of the report it will be determined whether or not the manual application of the pattern was a sufficient means to capture the deck deformations in a precise manner.

3.8 Accelerometers

Accelerometers are used to measure the responses of the model to the wave loads. In total, eight sensors will be used to capture the responses in the whole model, three in each side-hull and two at the front and back of the deck. The sensors are going to determine the global whipping responses induced by wet-deck slamming. The value of the sensor measurements will become indicative of the structure responses and will trigger the high speed cameras in the event of wet deck slamming occurring.

The sensors are small and are not expected to affect the structural stiffness of the model. The cables connecting the sensors to the DAQ box need to be loose so that no additional stiffness is introduced to the system while it needs to ensure that the cables will not come in contact with the water during test runs. The DAQ box needs to be close to the model and the main computer. Hence, it is decided that the box will be placed in a specially crafted position by the flume tank, while the cables of the sensors will be supported by special item beams to stay away from water while still providing for sufficient length for good connection with the model at all excursions during testing.

As the accelerometers are positioned so that the responses of the first four flexural modes can be captured adequately. Based on the mode shapes calculated in the dry and wet modal analysis, the sensors are placed at model locations of significant deflection.

3.9 Complete tank set up

In the following pictures the complete set up at the flume tank can be seen with all the systems active and ready for measurements. The acceleration sensor locations are presented, as well as the surface covered by the speckle pattern.

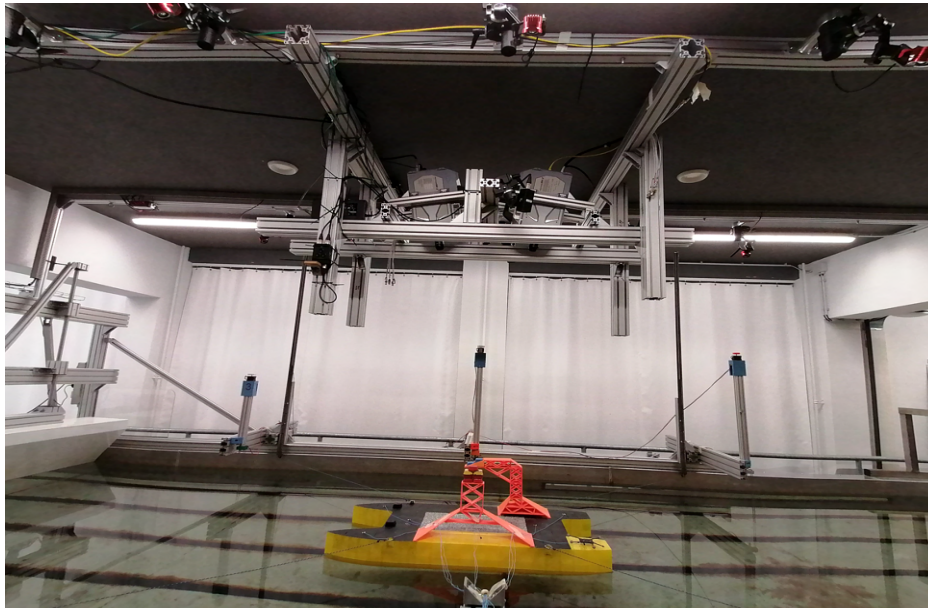


Figure 3.7: Completed measurement set up.

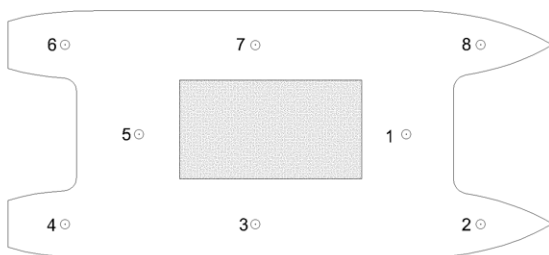


Table 3.2: Sensor Placement

Sensor	X(mm)	Y(mm)
1	850	0
2	955	-180
3	500	-180
4	115	-180
5	265	0
6	115	180
7	500	180
8	955	180

Figure 3.8: Model Instrumentation

3.10 Limitations

A thorough description of the the experimental set up has been given. The limitations of the facilities and the instrumentation used should be mentioned. Initially, the limitations of wave making need to be discussed. The recirculation flume tank is equipped with a current generator as well as a wave flap generator, as such the two functions of the tank can be used simultaneously. The parallel operation of the two generators has implications, as the wave height of the waves generated drops with the increase of the current speed. Since wet deck slamming on a low speed twin hull vessel is investigated, high amplitude waves are important, while the investigation of different forward speeds dictates the use of more than one current speeds during the wave impact tests. Fine tuning is necessary to determine the range of the wave amplitudes to be tested, as well as the most relevant current speeds for the present model. The wave generator also exhibits limitations in the frequency range of the wave components it can generate consistently. After testing, it is found that for wave frequencies above 7 rad/s refraction phenomena at the beach and side walls are increased, causing standing wave formation.

Aside from the wave and current conditions, the instrumentation used on the model also introduces some uncertainty. As fully elastic models are not usually mobilised, most frameworks that have been developed for the hydroelastic investigation are not directly applicable. In the current set up, no sensor is placed on the wet deck surface, meaning there are no direct measurements of the wave impact on the structure. It is also important to note that the wave probes placed in the tank are not able to measure the free surface elevation between the side hulls of the structure. As such the side-hull interaction that causes the incident waves to form standing waves below the wet deck surface is not quantified.

Another point to be made about the measurements is that the DIC set up does not capture the whole deck deformation field. This limitation is due to the practical field of view of the high speed cameras. Based on the available distance from the model upper deck and the lens capabilities in terms of focal depth and focal length, the field of view is determined to be approximately around 35 centimeters. This shortcoming could have been solved by acquiring new lenses of shorter focal length. Unfortunately, due to the scheduling of the experimentation and the time necessary for new lenses to be acquired, this solution was not feasible, and a limited area of the deck deformations was captured by the stereo DIC system. Additionally, the weight of the cameras also necessitates the construction of a heavy support frame which consumes significant amount of time and effort.

Last but not least, the fragility of the model should be addressed. The use of PETG material and the wall thickness of 0.56 mm make the model particularly susceptible to delamination and cracking. handling the model requires particular attention, at least two people are needed to lift the model and place it in the tank. During the first attempt to place the model, delamination in the bottom of one side hull was observed. The point of failure was mended with special epoxy 3.9. No water leakage was observed.

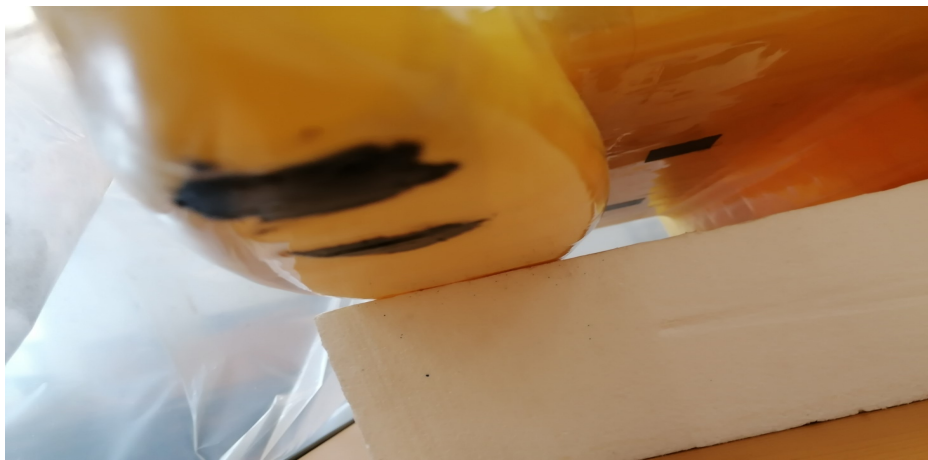


Figure 3.9: Epoxy treatment to cover hull delamination

Chapter 4

Modal Analysis

4.1 Impact Hammer Tests

The verification of the model dynamic characteristics is achieved through impact hammer modal tests. The test configuration is described as a single input-multiple output testing (SIMO), with a single impact hammer hitting the model and multiple acceleration sensors measuring the response of the structure. The Dewesoftx data acquisition system is used for modal tests. The behavior of the model is evaluated using the frequency response function, the coherence of the signal and the mode indication function. The high speed cameras are also used to capture the responses under hammer impacts and evaluate the modal behavior via Digital image correlation.

4.1.1 Test process

The model is placed in the recirculation flume tank, under still water conditions. It is established that the structure can not withstand direct hits on the deck, as damage of the structure would be unavoidable. Considering the fragile nature of the model, the hammer hits are applied on the foot of the support structure that is placed on the deck. The support structure is comprised of thicker material and can withstand the impact loads better. Since the loads are not applied directly to the model hull, the load transfer may not be optimal. Additionally, the wet modal analysis configuration introduces added damping that can result in less straightforward analysis results. Moreover, the placement of the model in the tank hinders the precise control of the hammer, increasing the probability of double impacts. Indeed, during the testing, double impacts were recorded, in those cases the impacts were rejected and the process was repeated. The use of a shaker in place of a hammer was discussed but was dismissed due to the complexity of the required set up close to the water. As mentioned earlier, the additional damping due to the surrounding water can introduce added complexities in the modal responses of the structure. Masking of the modes is observed, while the peaks detected at the frequency response function may not align completely with the natural frequencies. To be able to determine the natural frequencies and mode shapes under these conditions, it is necessary to investigate the response of the structure with as many tools as possible. Firstly, the frequency response function (FRF) is investigated to obtain information on the maximum responses of the structure. In case of resonance, the transfer function amplitude presents a peak, while the phase of the transfer function should shift. In cases of systems with additional damping such as the present study, the phase change might not be as drastic as in other systems. Additionally, the validity of the peaks observed needs to be ensured. To that end the coherence of the signal must be checked. Coherence shows to what extent the excitation input and response output of the modal analysis are correlated linearly. In other words, when the coherence value is close to unity, the FRF transfer function can be considered realistic. Hence, the peaks of the FRF, where the coherence is close to unity, probably indicate a resonance peak. As a last measure to evaluate the modal test findings, the modal indicator function (MIF) may be used. The MIF can be calculated by the dewesoftx software. It can indicate at which frequencies the response of the structure represents a mode shape. MIF values close to unity represent mode shapes.

4.1.2 Impact Hammer Results

The analysis of the structure made use of the methodology presented above to experimentally identify the mode shapes and natural frequencies. The definition of the natural frequencies based on all of the disposable analysis tools is presented in detail in the following figures :

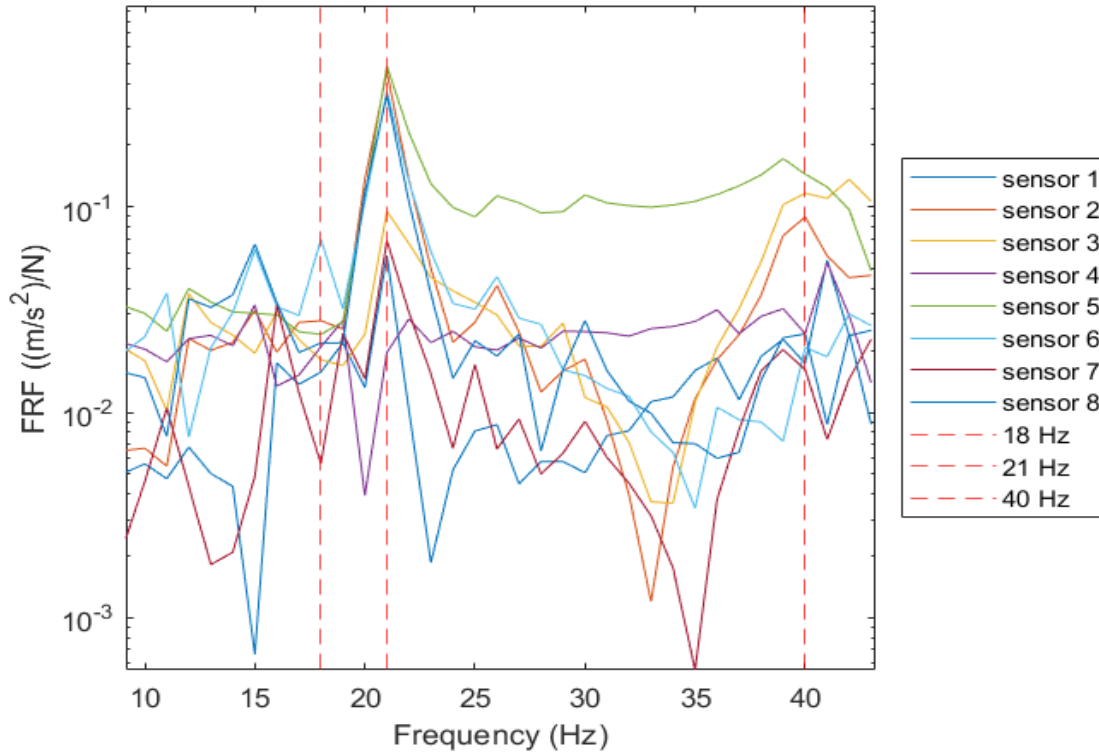


Figure 4.1: Frequency Response Function from SIMO impact hammer tests

The figure 4.1 shows the peaks observed at the transfer function. It is evident that the peaks do not show resonance peaks with clarity. The dashed lines show the frequencies that are determined to represent the wet system natural frequencies. It can be seen that many sensors show increased responses for various frequencies, that is due to the mode masking that prevents the system's modes from manifesting clearly. In the following graphs it is shown that the chosen frequencies are the ones closest to fulfilling all the requirements for natural frequencies.

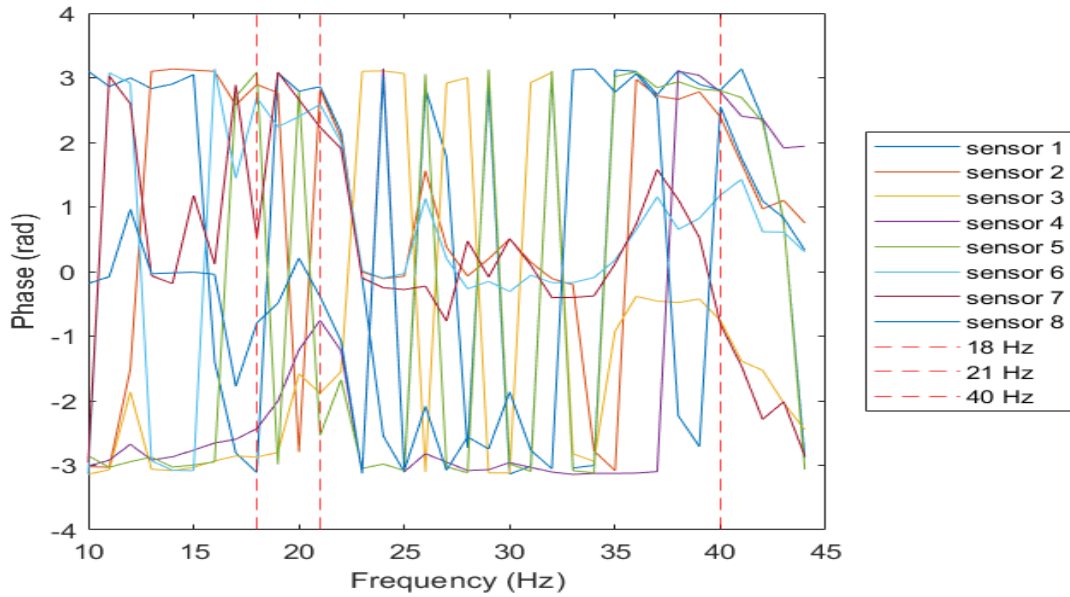


Figure 4.2: Phase of the transfer function from SIMO impact hammer tests

By following the dashed lines indicating the natural frequencies of the figure 4.2, it can be seen that the phase undergoes change for these values. What is also evident is that substantial change is also met for other frequencies. This makes the distinction of resonance harder as there is no absolute indication of the natural frequencies.

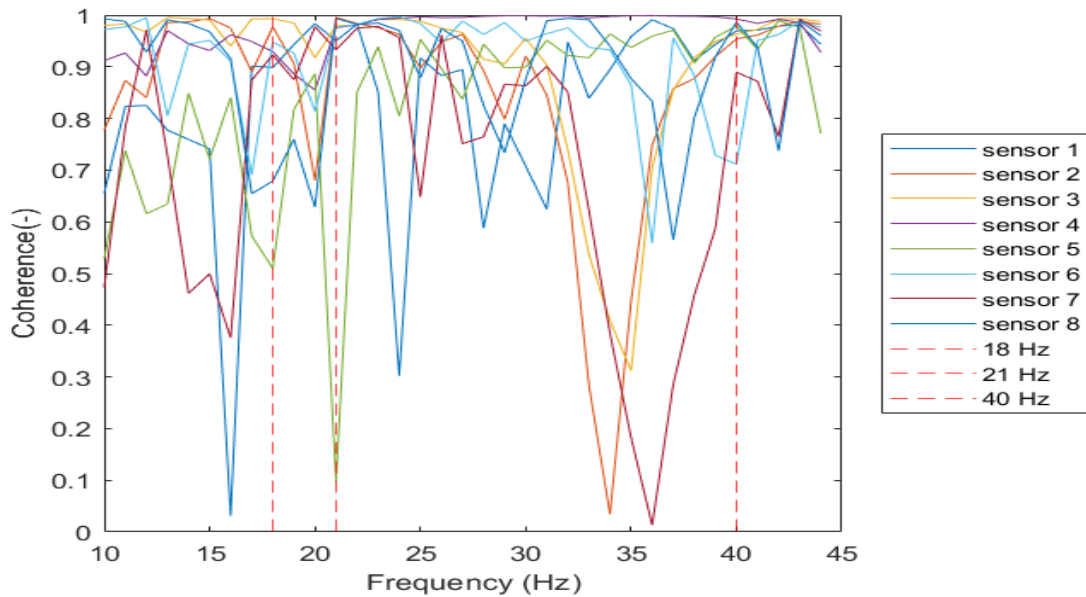


Figure 4.3: Coherence for the SIMO impact hammer tests

The coherence figure 4.3 assists in excluding numerous frequencies. It can be seen that the coherence values of sensor 5 take low values in the selected natural frequencies of 18 and 21 Hz. As the rest of the sensors seem to maintain values close to unity for these frequencies, it is decided not to exclude them as possible natural frequencies and consult the MIF function for further insight.

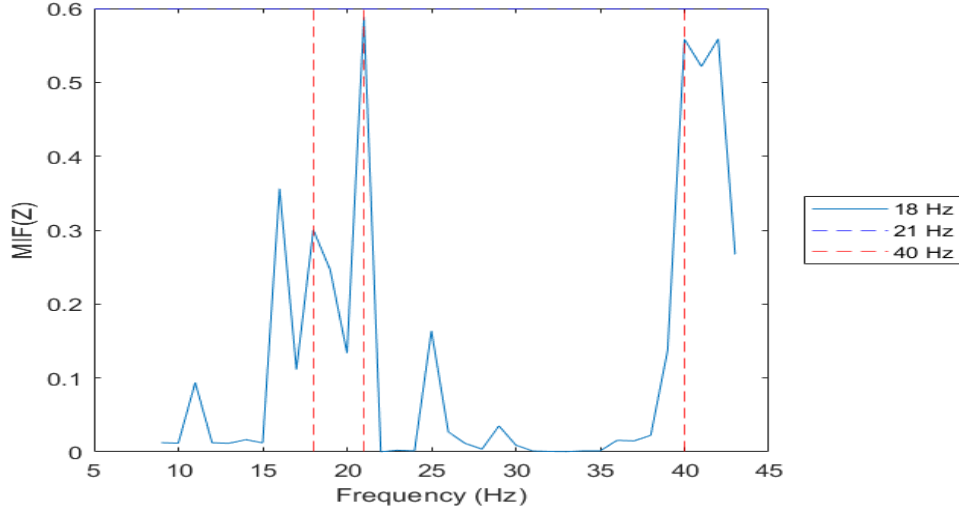


Figure 4.4: Mode Indicator Function for the SIMO impact hammer tests

The MIF function shows five substantial peaks in 16, 18, 21, 40 and 42 Hz. Although the MIF indication of frequency 16, is stronger than frequency 18 Hz, the findings from the previous tools, such as the coherence and the frf peaks, shows that resonance behaviour is more likely in the frequency of 18 Hz. The MIF indication of frequency 21 Hz also matches with the FRF response, the phase shift and the high coherence values, with the exception of sensor 5. Finally, frequencies 40 and 42 appear to have similar behavior with regards to the MIF indication, the coherence and the phase change. Nevertheless, the FRF response at frequency 40 Hz reaches higher values than frequency 42 Hz and hence, frequency 40 Hz is chosen as the third natural frequency. It is worth mentioning that the expected natural frequencies were four. The analysis tools used did not indicate more wet natural frequencies. This is further backed by the previous modal tests that were conducted on the vessel [14].

4.1.3 Comparison of experimental and numerical results

The experimental investigation of the modal characteristics of the model, surrounded by water yielded three wet natural frequencies. The numerical investigation used the structural modes and conducted a numerical method to account for the hydrodynamic mass using potential theory, concluding in four wet natural frequencies of the floating model.

Both methods include uncertainties in their approaches. For the numerical method, a convergence study was conducted to determine whether the added mass calculation is sufficient for lower frequencies than the structural natural frequencies as presented in chapter 2. The results showed sufficient convergence 2.22.3. On the other hand, the experimental method was met with challenges due to mode masking. The surrounding water introduced additional damping, while the first and second natural frequencies are relatively close. Additionally, the impact hammer tests in the tank pose difficulties in the practical aspects of the test, such as reaching the model in the tank and conducting valid hits while avoiding double hits. Four tools were used to analyse the experimental data and conclude to the models structural frequencies. The results of both approaches are presented in the following table, accompanied by the relative error between the two values.

Table 4.1: Comparison of numerical and experimental modal characteristics

Mode	Numerical $f_n(Hz)$	Experimental $f_n(Hz)$	Relative error (%)	M.A.C.
1	17.42	18	3.3	0.803
2	22.09	21	5.2	0.6525
3	36.58	-	-	-
4	38.79	40	3.12	0.7595

The mode shapes resulting from the accelerometer sensors show good agreement with the numerical estimations. The Mode Assurance Criterion was applied to compare the two approaches. It can be seen that the mode shapes are correlated but not identical, with the second mode shape being the most poorly represented by the numerical analysis. Nevertheless, the general deformation pattern is captured by all modes.

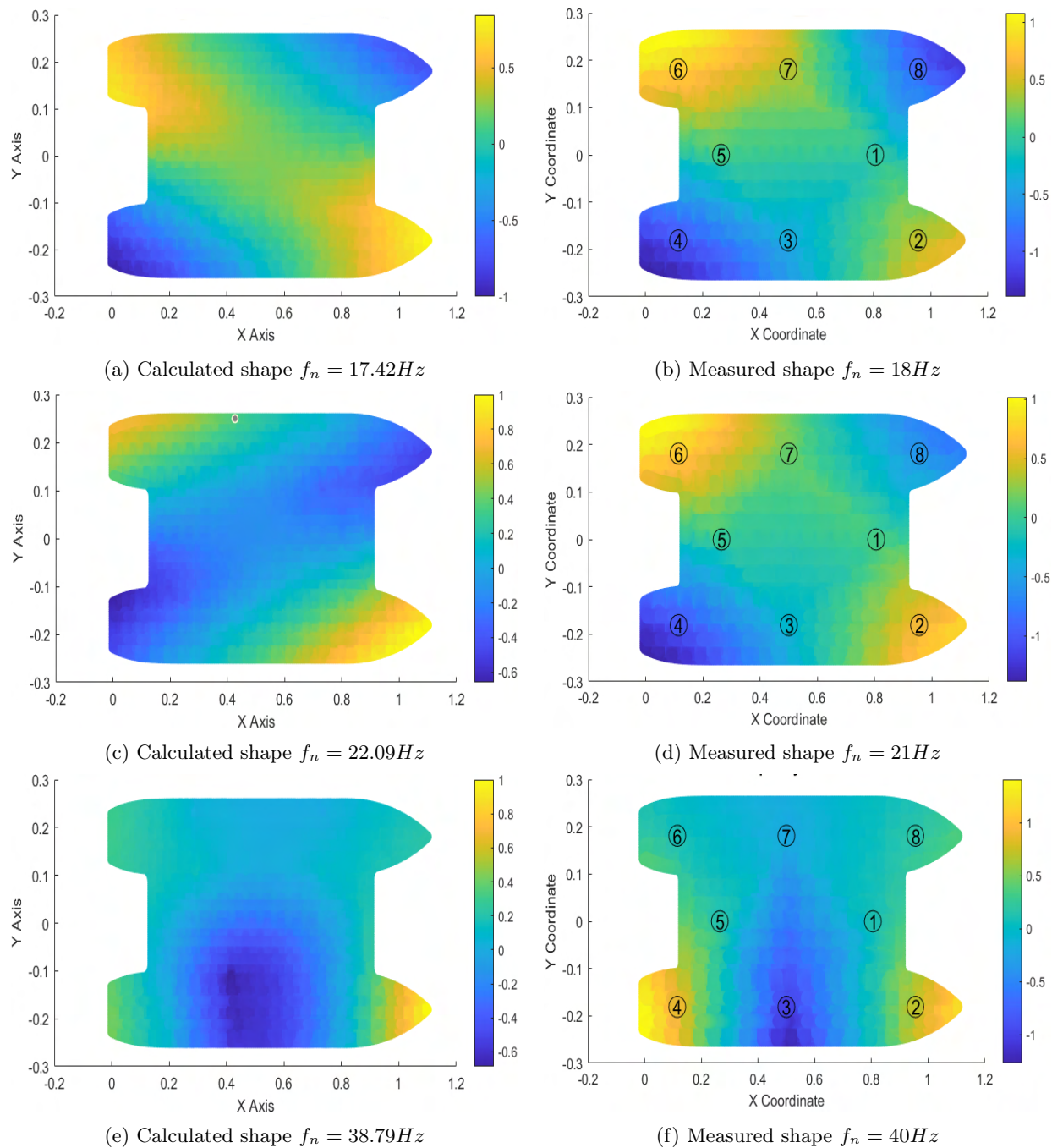


Figure 4.5: Comparison of calculated and measured mode shapes

4.2 DIC measurements

The high speed camera set up was used to compliment the accelerometer measurements. The high speed cameras were used in the same set up as the accelerometers, but for different hammer impacts. The reasoning was that the often occurrence of double hits during the hammer tests and the consequent rejection of measurements for the dewesoft acquisition system, could not be followed efficiently by the high speed camera system. As such the high speed camera recording was conducted for five hammer hits that were also measured by the dewesoft system, as simple acceleration and excitation recordings.

The recording was post-processed with the Digital Image Correlation (DIC) software istra4D. A mask was defined to mark out the surface of interest, while a starting point was set to activate the mask. Appropriate resolution settings were chosen, while each frame was evaluated to obtain the three-dimensional displacement field. The grid and facet size produces 1024 measurement points on the surface. The data were exported in text file format, each file containing the evaluated values for each measurement point at a set time step. The files were processed appropriately for further treatment in the Matlab environment.

It is worth noting that parts of the speckle pattern surface were not evaluated. As discussed earlier, the speckle pattern quality is not uniform throughout the total pattern surface. Small points have been aliased due to the larger than optimal size of the speckles. These points are limited, with the majority of the grid being represented in the evaluated data. Additionally, the four orifices on the top deck that were originally meant for pressure sensor placement were not covered by the speckle pattern. Finally, due to practical reasons, a cable of one of the acceleration sensors crossed the pattern transversely, the cable had been stabilized on its other end at the rigid support structure at the other side of the deck to minimize its movement. During the evaluation of the results, the cable interference caused a fine transverse line on top of the pattern, leading for absence of evaluated data for that fine line location. During the modal tests, the total evaluated surface is established to give a good representation of the upper deck surface, with any empty points remaining secluded, and not causing substantial lack of results.

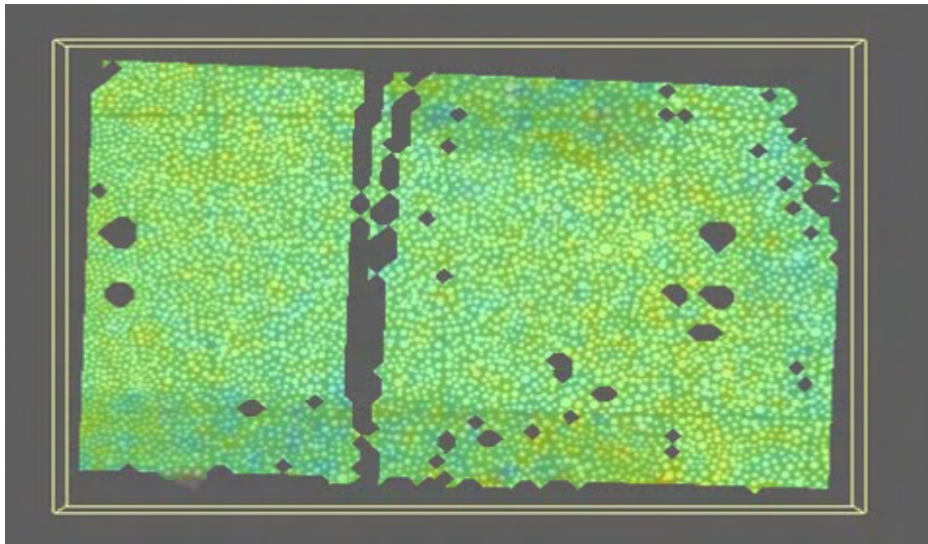


Figure 4.6: Evaluated surface usnig istra4D software.

4.2.1 DIC Modal Results

The main objective of this analysis is to investigate the modal characteristics of the model based on the DIC evaluated responses. The vertical displacement data are used. OMA is applied, due to uncertainty in the force signal measurement. The data points used are shown in the following figure 4.7.

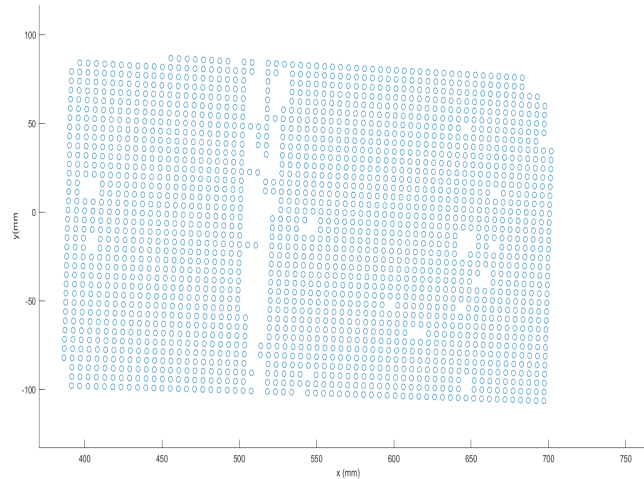


Figure 4.7: Data points used for the modal analysis.

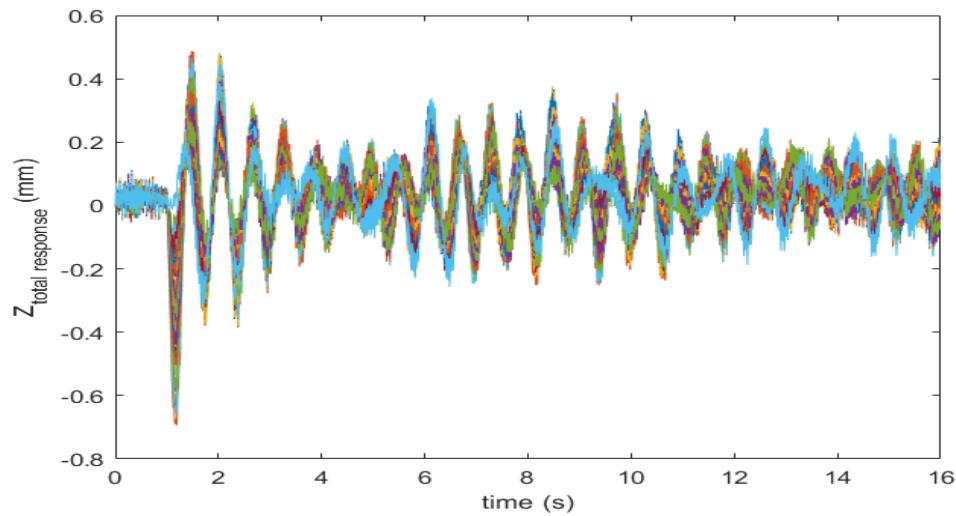


Figure 4.8: Total z displacement (mm) for hammer impact.

Figure 4.8 shows the total vertical displacement of the evaluated points. The recording includes a second before the actual hammer impact. The figure also serves as a validation to the triggering settings of the DIC system, as the high speed cameras are able to capture frames before and after the impact. The difference in amplitude and phase of some data points indicates the presence of flexible motions.

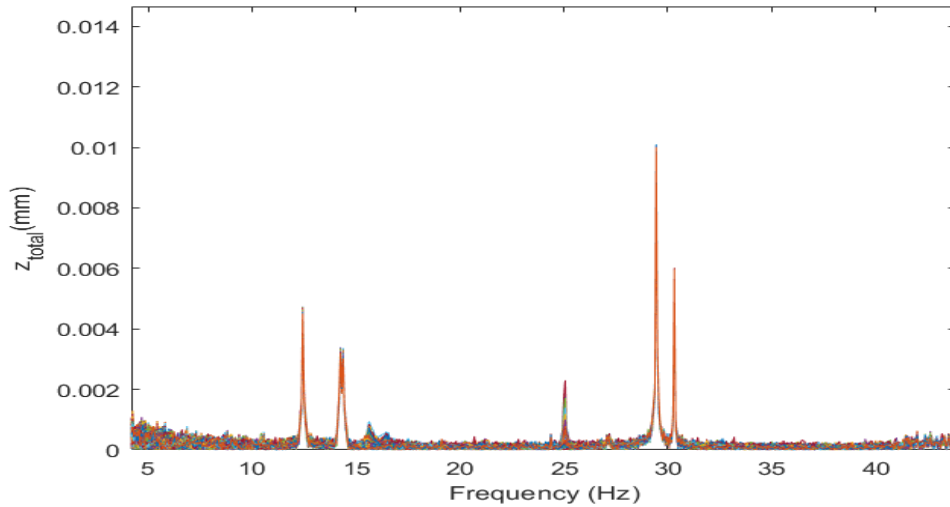


Figure 4.9: Frequency dependency of total vertical displacement.

Calculating the frequency dependency of the vertical responses shows some frequencies are dominated by significant rigid vertical displacement. These frequencies are not resonance frequencies, and do not demonstrate mode shapes when the data are analysed further. From the above behaviour, it is determined these instances present a systematic error of the DIC set up and should be ignored. The DIC software offers the possibility to omit the rigid body motions of the structure, making it easier to evaluate the hydroelastic responses of the model in the wet modal test configuration. The following figures show the results extracted while only the flexible motions are considered.

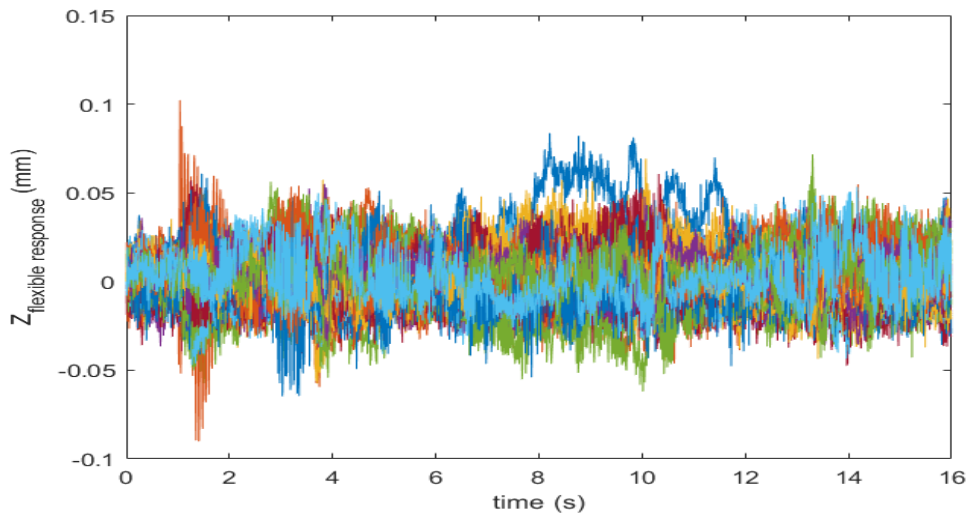


Figure 4.10: Flexible motion z displacement (mm) for hammer impact.

Figure 4.10 shows the vertical displacement of the data points while the rigid body motions is removed, the response amplitudes are significantly lower, while the displacement pattern of each data point follows a different pattern. The data were transferred in the frequency domain to investigate the occurring peaks.

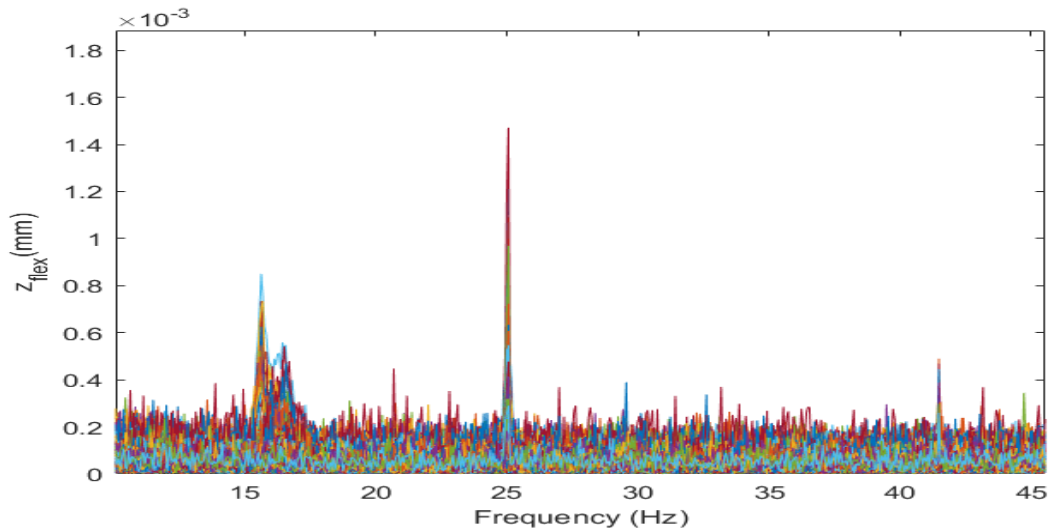
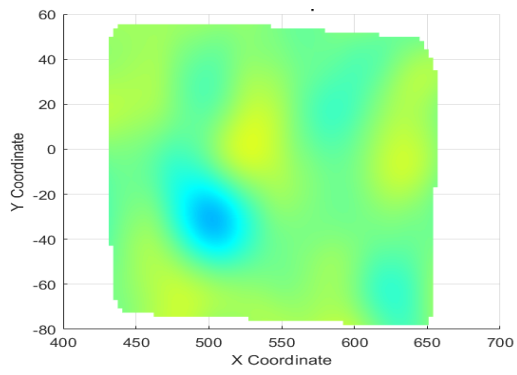
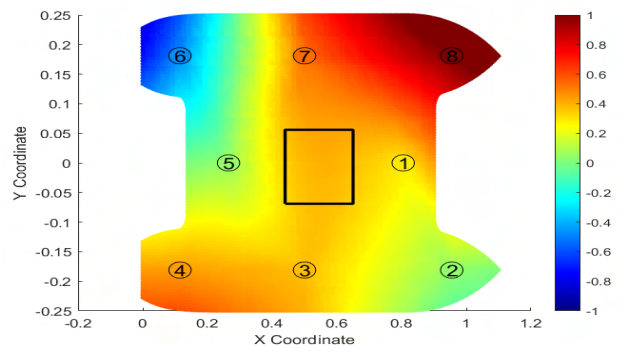


Figure 4.11: Frequency dependency of flexible vertical displacement

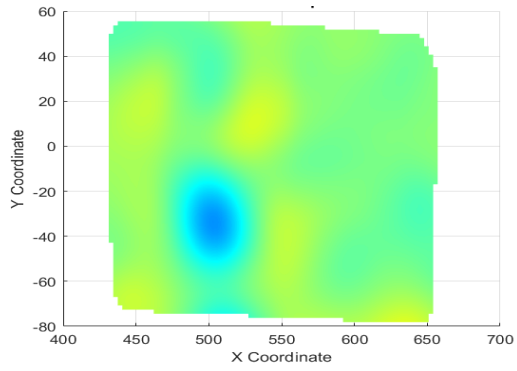
Figure 4.11, shows the frequency domain responses. Peaks are observed for the frequencies 15.55, 16, 25 and 41.5 Hz. More peaks are present as well, but only consist of single point data, meaning they are products of aliasing in a specific point, rather than a total response of the measured surface. The peaks observed from the DIC results demonstrate differences with the accelerometer responses. Most peaks are not clear, while the most pronounced frequency response is found at 25 Hz. This value is not showing significant amplitudes in the FRF calculated from the impact hammer modal tests. Nevertheless, some values appear relatively close to the accelerometer natural frequencies.



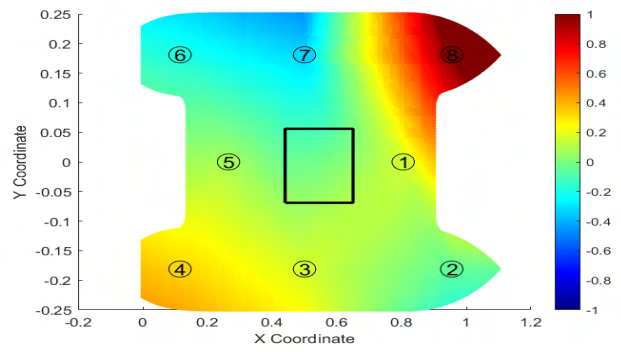
(a) DIC measured shape $f_w = 15.6$ Hz



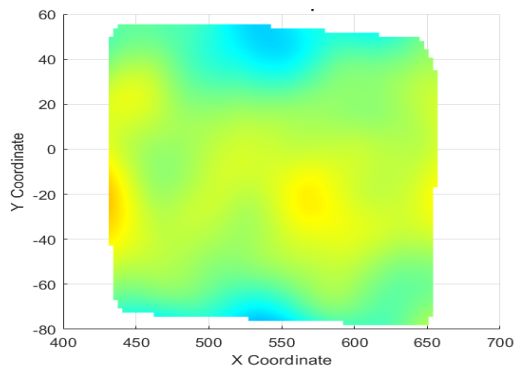
(b) Accelerometer measured shape $f_w = 15.6$ Hz



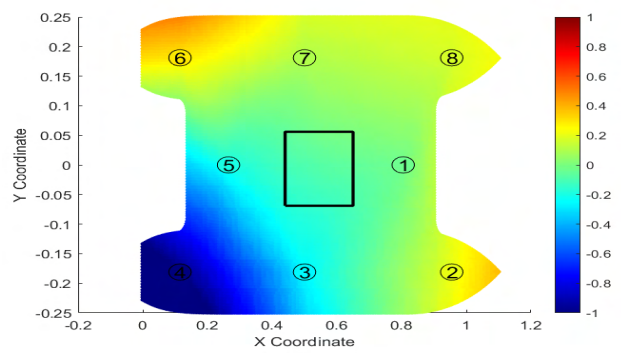
(c) DIC measured shape $f_w = 16.5$ Hz



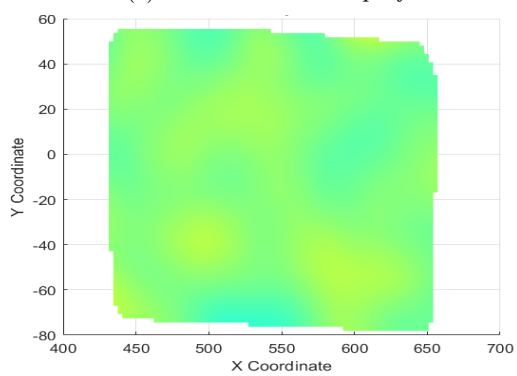
(d) Accelerometer measured shape $f_w = 16.5$ Hz



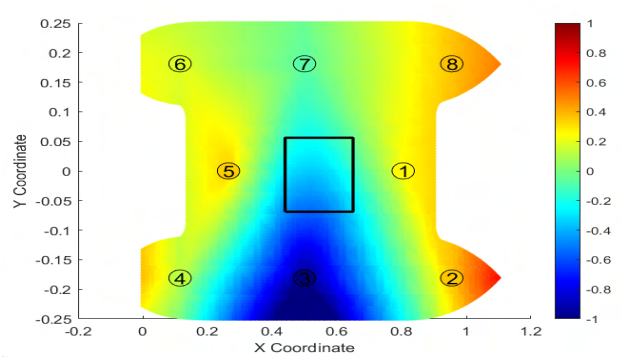
(e) DIC measured shape $f_w = 25$ Hz



(f) Accelerometer measured shape $f_w = 25$ Hz



(g) DIC measured shape $f_w = 41.5$ Hz



(h) Accelerometer measured shape $f_w = 41.5$ Hz

Figure 4.12: Comparison between DIC and Accelerometer measured shapes

Although the field of view of the DIC measurements is limited to a part of the upper deck structure, a distinct mode shape can still be seen for frequency 25 Hz. The figure above 4.12 compares the mode shapes emulated from DIC with the calculated mode shapes. Local variations of the deformation can be seen in the mode shapes. No significant correlation between the DIC and accelerometer measurements can be seen. The local irregularities of the patterns and the limited area captured do not allow for a clear cross reference. Additionally, the first two frequencies examined, are influenced greatly by the sensor cable crossing the speckle pattern, as mentioned earlier. The changes in displacement in those shapes can only be seen in the region of the cable, indicating the cable motion is what triggers the evaluation of significant displacements, not the deck surface. In any case, clear relation between the two approaches is difficult. Although, the measurements from the cameras do not agree well with the expected mode shapes, the findings show that displacement fields can be captured. It is believed, that if a wider field of view was possible and the speckle pattern quality was improved, so would the accuracy of the modal analysis using this measurement system. Additionally, if the measurement area had some common points of measurements with the accelerometers, the comparison would be more substantial. Since the presence of the sensors hinders the evaluation of the camera recordings by the DIC software, such a thing was not possible for the current project. It should be investigated how a wider field of view can be achieved without the two measurement systems interfering with each other.

4.2.2 Conclusions

The modal characteristics of the vessel were investigated experimentally using both acceleration sensors and DIC (Digital Image Correlation) recordings. The acceleration setup employed EMA (Experimental Modal Analysis), while DIC was analyzed using OMA (Operational Modal Analysis). Both configurations faced challenges: mode masking and difficulty performing hammer impacts in the flume tank hindered the clear identification of natural frequencies and mode shapes.

Using multiple analysis tools, natural frequencies and mode shapes were successfully identified for the accelerometer setup. However, the DIC measurements faced issues, primarily due to the limited field of view and the quality of the speckle pattern. While natural frequencies were estimated, some results were ambiguous.

When comparing the experimental findings with numerical estimations, the accelerometer setup showed reasonably good correlation, while the DIC deviated more significantly. Improving the speckle pattern application and expanding the field of view, possibly with different lenses or cameras, would enhance DIC results.

In conclusion, the modal analysis using accelerometers was successful, and closer alignment between accelerometer and DIC measurement points would improve the comparison between the two methods. Better instrumentation configuration and additional measurement points would further enhance the quality of the results. Further work is necessary to ensure the two measurements do not interfere with each other significantly.

Chapter 5

Monochromatic Regular Wave Runs

5.1 Introduction

The model is subjected to regular waves of low amplitude to measure the hydrodynamic responses in the vertical degrees of freedom. A current speed of 0.1 m/s is implemented to reduce the reflection of the waves once they reach the tank beach. The tests have been conducted for a wave frequency range of $2 - 10\text{ rad/s}$. As the experiments progressed, it was observed that the current speed induced vortices in the flow. This caused the model to rotate in yaw and roll motions. The experiments were repeated for additional pretension of the mooring lines to mitigate these rotations.

5.2 Results & Comparison to Numericals

In the graphs below, the results of the two test run configurations are presented together with the computed RAOs presented in an earlier chapter.

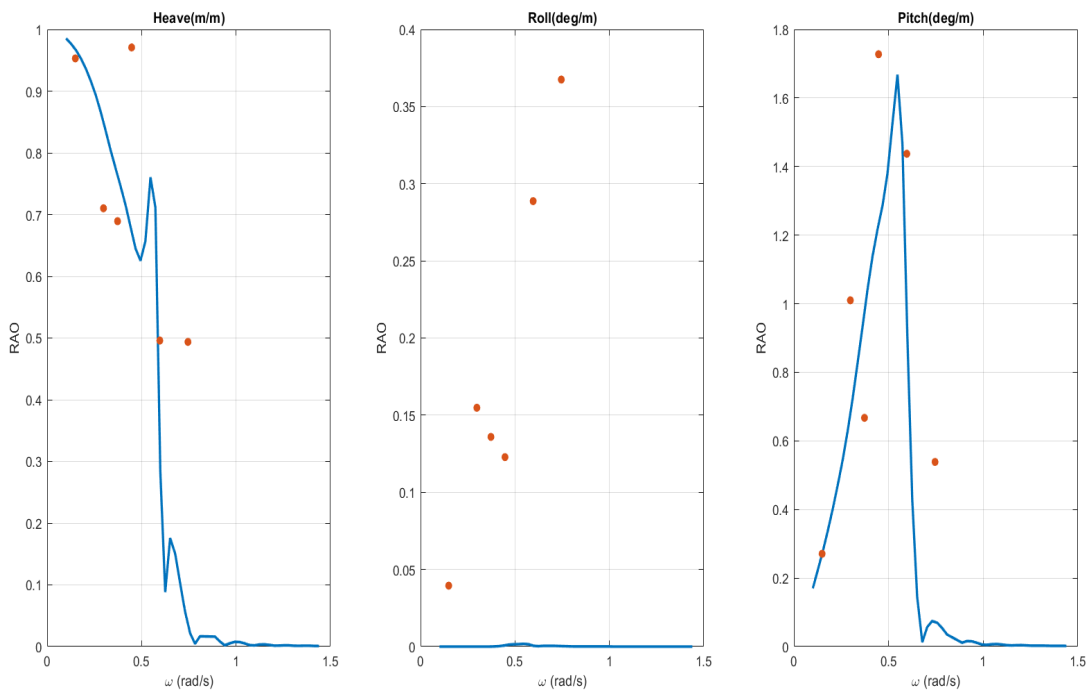


Figure 5.1: R.A.O. measured and compared to AQWA estimation, initial configuration

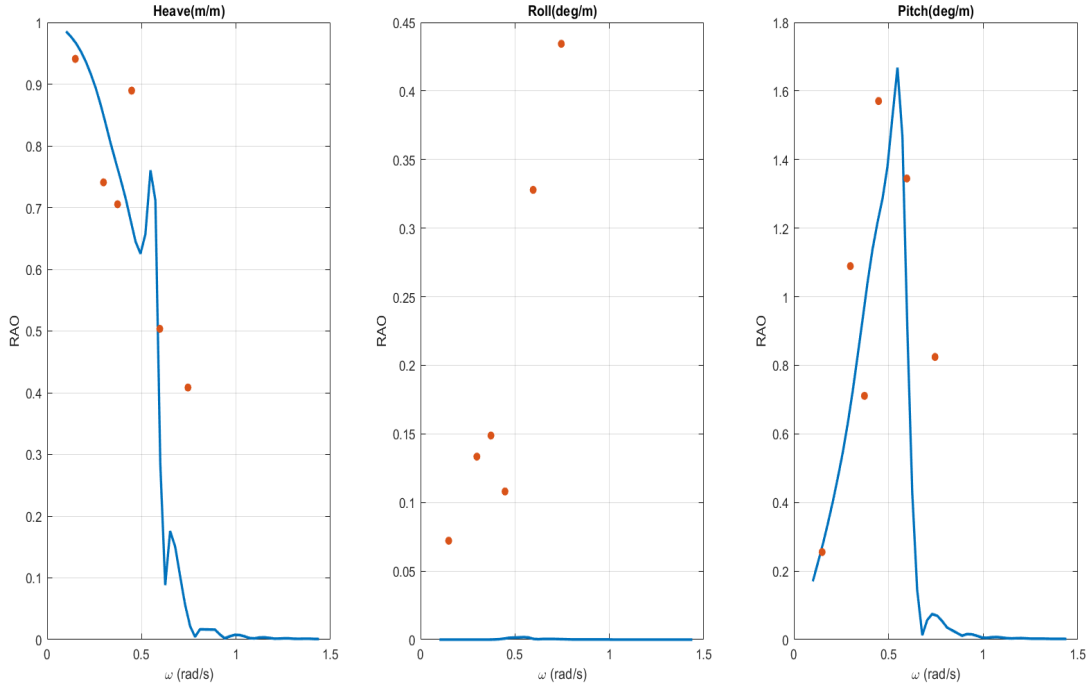


Figure 5.2: R.A.O. measured and compared to AQWA estimation, final configuration

The comparison between the experimentally measured values and the expected numerical calculations show good agreement for the heave and pitch motions. Roll rotation is found to be exponentially higher than the numerical estimation. The additional pretension does not seem to affect the rotation around the longitudinal axis, since the rotation itself remains relatively small. Constraining such a low motion would mean the other vertical degrees of freedom would also be constraint by the mooring lines, which is not a desirable outcome.

Another source that could produce such an irregularity for Roll, could be that the waves generated do not maintain a uniform height throughout the width of the tank. To investigate this possibility, the wave probes were placed in the same vertical distance between the model and the wave generator in different transverse directions. That way the wave profile could be captured.

Indeed, the wave height was not constant along the width of the tank. It is not certain whether this inconsistency captured by the wave probes is the result of the turbulent flow caused by the current or the function of the wave generator itself also contributes to more inconsistencies of the wave profile along its width. Nevertheless, the findings suggest that the discrepancies in the roll motion are products of the facility function and not the model itself.

5.3 Conclusion

The measured RAOs of the vertical motions show good agreement with the numerical estimations for the Heave and Pitch motions. Roll exhibits major differences as high as two orders of magnitude. The incident flow on the vessel is not uniform due to the current speed, the wave height along the width of the tank is also measured and found to be varying. These findings suggest that the differences between the measured and estimated values for Roll are the result of inaccuracies in the flow recreation in the experimental set up.

Chapter 6

Bichromatic Wave Impact Runs

6.1 Introduction

As earlier mentioned, the wet deck wave impacts are investigated using bi-chromatic waves. The utilised waves have varying wave height and frequency, while the current speed simulating the forward speed also takes different values. Eighteen cases are investigated in total. Since the current speed induced non-uniformities in the flow, additional yaw and sway motions were originally observed. To mitigate those effects and limit the change of direction of the attack angle, additional pretension was enforced on the mooring system as mentioned in the previous chapter. The tests were repeated for the additional pretension regime. In this chapter, the measurements from the wave impact test runs are analysed to identify the slamming events. The term slamming will refer to wave impacts while whipping will address the slams that have resulted in some level of flexible response of the model. The acceleration signals carry the information regarding the model responses and will be used to identify whipping events. Two different approaches will be followed to process the signals and identify slamming behavior. The two approaches will be compared and their performance will be evaluated. Conclusions regarding hydroelasticity during wet deck slamming for the present model will be made as a final step. The factors contributing to hydroelastic responses are identified and discussed as well. In the following table, the investigated wave conditions are presented, containing information about the nominal maximum wave height, the frequencies of the two monochromatic wave components that constitute the total bi-chromatic wave signal, as well as the implemented current speed and the presence of additional pretension to the system.

Table 6.1: Test Runs without Added Pretension

Test Run	$H_{max}(m)$	$\omega_1(rad/s)$	$\omega_2(rad/s)$	$u_{cur}(m/s)$	Ad. Pret.	Slamming	Global Whipping
5_38	0.05	4	5	0.1	No	Yes	No
5_39	0.05	4	6	0.1	No	No	No
5_40	0.05	4	7	0.1	No	No	No
5_41	0.05	5	6	0.1	No	Yes	No
5_42	0.06	4	5	0.1	No	Yes	No
5_43	0.06	4	6	0.1	No	Yes	Yes
5_44	0.06	4	7	0.1	No	No	No
5_45	0.06	5	6	0.1	No	Yes	No
5_46	0.07	4	5	0.1	No	Yes	Yes
5_47	0.07	4	6	0.1	No	Yes	Yes
5_48	0.07	4	7	0.1	No	Yes	Yes
5_49	0.07	5	6	0.1	No	Yes	No
5_50	0.04	4	5	0.2	No	No	No
5_51	0.05	4	6	0.2	No	Yes	No
5_52	0.04	5	6	0.2	No		
5_54	0.05	4	5	0.2	No	Yes	No
5_55	0.055	4	6	0.2	No	Yes	No
5_56	0.05	5	6	0.2	No	No	No

Table 6.2: Test Runs with Added Pretension

Test Run	$H_{max}(m)$	$\omega_1(rad/s)$	$\omega_2(rad/s)$	$u_{cur}(m/s)$	Ad. Pret.	Slamming	Global Whipping
5_66	0.05	4	5	0.1	Yes	No	No
5_67	0.05	4	6	0.1	Yes	No	No
5_68	0.05	4	7	0.1	Yes	No	No
5_69	0.05	5	6	0.1	Yes	Yes	No
5_70	0.06	4	5	0.1	Yes	Yes	No
5_71	0.06	4	6	0.1	Yes	Yes	Yes
5_72	0.06	4	7	0.1	Yes		
5_73	0.06	5	6	0.1	Yes	Yes	No
5_74	0.07	4	5	0.1	Yes	Yes	Yes
5_75	0.07	4	6	0.1	Yes	Yes	Yes
5_76	0.07	4	7	0.1	Yes	Yes	Yes
5_77	0.07	5	6	0.1	Yes	Yes	No
5_78	0.04	4	5	0.2	Yes	Yes	No
5_79	0.05	4	6	0.2	Yes	Yes	No
5_80	0.04	5	6	0.2	Yes	No	No
5_81	0.05	4	5	0.2	Yes	Yes	No
5_82	0.055	4	6	0.2	Yes	Yes	No
5_83	0.05	5	6	0.2	Yes	No	No

6.2 Slamming Identification

To identify slamming events many different approaches have been followed. The different methodologies can be categorised into two general approaches. The first relates the slamming events with the kinematics of the vessel at the section of impact [15],[16]. The second category relates slamming to the consequent induced responses [3],[17].

The kinematic criterion method, known as the Ochi criterion has been the most wide spread method regarding slamming occurrence. The approach is easy to use in the design phase but is met with certain challenges when applied in an experimental set up. The measurement of the relative motion and velocity at each section of interest is not always known. Additionally, the assumption of the free surface elevation not being affected by the vessel radiation potential adds to the level of complexity for the experimental measurements. In the current set up specifically, the interaction between the model side-hulls increases the uncertainty of the free surface elevation below the wet deck surface. The measurement set up for the wave elevation can not collect data between the model side-hulls, as such the direct measurement of the relative motion and velocity at each section of interest is not possible. The kinematic criterion has also met opposition regarding the way slamming events are treated as independent to each other, while recent studies have debunked that assumption.

The response based criteria have been established in recent years and rely on the loading and acceleration hull measurements. Dessi uses continuous wavelet transform to distinguish the high frequency component of the moment, which is treated as an indicator of whipping. Dessi also proposes an alternative to continuous wavelet transform by applying Hilbert transform. In a more recent work, Alsalah used the acceleration signals of a fast catamaran hull, decomposed it into different intrinsic mode functions and determined the component of the total signal representing the response due to global flexible response. The difference between the two methods comes to the way the high component signal is sorted from the total measurement. Dessi, uses filtering techniques while Alsalah uses decomposition. Both approaches are used on the measured signals. The acceleration signals will be used for both approaches while Hilbert transform and the instantaneous energy quantity will be used for the identification of slamming events.

The analysis of the measured signals has shown that hydroelastic responses are significant for the test runs with maximum nominal wave height of 7 cm. Added pretension runs show higher hydroelastic responses. The results for the slamming identification process are presented in the following pages, with comparison of the findings of exact method. The criterion established by Dessi will be referred to as the whipping criterion, while the criterion established by Alsalah will be referred to as EMD (Empirical Mode Decomposition).

6.2.1 Threshold values for slamming identification

The response based criteria require the slamming related measured values to be equal or greater than a set threshold value. The said threshold is chosen by the user and differs for each case study. In the present work it is determined that the IE of global responses is used to determine slamming. Slamming identification analysis showed that slams generally yield IE greater than 0.1 (m/s^2)². To automate the identification process for long test runs, the criteria used specify that each slamming event needs to yield $IE \geq 0.1$ and needs to have occurred at least 0.5 seconds (about half the pitch period) after the previous slam. That is to separate each event.

In order for the global responses to be accounted for, the local ones need to be also estimated. In the modal analysis of the model, it is seen that the natural frequencies are covering a frequency range of 18-40 Hz. Lower frequencies are also found that are too high to correspond to wave excitation, while there are also higher frequencies that could correspond to natural frequencies higher than the first four global ones that have been examined. A modal analysis is conducted for the various plates on the deck of the model. The boundary conditions are chosen as clamped-clamped, 5 different plates are examined and the first natural frequency of each plate is calculated to determine the threshold between global and local responses. The results are shown below:

Table 6.3: First mode frequencies of the model deck plates (clamped-clamped)

Plate	X(mm)	Y(mm)	$f_1(Hz)$
1	66.7	37.5	52.58
2	33.4	48.6	71.71
3	49.4	48.6	43.2
4	50	48.6	42
5	50	37.5	59.5

The identification criteria used, focus on wet deck slamming, as such the readings of sensor 1 are used. Plate of type 1 are in the proximity of sensor 1, meaning that the readings up to 52 Hz should correspond to global responses. The identification criteria, use the frequency range of 10-50 Hz to identify global whipping responses, other frequency ranges are chosen for following analyses, when all sensors are investigated for slamming, more strict frequency limits are used such as 10-45 Hz and 10-41 Hz. Slight modification occur at times to ensure smooth analysis, for example, in EMD the threshold used starts at 10.5 Hz to tackle an abnormal IMF behaviour in one case.

6.2.2 Empirical Mode Decomposition

The acceleration signal is decomposed to eleven distinct intrinsic mode functions (IMF) using empirical mode decomposition (EMD). The spectral energy of each IMF is computed. The IMFs are categorised based on their frequency content. If 80% of the spectral energy is below 10.5 Hz, the IMF is considered to represent quasi-static and hydrodynamic responses. If 20% of the spectral energy is above 50 Hz, the IMF is considered to represent noise and wave impacts. The IMFs that fall between those thresholds are treated as a global whipping responses due to slamming. The signal is reconstructed based on the three categories mentioned. Hilbert transform is applied on the global response signal and the instantaneous energy is calculated. The numbering of the IMFs corresponds to their frequency content, with the first IMF corresponding to the highest frequency content, while the last IMF is related tot he lowest frequency content.

The thresholds used attempts to provide the best representation of the global flexible responses. By inspecting the CSD of each case it is concluded that the thresholds set above are separating the responses as best as possible.

6.2.3 Whipping Criterion

The application of the criterion will take advantage of prior knowledge of the global response wet natural frequencies. A band-pass Butterworth filter is applied resulting in a signal of frequency range 10-50 Hz. Hilbert transform is then applied to the filtered signal. The instantaneous energy is calculated and the slamming occurrences are identified for peaks greater than 0.1 that occur for a time interval greater than 0.5 seconds between each other. The same peak identification criterion is used for EMD

6.2.4 Slamming identification results for run 5_74

EMD Run 5_74

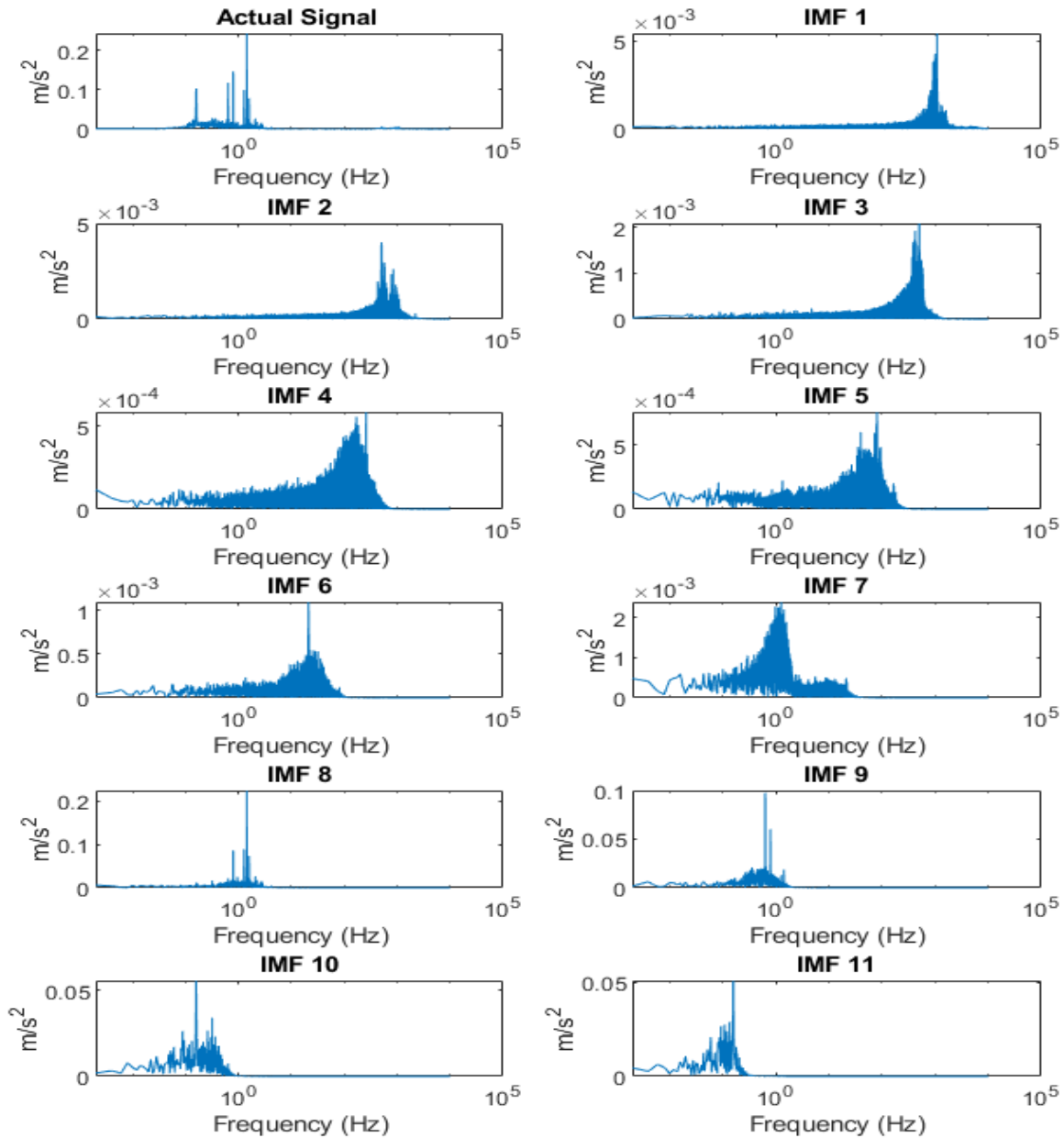


Figure 6.1: Intrinsic Mode Functions in frequency domain run of 5_74

Figure 6.1 shows the IMFs that are produced from EMD, the first IMF corresponds to noise of the signal, while the higher the IMF number, the lower the frequency range. The magnitudes of the IMFs in the frequency domain are normalised by the signal length. Below, the time domain IMFs are presented.

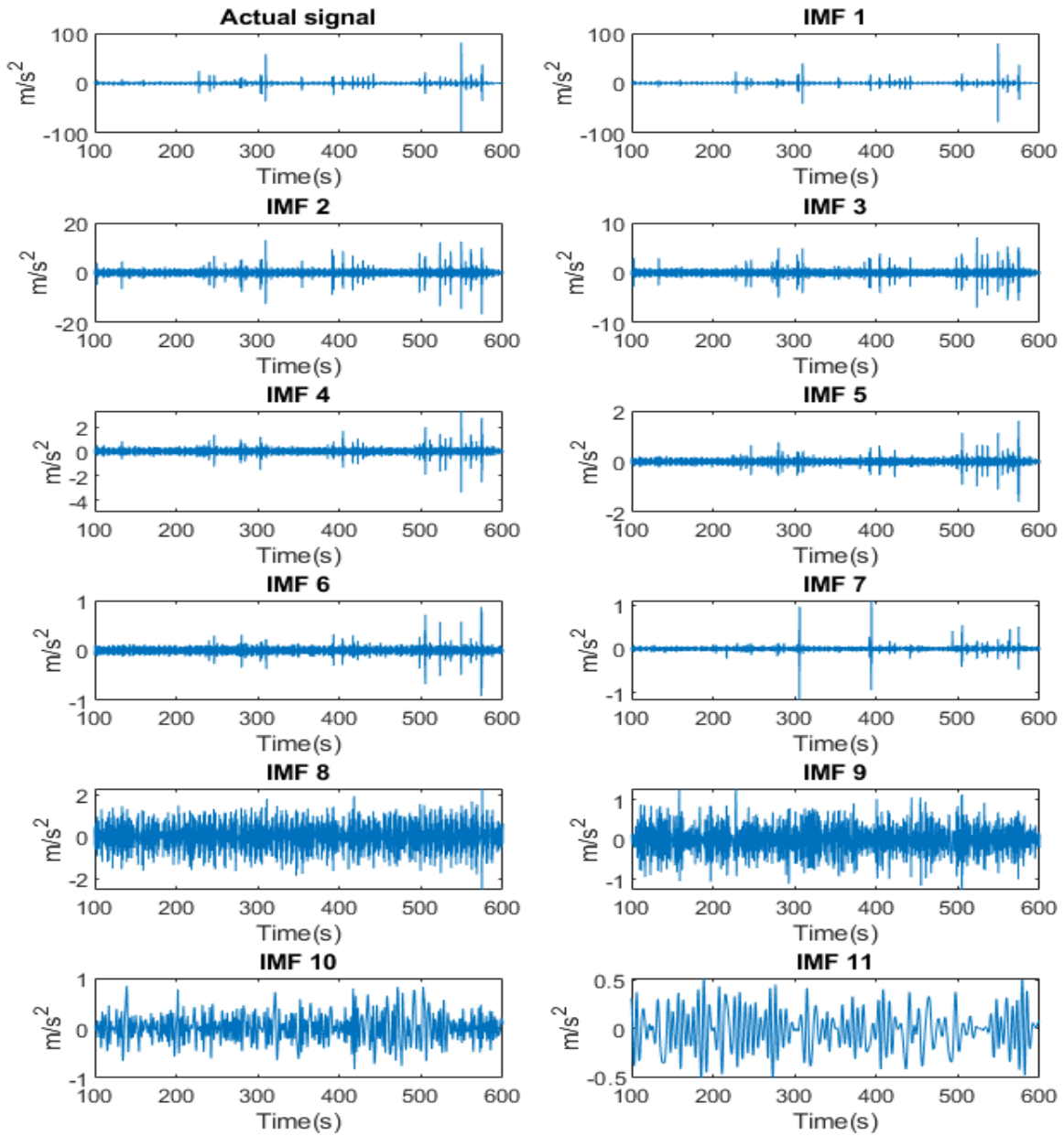
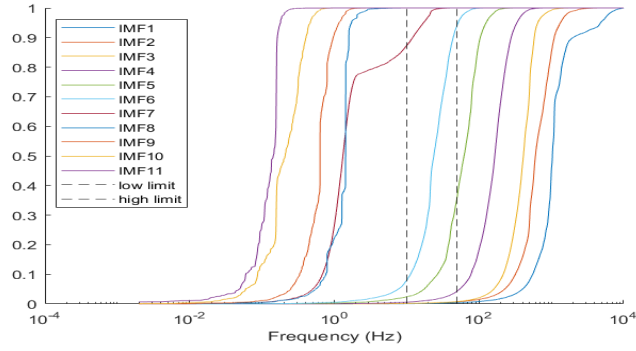
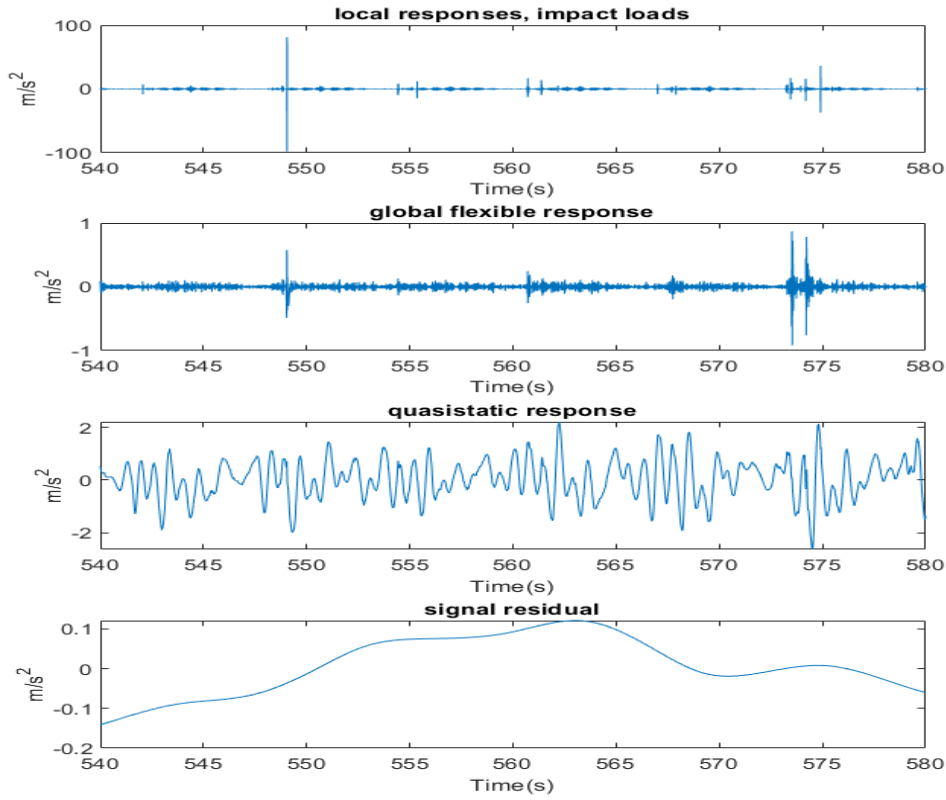


Figure 6.2: Intrinsic Mode Functions in time domain run of 5_74

Figure 6.2, shows a different representation of the IMFs, in a way that the signal can be interpreted more clearly. IMF 1 is stated to mostly show noise from the previous figure. The acceleration signal has a lot of noise, causing the peaks of the signal to have overestimated values. The IMFs for the rest of the test runs can be found in the appendix.



(a) CSD signal run of 5_74



(b) Reconstructed signal of run 5_74

Figure 6.3: EMD process for reconstruction of signal for run 5_74

The CSD shows clear separation between the high IMFs that tend to represent the hydrodynamic and quasi-static responses while the lower IMFs show closer proximity. The seventh IMF experiences a spike in frequency content, but still does not surpass the lower threshold set and is not included in the global flexible responses. The criterion used for the CSD threshold value defines the sixth IMF as the one representing the global flexible responses. Figure 6.3b shows the reconstructed signal and the residual of the initial signal that was lost during the EMD process.

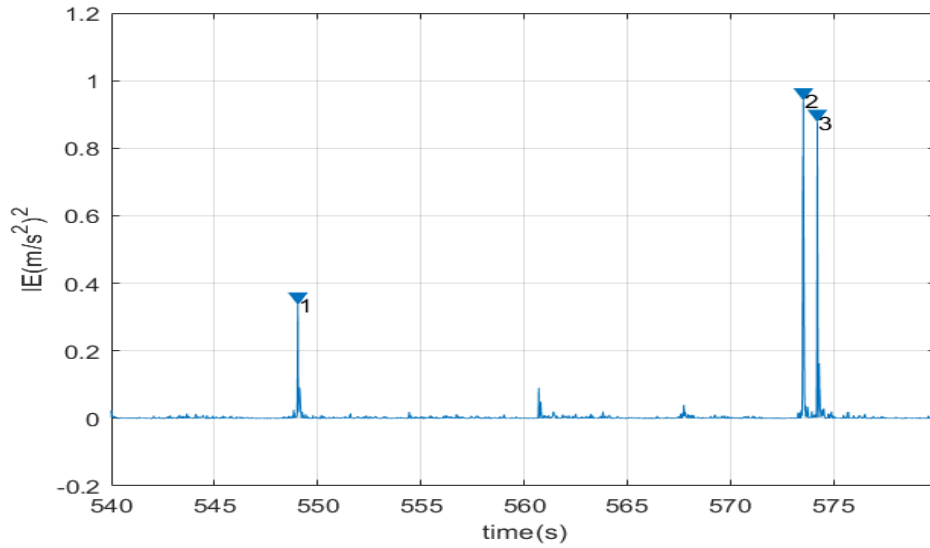


Figure 6.4: Slamming events identified by the EMD of run 5_74

Whipping Criterion Run 5_74

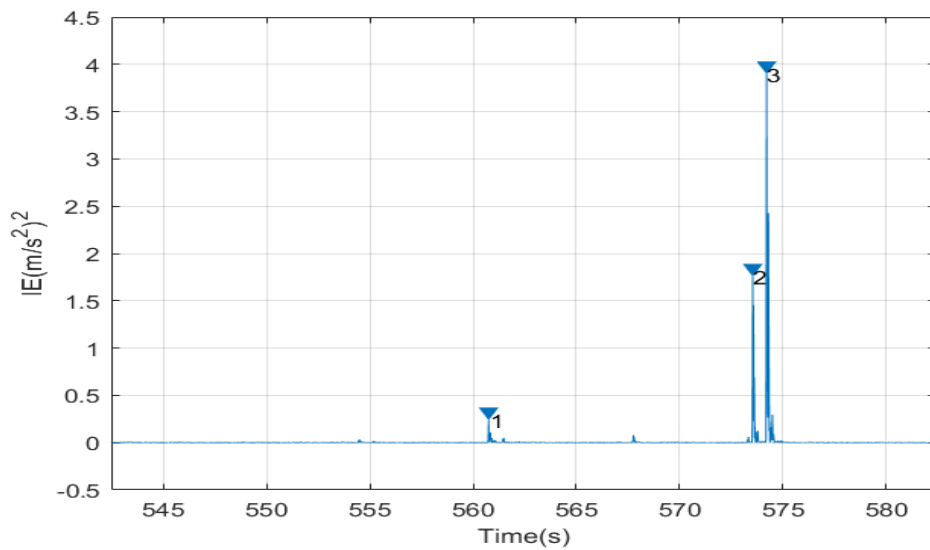
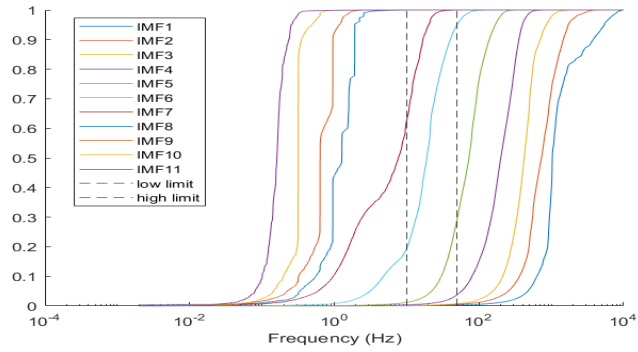


Figure 6.5: Slamming events identified by the whipping criterion of run 5_74

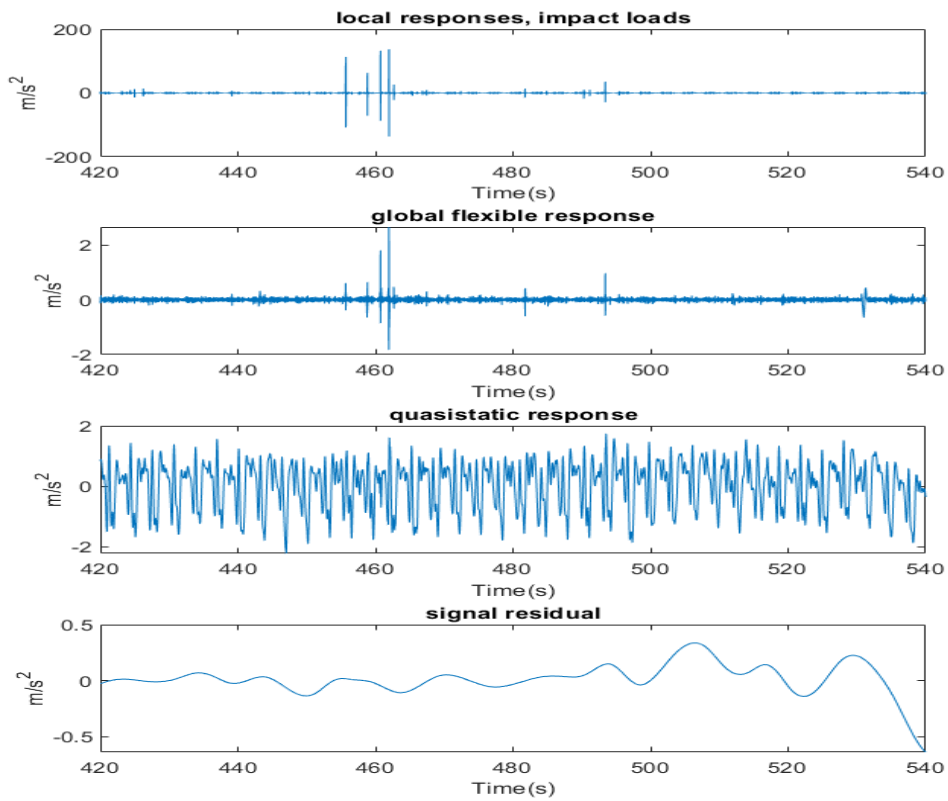
Whipping criterion identifies 3 slamming events, resulting in whipping. It is seen that the approach presents similarities with the EMD identification method. While some points of agreement can be seen in two identified events, it also becomes apparent that the two approaches read different quantities as relevant to slamming. The frequency ranges considered vary, resulting in different identification of the first slamming occurrence, while all identified slams contain different IE magnitudes.

6.2.5 Slamming identification results for run 5_75

EMD Run 5_75



(a) CSD signal run of 5_75



(b) EMD process for reconstruction of signal for run 5_75

Figure 6.6: Reconstruction of signal of run 5_75

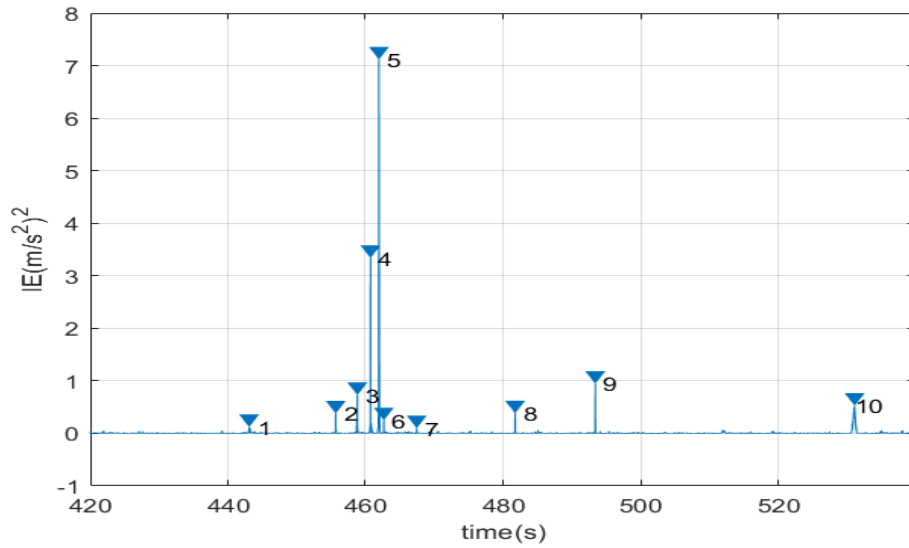


Figure 6.7: Slamming events identified by the EMD of run 5_75

Whipping Criterion Run 5_75

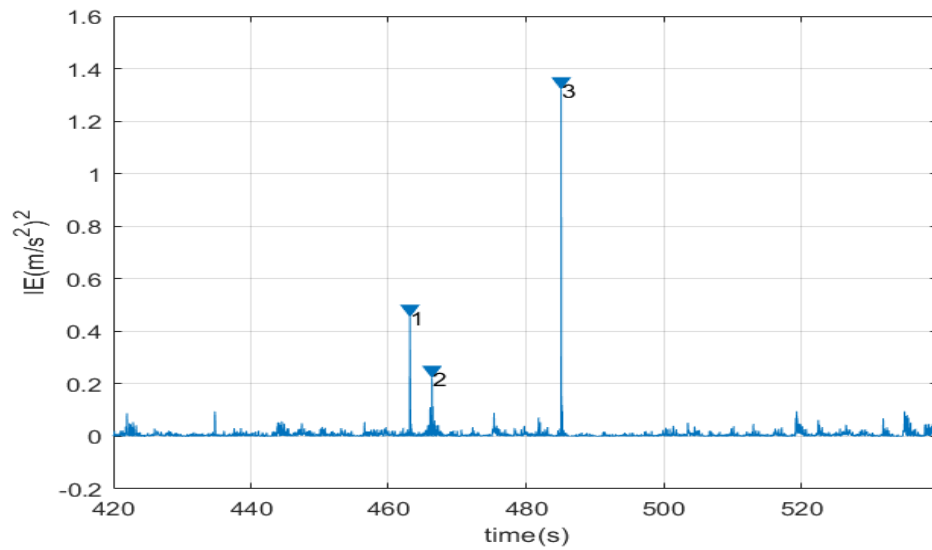
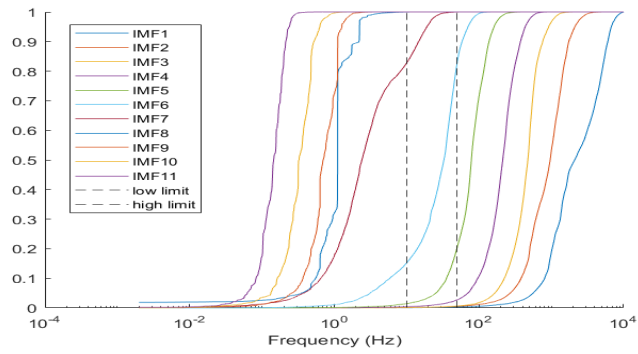


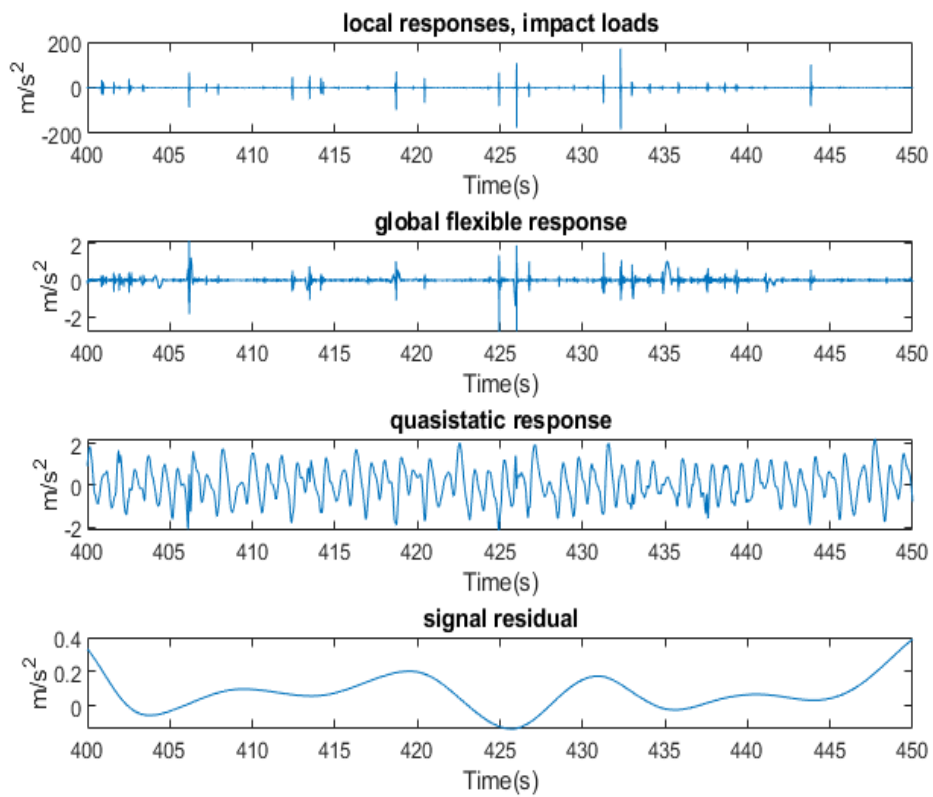
Figure 6.8: Slamming events identified by the whipping criterion of run 5_75

6.2.6 Slamming identification results for run 5_76

EMD Run 5_76



(a) CSD signal run of 5_76



(b) Reconstructed signal of run 5_76

Figure 6.9: EMD process for reconstruction of signal for run 5_76

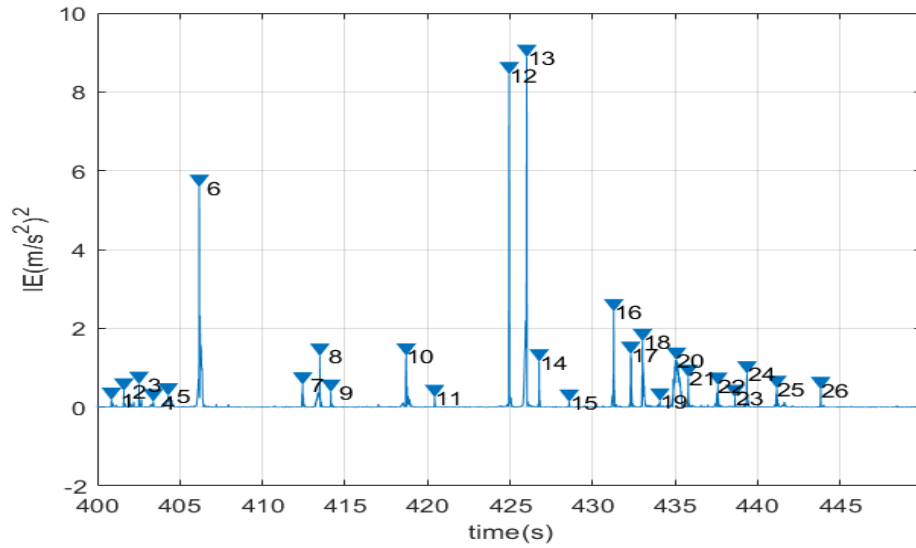


Figure 6.10: Slamming events identified by the EMD of run 5_76

Whipping Criterion Run 5_76

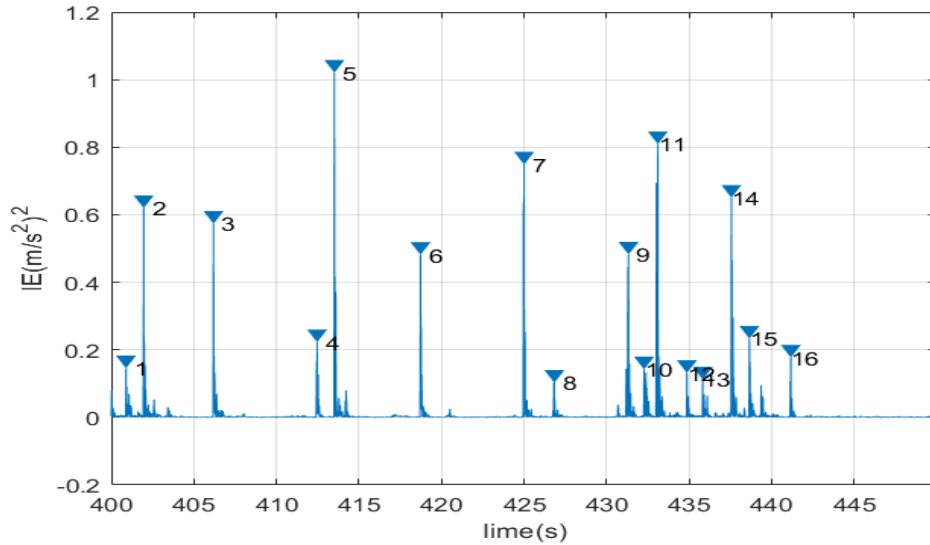
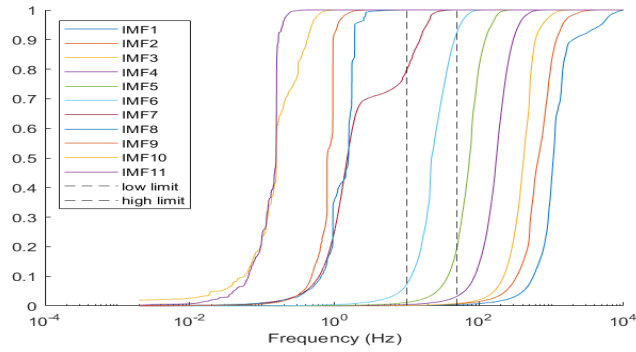


Figure 6.11: Slamming events identified by the whipping criterion of run 5_76

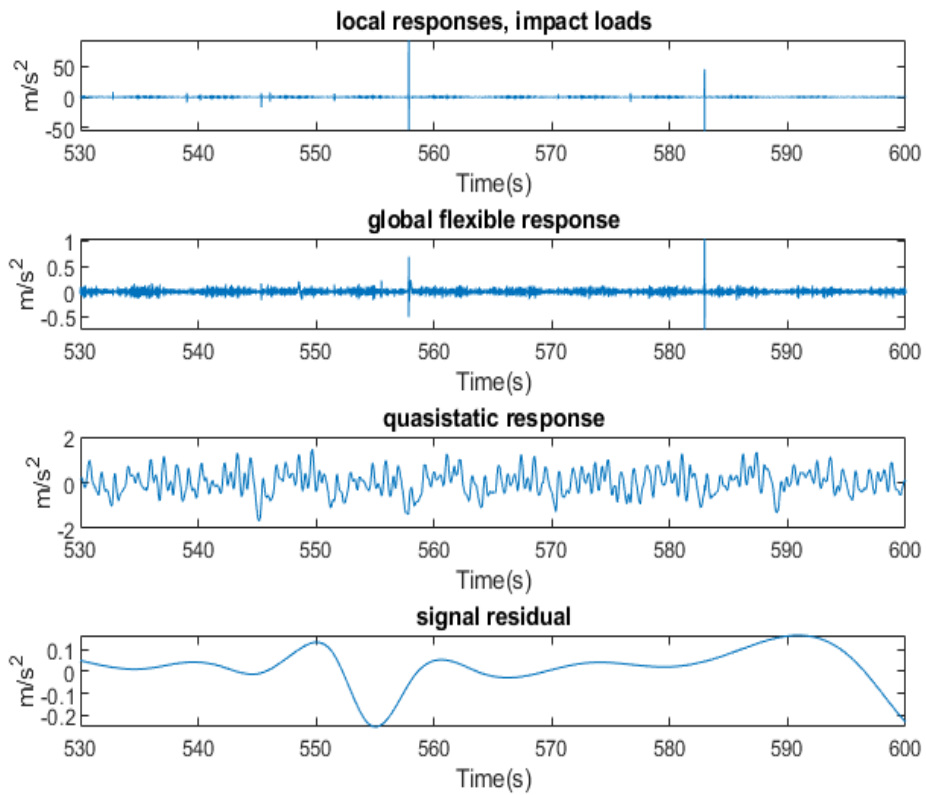
The whipping criterion has identified 60 events, with occurrences 1,25,31 and 36 having substantial instantaneous energy values. This test run is characterised by the most intense hydroelastic responses, the number of identified events is far higher than the rest of the test runs.

6.2.7 Slamming identification results for run 5_77

EMD Run5_77



(a) CSD signal run of 5_77



(b) Reconstructed signal of run 5_77

Figure 6.12: EMD process for reconstruction of signal for run 5_77

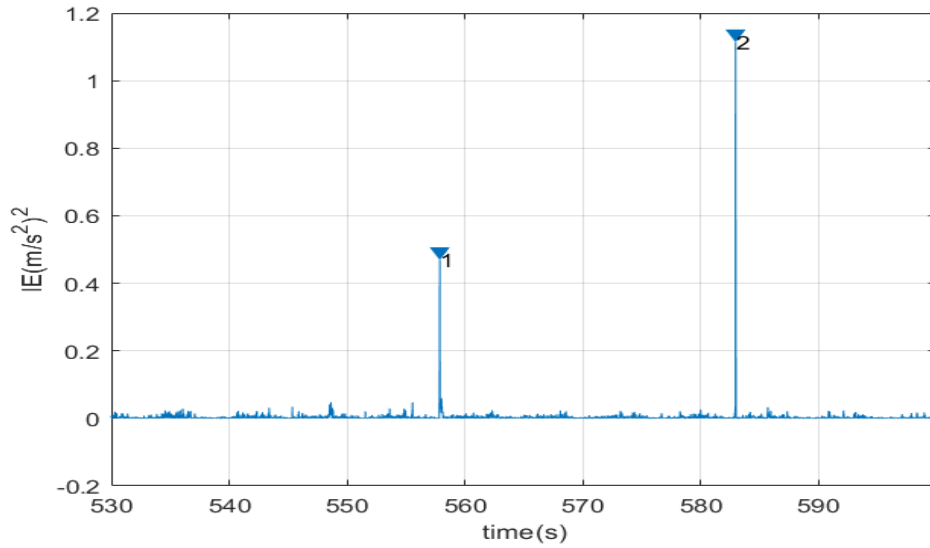


Figure 6.13: Slamming events identified by the EMD of run 5_77

The EMD identified four slamming events, the magnitude of the values is relatively low for most cases. Nevertheless, the values do surpass the threshold value of $0.1 (m/s^2)^2$.

Whipping Criterion Run 5_77

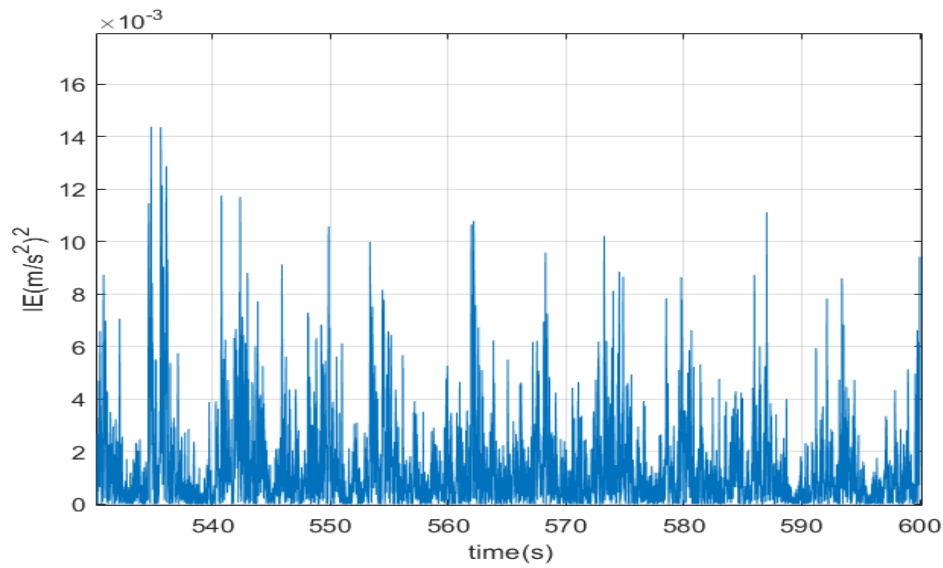


Figure 6.14: Slamming events identified by the whipping criterion (run 5_77)

The whipping criterion has not identified slamming events for this test run. The instantaneous energy for the band-pass filtered signal maintains values much lower than the threshold value of $0.1 (m/s^2)^2$.

6.2.8 Comparison between whipping criterion and EMD

Differences between the two applied criteria can be found in the various test runs. For run 5_74, EMD identifies more events with the instantaneous energy amplitude being steadily lower than the amplitude of the identified events using the whipping criterion ???. In test run 5_75, EMD identifies more events???. The instantaneous energy amplitude remained similar between the two methods, with the exception of some events identified by EMD after time 450 seconds. Run 5_76 exhibited the most identified events for both methods, once again EMD traced more slams???. Most occurrences had similar instantaneous energy amplitudes, while again some EMD occurrences had overestimated energy amplitudes compared to those of the whipping criterion. Finally, run 5_77 identified no slams with the whipping criterion, while EMD found a few events of low energy.

It becomes evident that the two criteria present differences with respect to the estimation of the number of slams occurred. The whipping criterion only considers the responses within the defined filter band pass, containing all the global flexible frequencies. EMD on the other hand defines the global flexible response based on the IMFs that fulfill the CSD threshold requirements. It is seen by the CSD figures 6.3a,6.6a,6.9a,6.12a that the IMFs used for the reconstructed global signal also contain local frequencies. At the same time, IMFs that do are not used in the reconstructed global signal contain some of the global flexible frequencies that are accounted for by the whipping criterion.

Considering the above it is clear that EMD is more inclusive of higher frequencies and can therefore identify more events, which however do not necessarily correspond to global flexible responses, or at least not as significantly as implied by the method. Defining the IMFs in a way that would only consider the desired 10-50 Hz bandwidth is not easy.

In any case, the current project has only considered the first four global deformation modes. The local responses have been calculated to be close to the global flexible responses bandwidth as the first local plate response frequency near the sensor used for the identification is found to be 52 Hz. It is therefore, hard to completely separate the global from the local responses. Both methods seem to yield, realistic results, with the whipping criterion being a bit more relevant for the current project application, as it separates the responses of interest more clearly.

6.3 Analysis in the time domain

The events where global hydroelastic response is induced have been identified using two response based criteria. It is now time to investigate the slamming behaviour in individual events. The analysis that follows is based on the time domain. Emphasis is given to significant slams with hydroelastic responses, the acceleration signals from different sensors are used. The acceleration responses are presented for all the available sensors, a low pass filter is applied to omit frequencies higher than 800 Hz. The signals are decomposed using CWT to discern the contributing frequencies. CWT is applied in time intervals where the whipping criterion has identified the most severe global whipping. The model dynamic response is also estimated by calculating the operating deflection shapes (ODS) resulting from the wave impacts.

6.3.1 Green Water

Before studying the slamming and whipping recorded during the test runs, it is also important to address other noteworthy phenomena that happened during testing. It was observed that waves with frequency components 4&7 rad/s and height of 7 cm induce green water, namely runs 5_48 and 5_76. Green water appears in both test runs with these wave conditions. For 5_48, where the attack angle changes more drastically, green water is more severe, while the hydroelastic responses are less severe compared to run 5_76. The following images show the water at the side hulls for the two distinct test runs.



(a) Green water at run 5_48



(b) Green water at run 5_76

Figure 6.15: Side by side comparison of green water runs

Aside for these two test runs there was no other occurrence of green water. It was also observed that more water accumulated in the starboard side-hull. The distinct difference of the effects of green water is seen after a number of slams has occurred and the motions of the model are built up.

The two test runs were both cut shorter than 10 minutes, the normal duration of tests. The presence of water on the top deck was not accounted for during the design of the instrumentation. As such, the test runs were terminated after excessive water had gathered at the top of the model.

6.3.2 Run 5_74

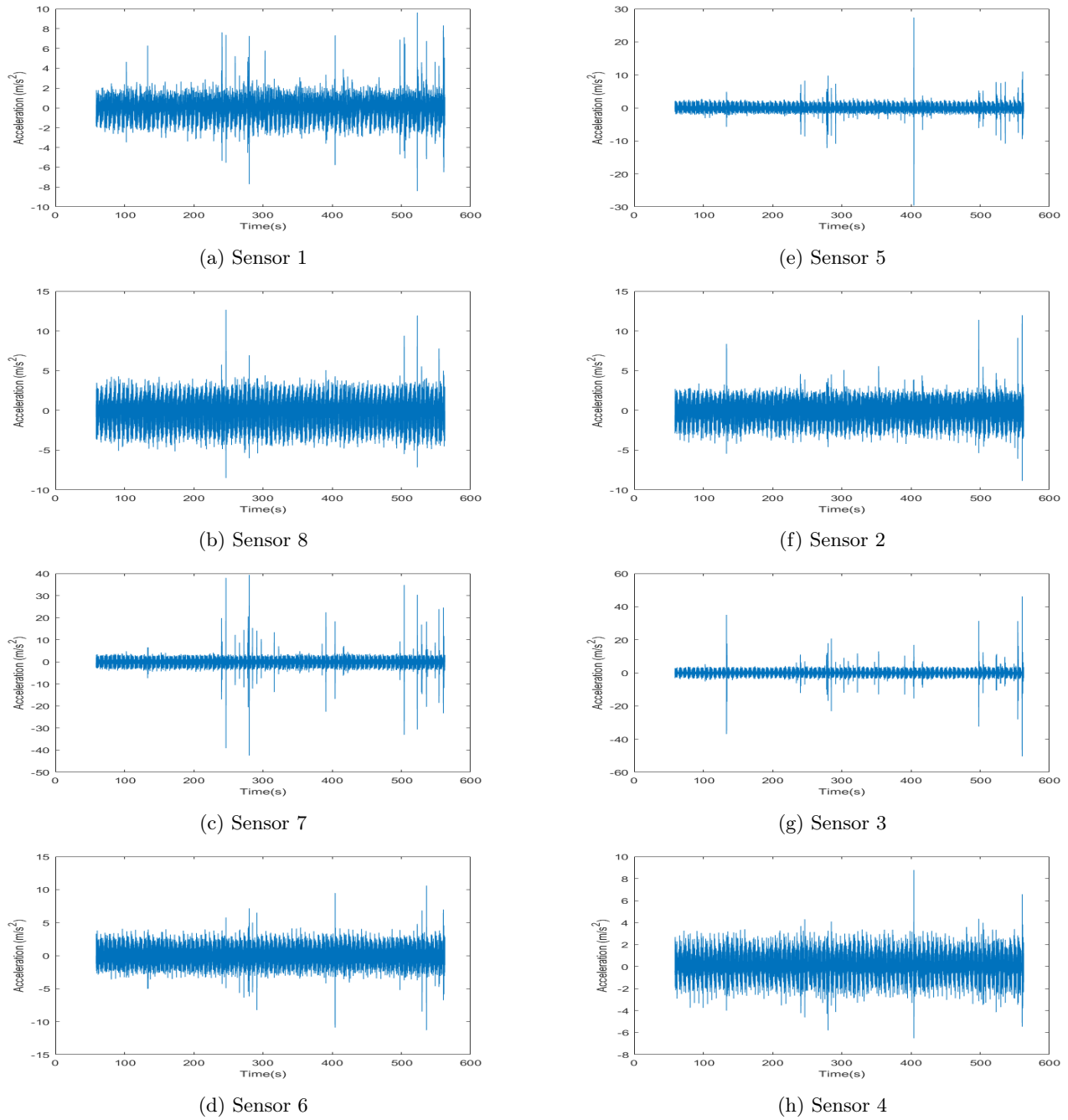
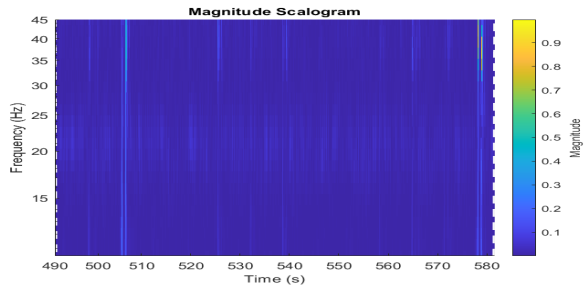
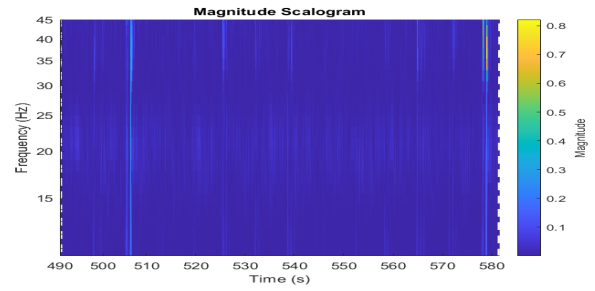


Figure 6.16: Acceleration recordings of run 5_74.

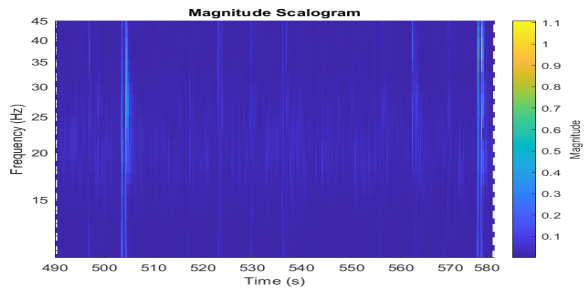
Run 5_74 does not experience many global slams, sensors 3 and 7 demonstrate the highest impulses which are not occurring with the same amplitudes simultaneously, midhull. Wet deck slams appear to occur mostly on the aft of the deck, as sensor 56.16e presents higher impulse amplitudes.



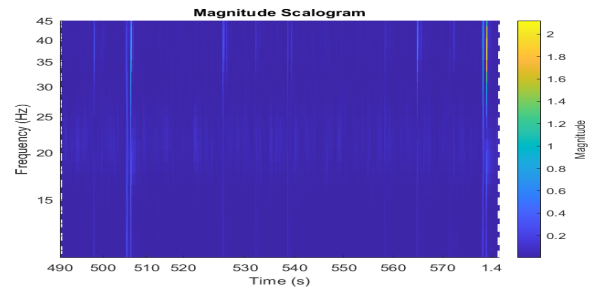
(a) Sensor 1



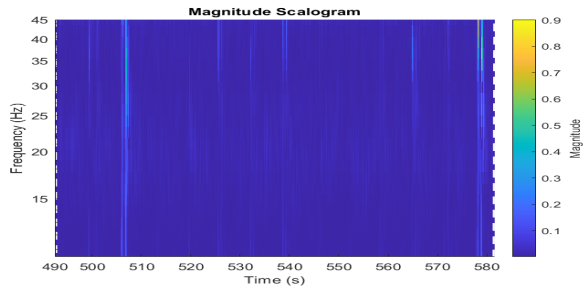
(e) Sensor 5



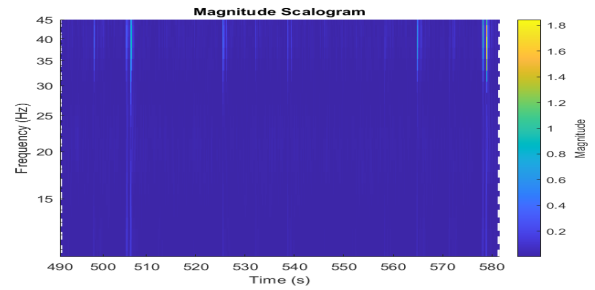
(b) Sensor 8



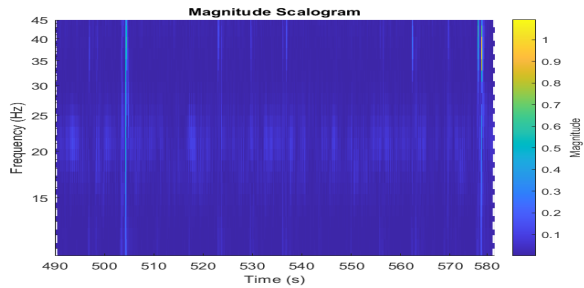
(f) Sensor 2



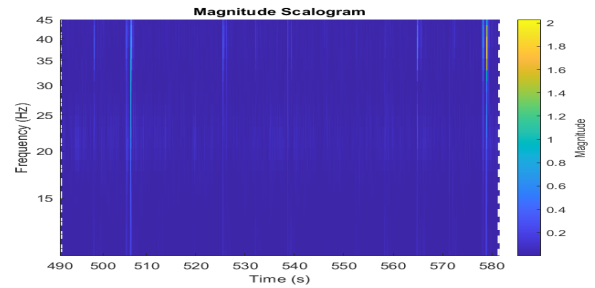
(c) Sensor 7



(g) Sensor 3



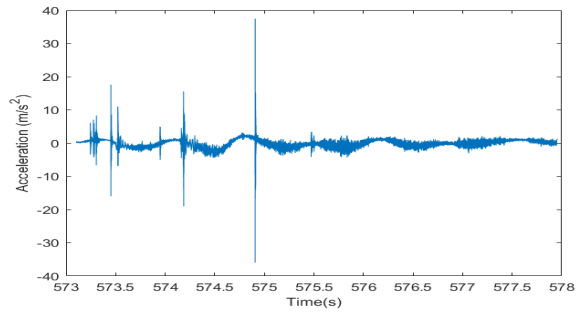
(d) Sensor 6



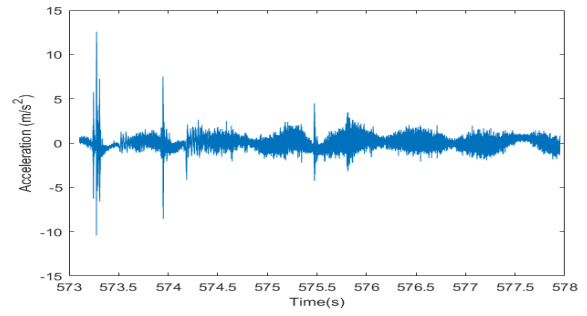
(h) Sensor 4

Figure 6.17: Scalogram of run 5_74.

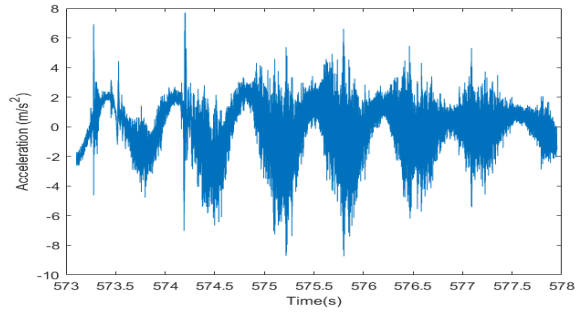
The cwt scalograms show that the slams between 500-510 s and 570-580 s correspond to significant flexible response frequency content. These time intervals correspond to dense slamming occurrences. It is evaluated that the slamming between 570-580 seconds has higher flexible frequency components. The time interval is further analysed.



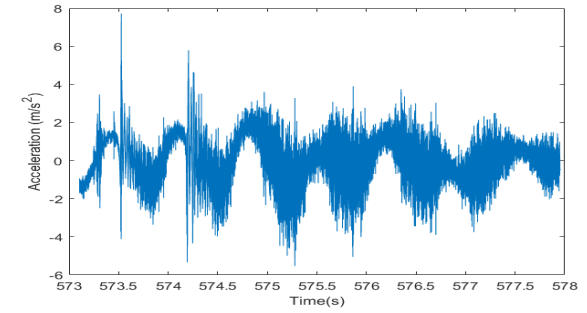
(a) Sensor 1



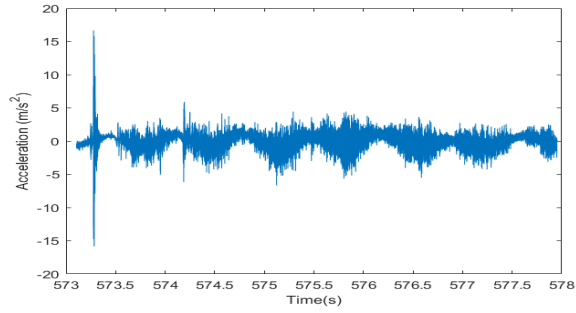
(e) Sensor 5



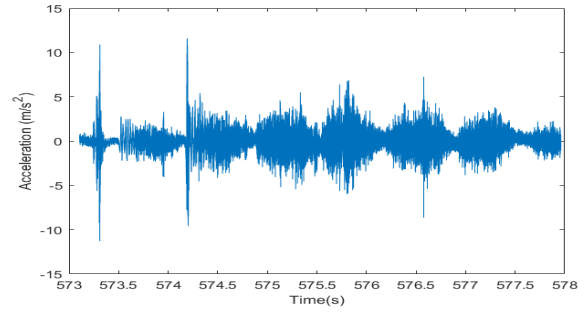
(b) Sensor 8



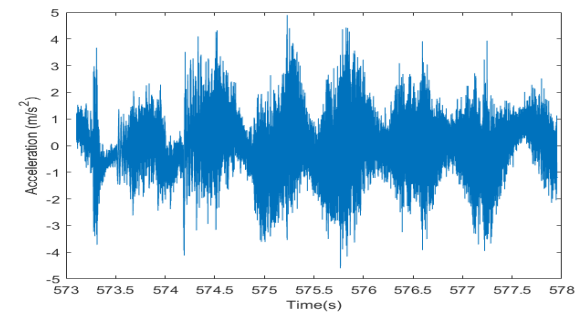
(f) Sensor 2



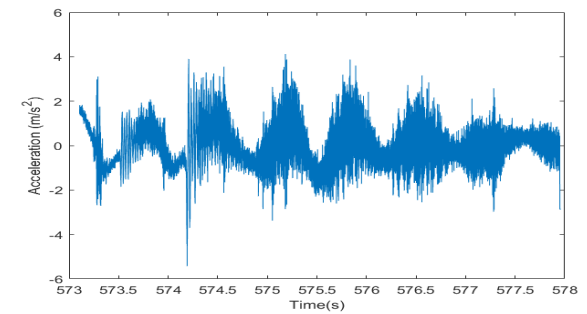
(c) Sensor 7



(g) Sensor 3



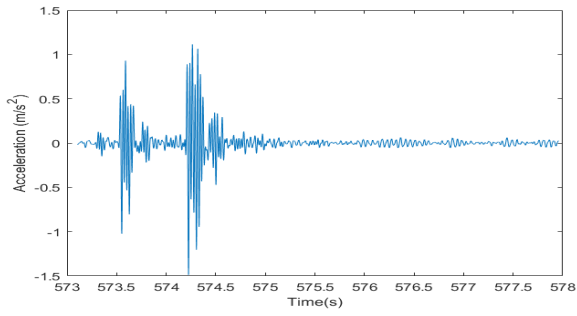
(d) Sensor 6



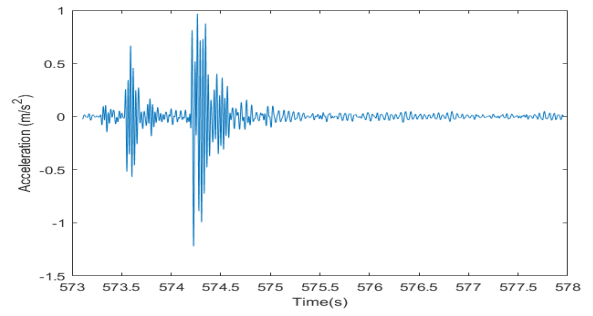
(h) Sensor 4

Figure 6.18: Zoomed in responses of slamming

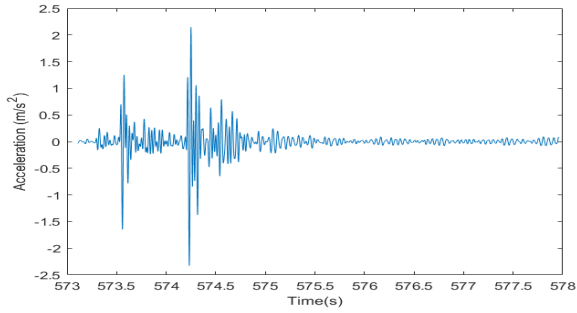
Sensors 1 and 5 capture slamming clusters at the beginning of the recorded signal 6.18a, 6.18e. The two sensors capture approximately the same magnitude of slams, indicating they occur in the middle of the deck, the slams recorded later show a tendency for the slams to occur closer to sensor 1. Band pass filtering of 10-41 Hz is applied to the signals to investigate the hydroelastic responses. The results are shown in 6.19.



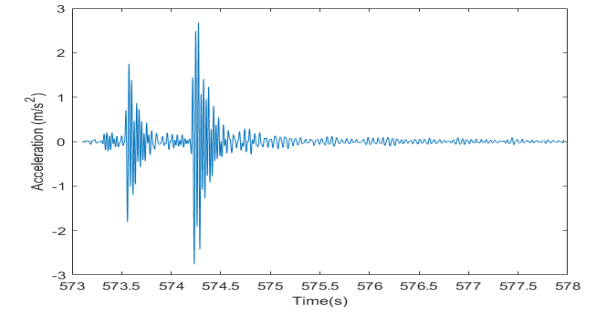
(a) Sensor 1



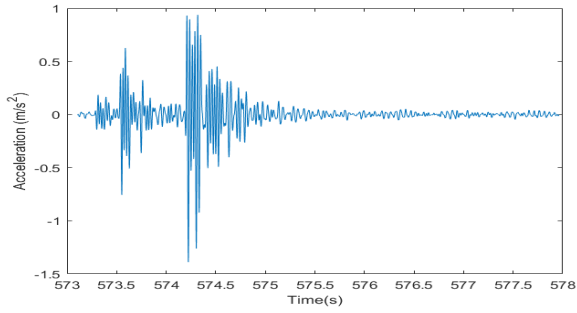
(e) Sensor 5



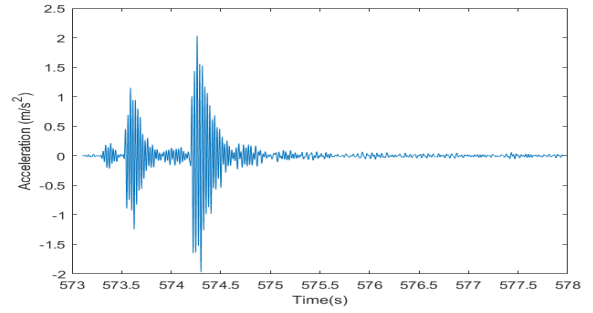
(b) Sensor 8



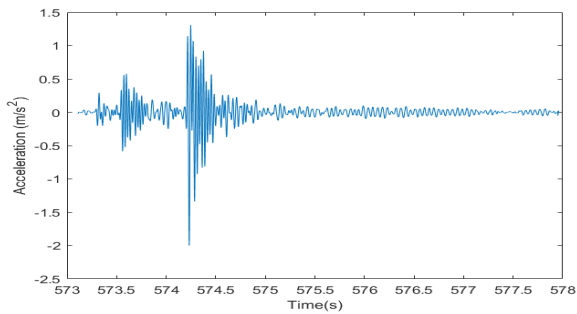
(f) Sensor 2



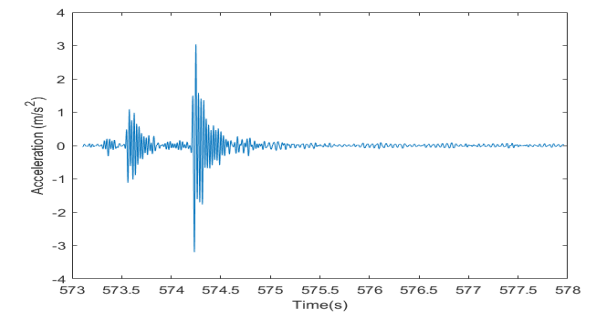
(c) Sensor 7



(g) Sensor 3



(d) Sensor 6



(h) Sensor 4

Figure 6.19: Zoomed in hydroelastic responses of slamming

The responses show a standard impact pattern, where the response amplitude changes abruptly, followed by a quasi-exponential decay of the response. Three distinct hydroelastic responses are captured. It is worth noting that the new responses are initiated before the previous ones have completely died out. The oscillation patterns differ slightly depending for each side hull. Starboard hull 6.19f,6.19g & 6.19h, exhibits higher responses and smoother oscillation pattern compared to the portside hull 6.19d,6.19c & 6.19b.

Using the responses from the above slamming event, the operating deflection shapes are calculated.

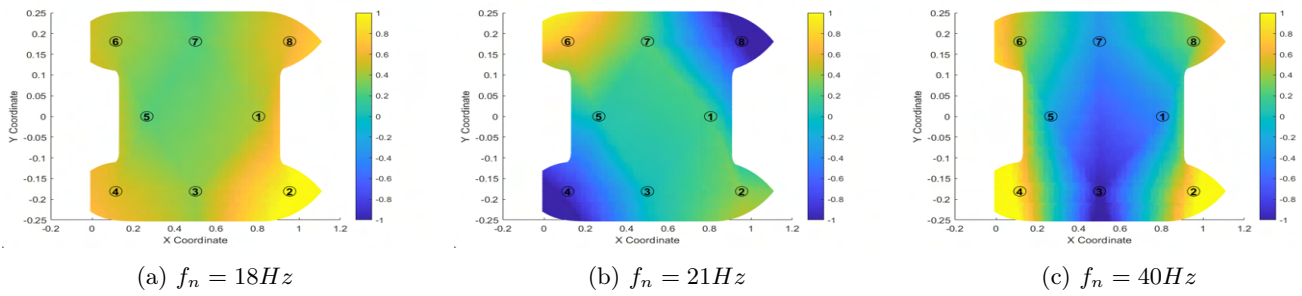


Figure 6.20: ODS for maximum hydroelastic response in run 5_74

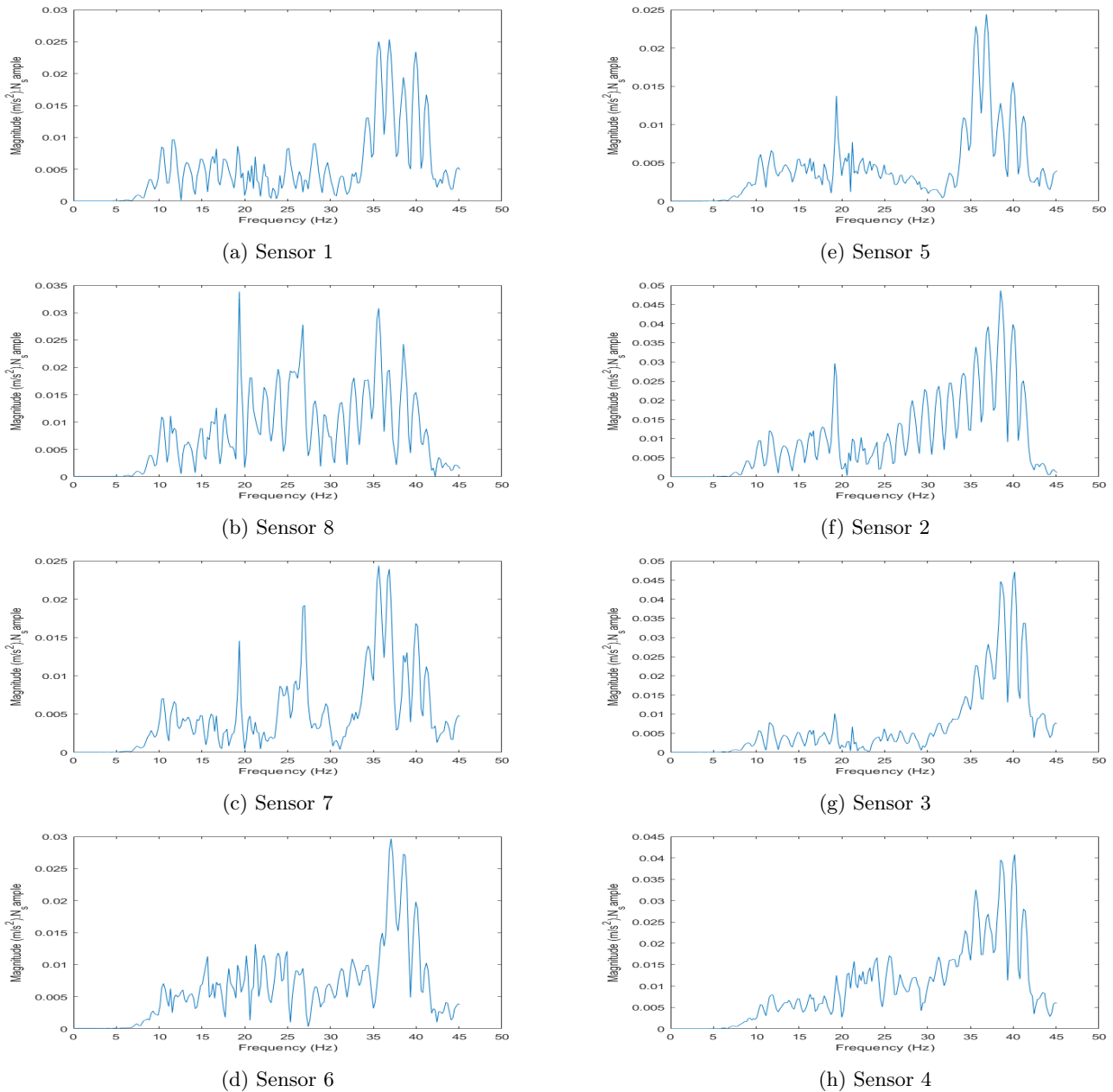


Figure 6.21: Fast Fourier Transform of investigated slam in run 5_74

6.3.3 Run 5_75

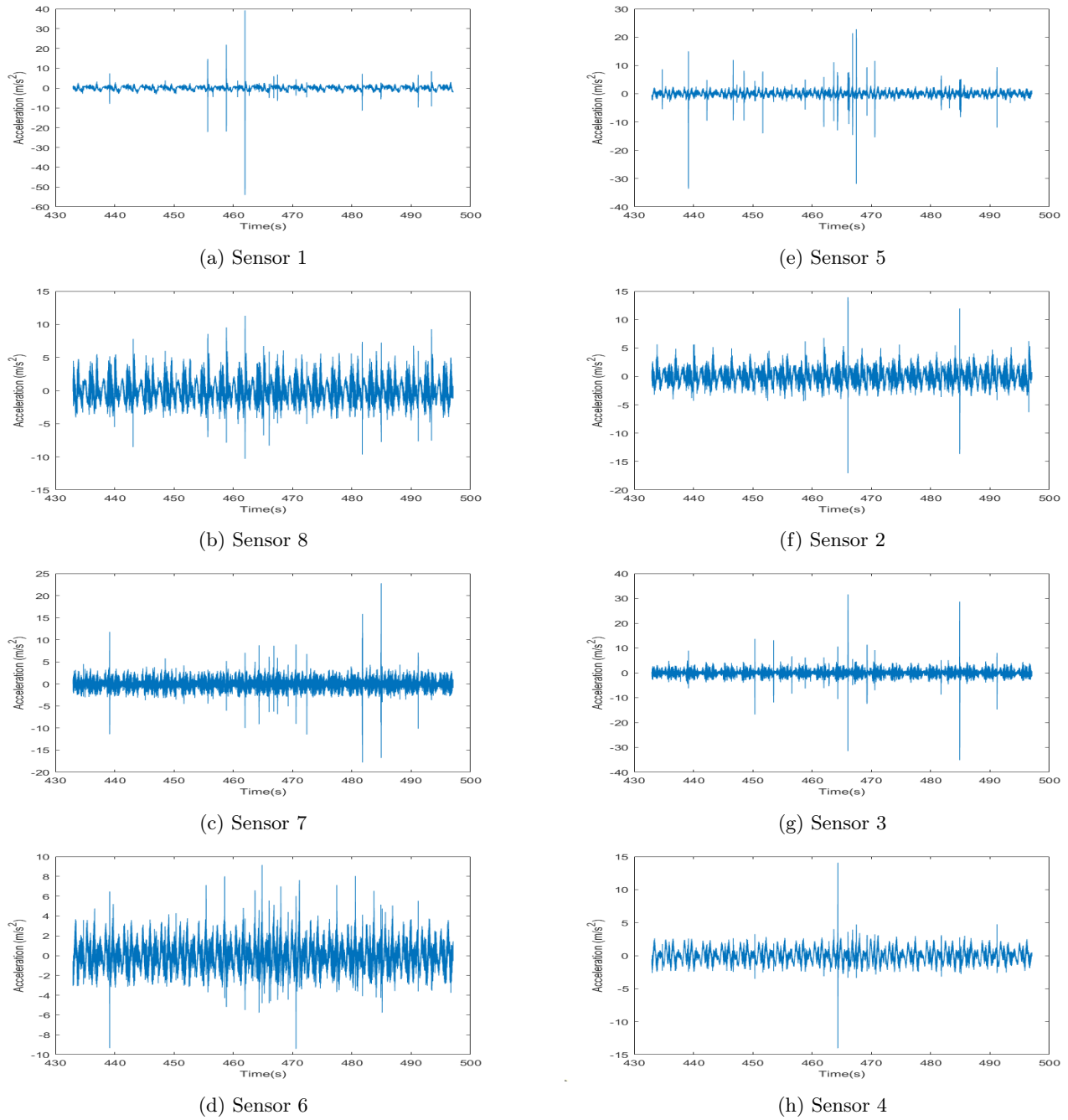
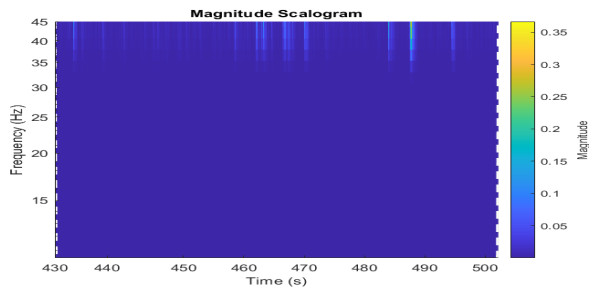
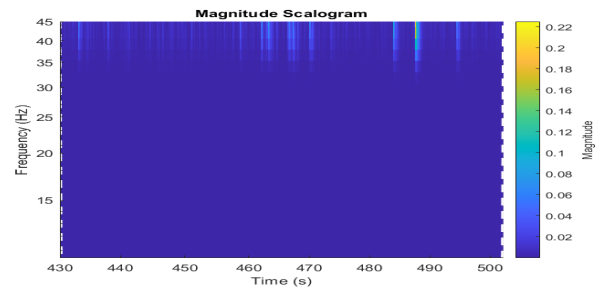


Figure 6.22: Acceleration recordings .

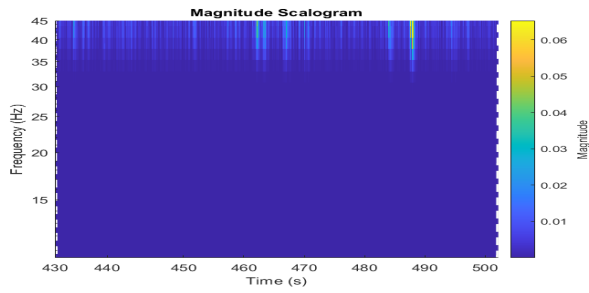
The impulse loads appear higher in the deck for this run, sensor 5 more slams than sensor 1 6.22a,6.22e.CWT is applied to determine the frequency content of the responses due to slamming.



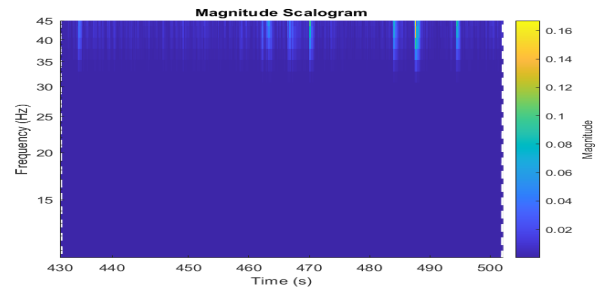
(a) Sensor 1



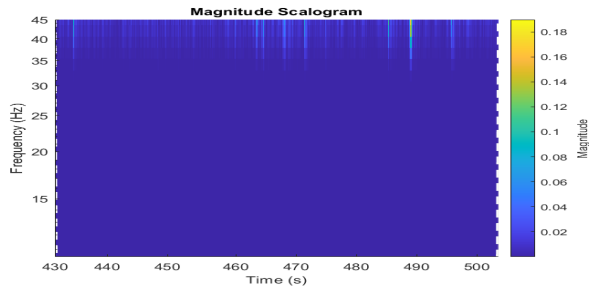
(e) Sensor 5



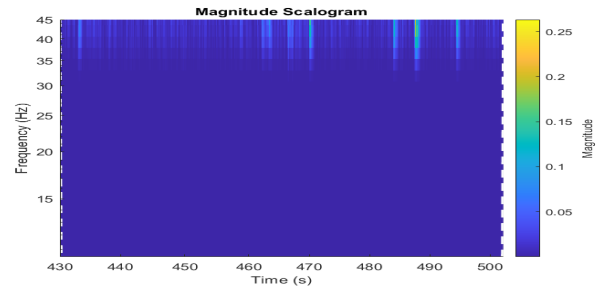
(b) Sensor 8



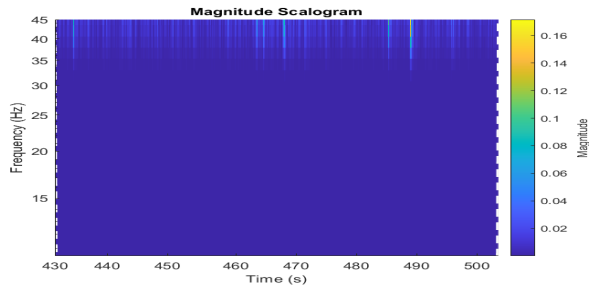
(f) Sensor 2



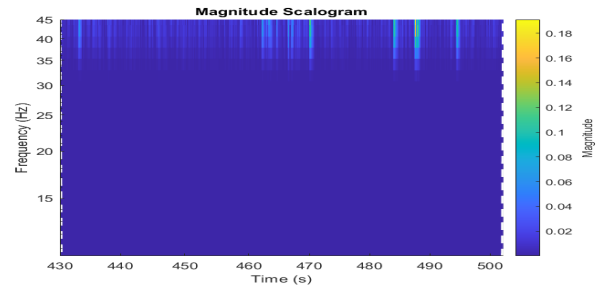
(c) Sensor 7



(g) Sensor 3



(d) Sensor 6



(h) Sensor 4

Figure 6.23: Scalogram of run 5_75.

The frequency content for this run is concentrated in the range 35-45 Hz, with the overall magnitude being fairly low. The highest concentration in flexible frequencies is found at time interval 484-490 s. The responses at that time interval are further studied.

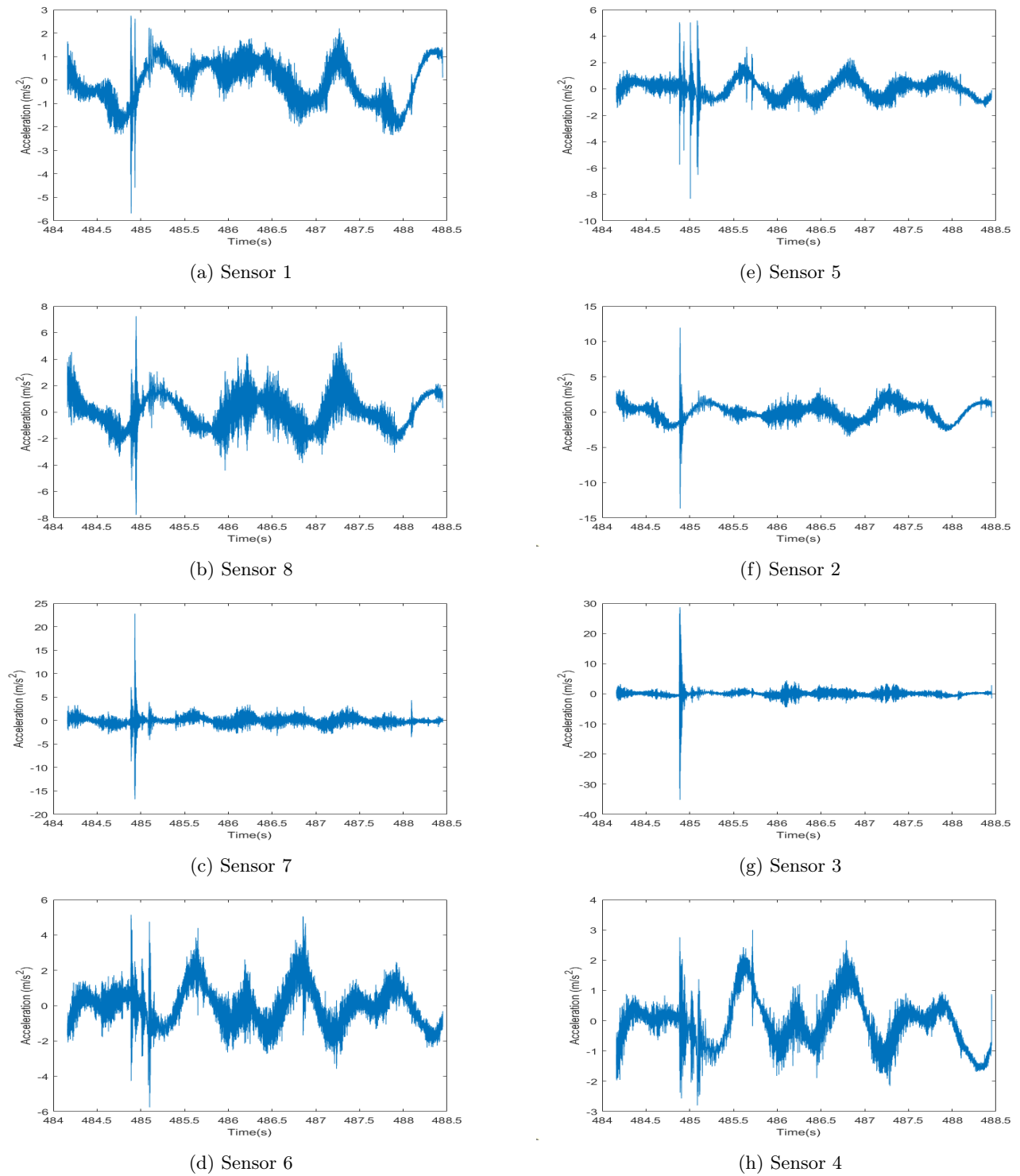
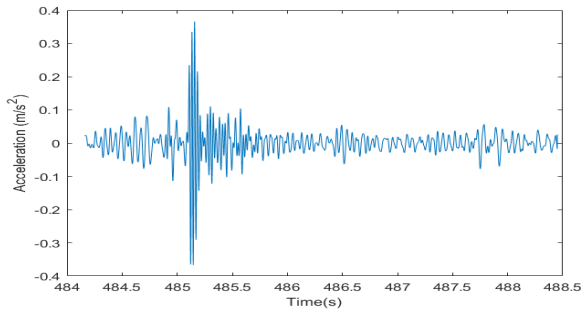
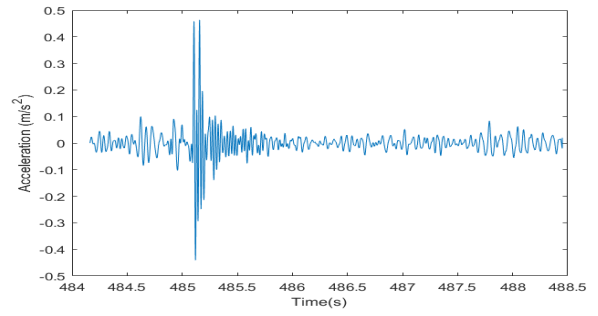


Figure 6.24: Zoomed in responses of slamming

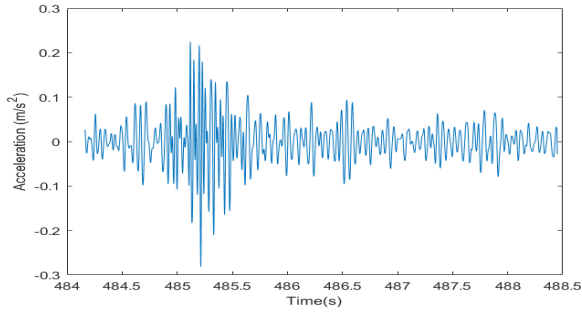
Slamming clustering is found once again in the deck sensors 6.24a,6.24e. Maximum impulse loads are recorded at the mid-span of the hulls in sensors 3 & 7, indicating the impacts occurred close to the middle of the model. It is noteworthy that the deck sensors record much lower responses. The hydroelastic responses from the investigated impacts are analysed below.



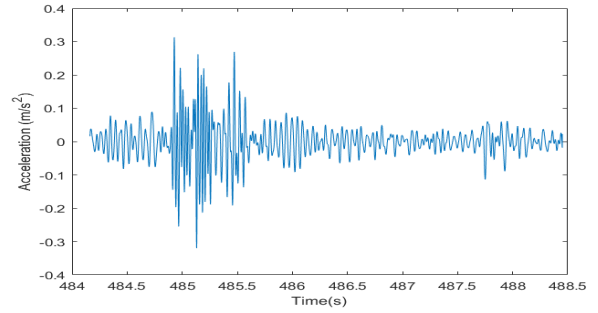
(a) Sensor 1



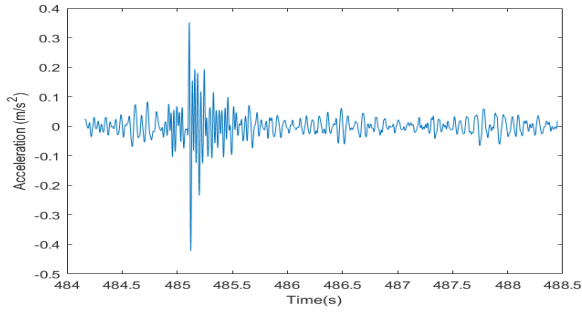
(e) Sensor 5



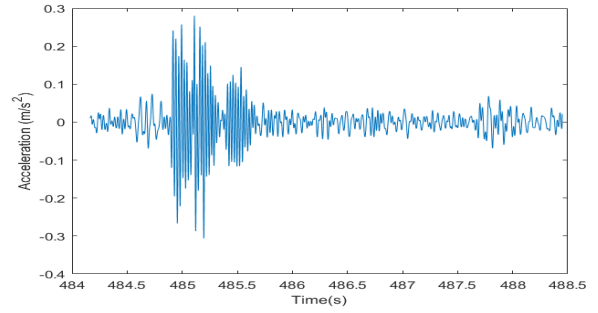
(b) Sensor 8



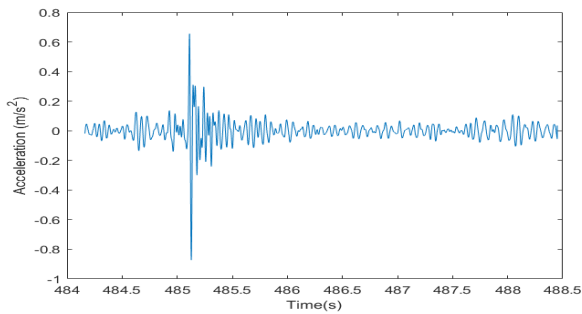
(f) Sensor 2



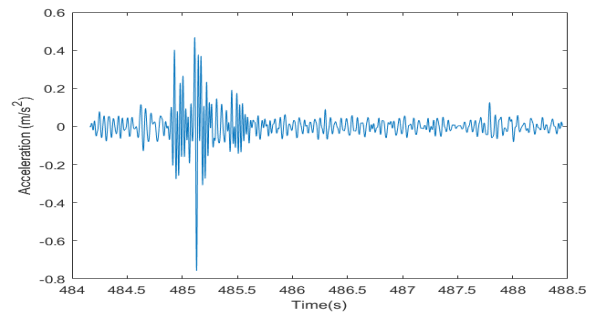
(c) Sensor 7



(g) Sensor 3



(d) Sensor 6



(h) Sensor 4

Figure 6.25: Hydroelastic responses of slamming

The maximum hydroelastic response is found in the aft sensors 6.25h & 6.25d. The oscillatory responses maintain distinct behaviour for the two side-hulls as seen in the previous test run. This time, the starboard hull exhibits three beats, while the portside hull maintains the form of a single oscillatory response. The response amplitudes captured are much lower than the hydroelastic responses of the previous run.

Using the responses from the above slamming event, the ODS are calculated as follows.

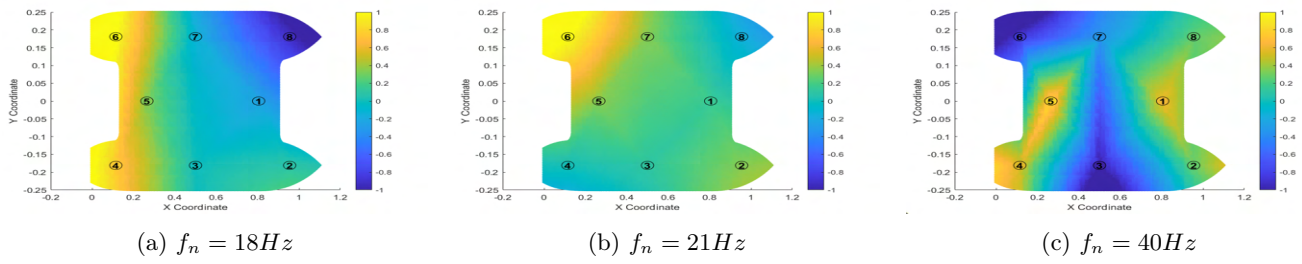


Figure 6.26: ODS for maximum hydroelastic response in run 5_75.

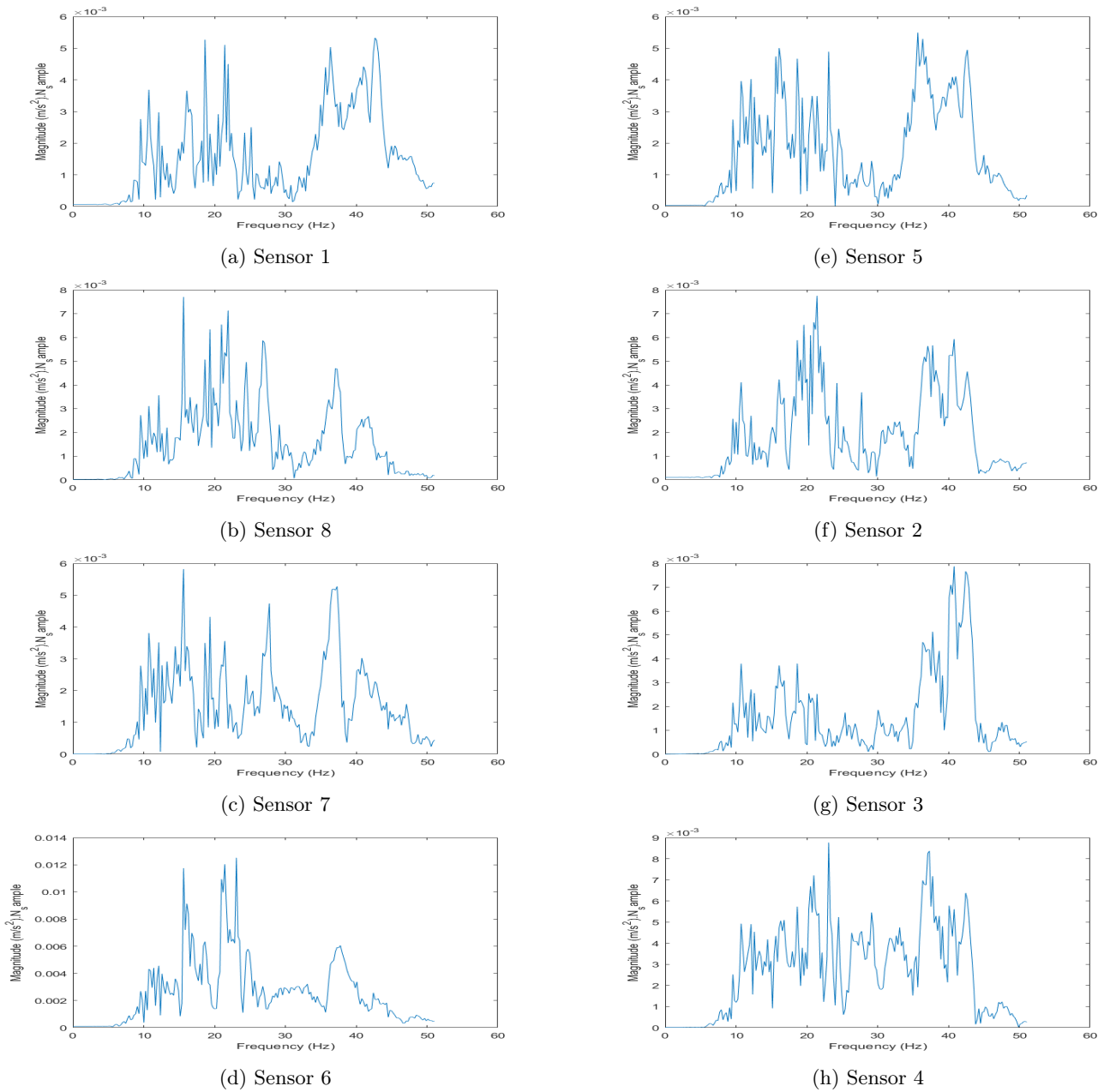


Figure 6.27: Fast Fourier Transform of investigated slam in run 5_75

6.3.4 Run 5_76

The highest slamming response is observed for test run 5_76.

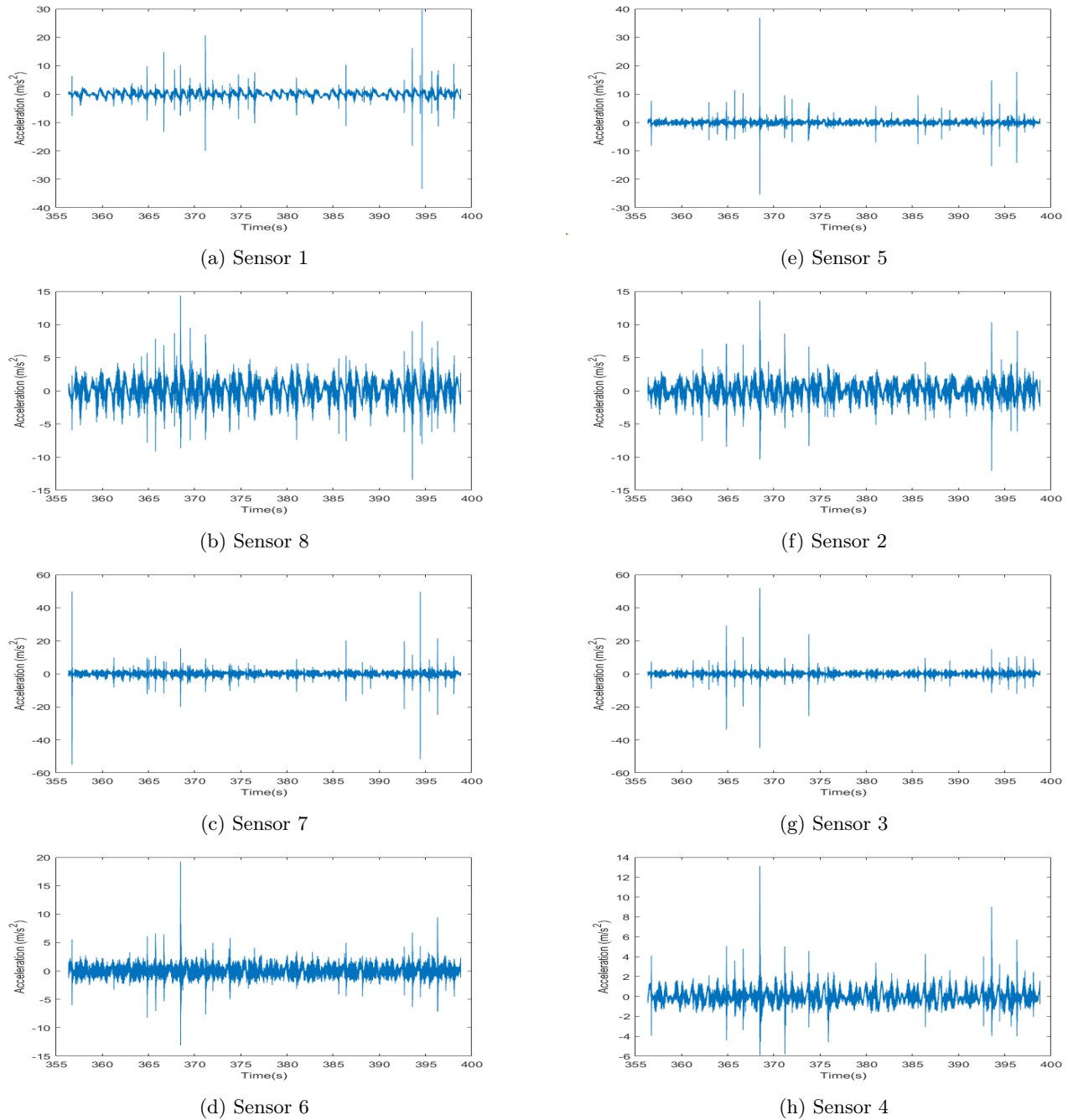
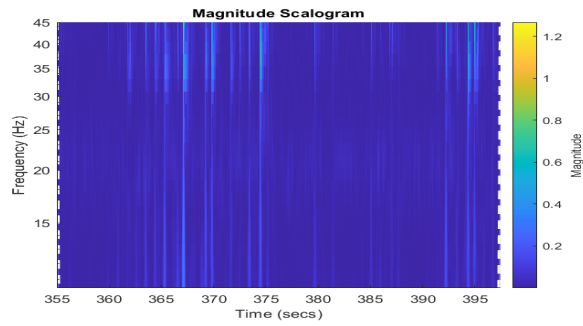
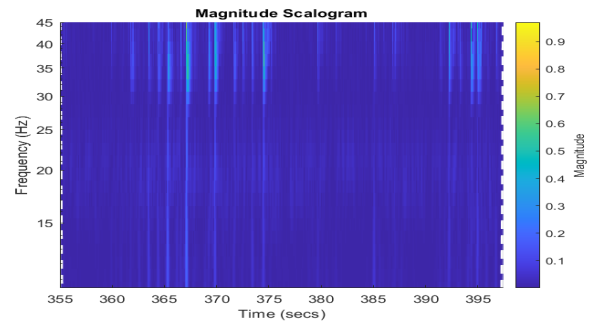


Figure 6.28: Acceleration recordings on the highest hydroelastic response recorded.

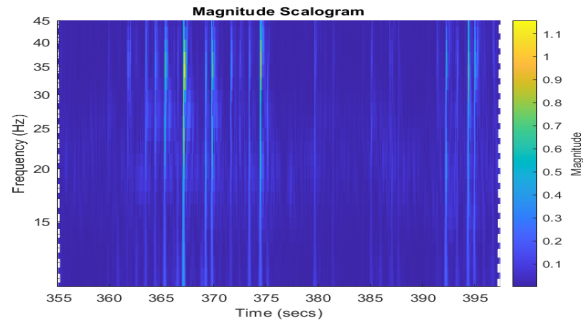
The sensor measurements show difference between the recorded loads at the fore and aft of the deck (6.28a, 6.28e, as well as for the different side-hulls (6.28f, 6.28h & 6.28g and sensors 6.28b, 6.28c, & 6.28d belong to separate side-hulls). The difference in measured loads suggests the wave loads do not occur at the middle of the wet deck but some eccentricity is involved. This can be explained by the increased roll rotation, detected during the RAO measurements. In order to analyse the slamming events thoroughly, shorter time intervals of study are necessary, while a narrower frequency band of the signal should be investigated.



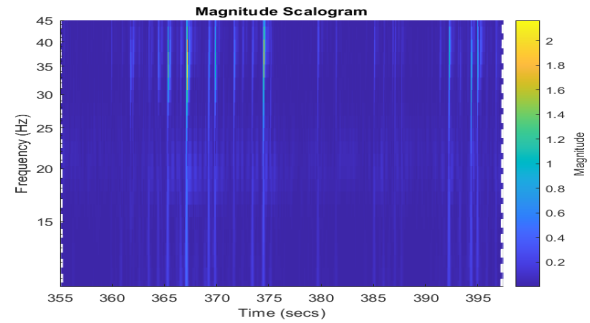
(a) Sensor 1



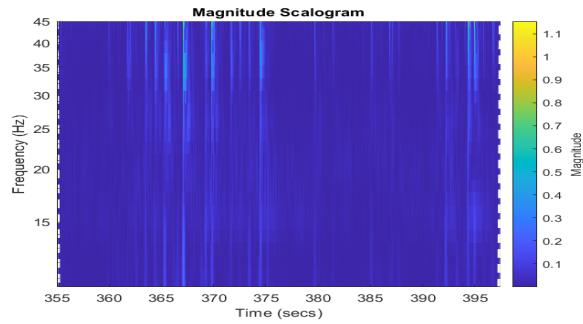
(e) Sensor 5



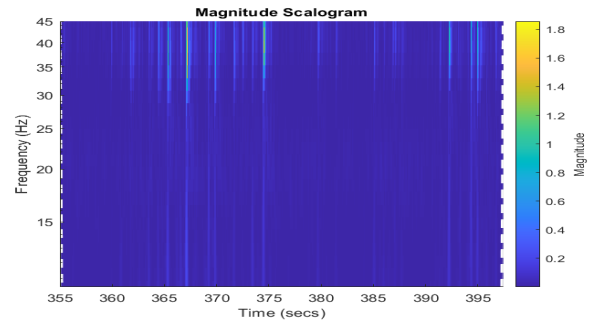
(b) Sensor 8



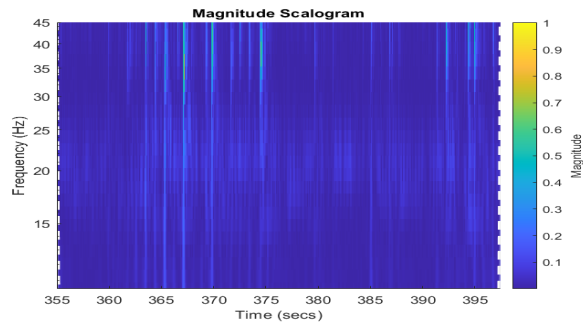
(f) Sensor 2



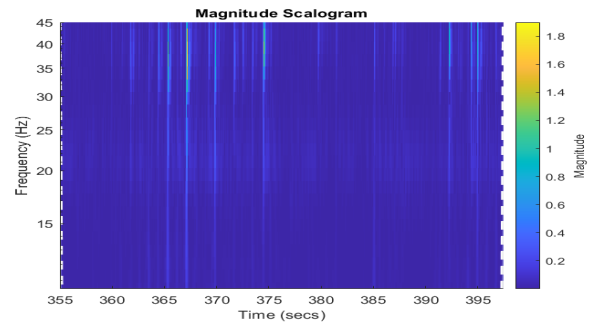
(c) Sensor 7



(g) Sensor 3



(d) Sensor 6



(h) Sensor 4

Figure 6.29: Scalogram for run 5_76

Using Continuous Wavelet Transform (CWT) the frequency content of each sensor is found for a range of 10-45 Hz. The particular frequency range is chosen, as the range 10-41 Hz is determined to be the most indicative of the global hydroelastic responses, according to the modal analysis findings. The slamming events are recognised by the sharp peaks covering all the frequencies of the figure. It can be seen that the most dense content is concentrated close to frequencies between 30-40. Seeing as the slamming event with the highest magnitude in the global flexible frequency range is located close to time 368 seconds, it is concluded that the maximum global hydroelastic response of the model is occurring at that time.

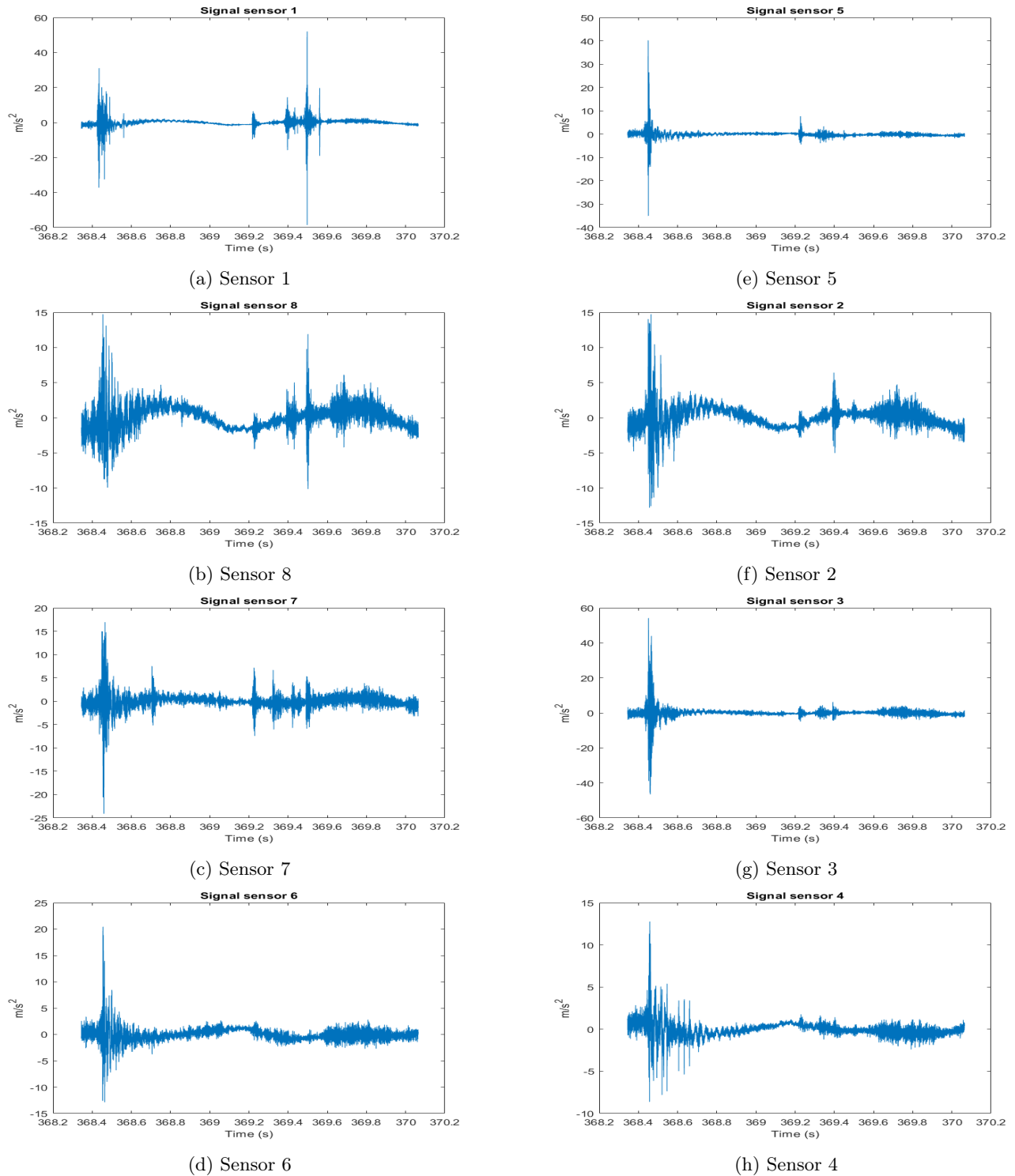


Figure 6.30: Zoomed in responses of slamming

It can be seen that the sensor measurements capture several slams, one occurring at time 368.4 s and then multiple peaks starting at 369.2 s up to 369.5 s. The initial slam recorded has caused the same magnitude of acceleration in the fore and aft deck sensors 6.30a,6.30e, suggesting the water impact happened in the middle of the wet deck. The cluster of slams seems to be best read by the fore sensors 6.30a,6.30f,6.30b,6.30c,6.30g, indicating the wave impacts occurred at the fore end of the wet deck. Considering the findings from the CWT applied earlier, a band pass filter is applied to the measurements for a range of 10-41Hz to quantify the hydroelastic responses caused by the impacts.

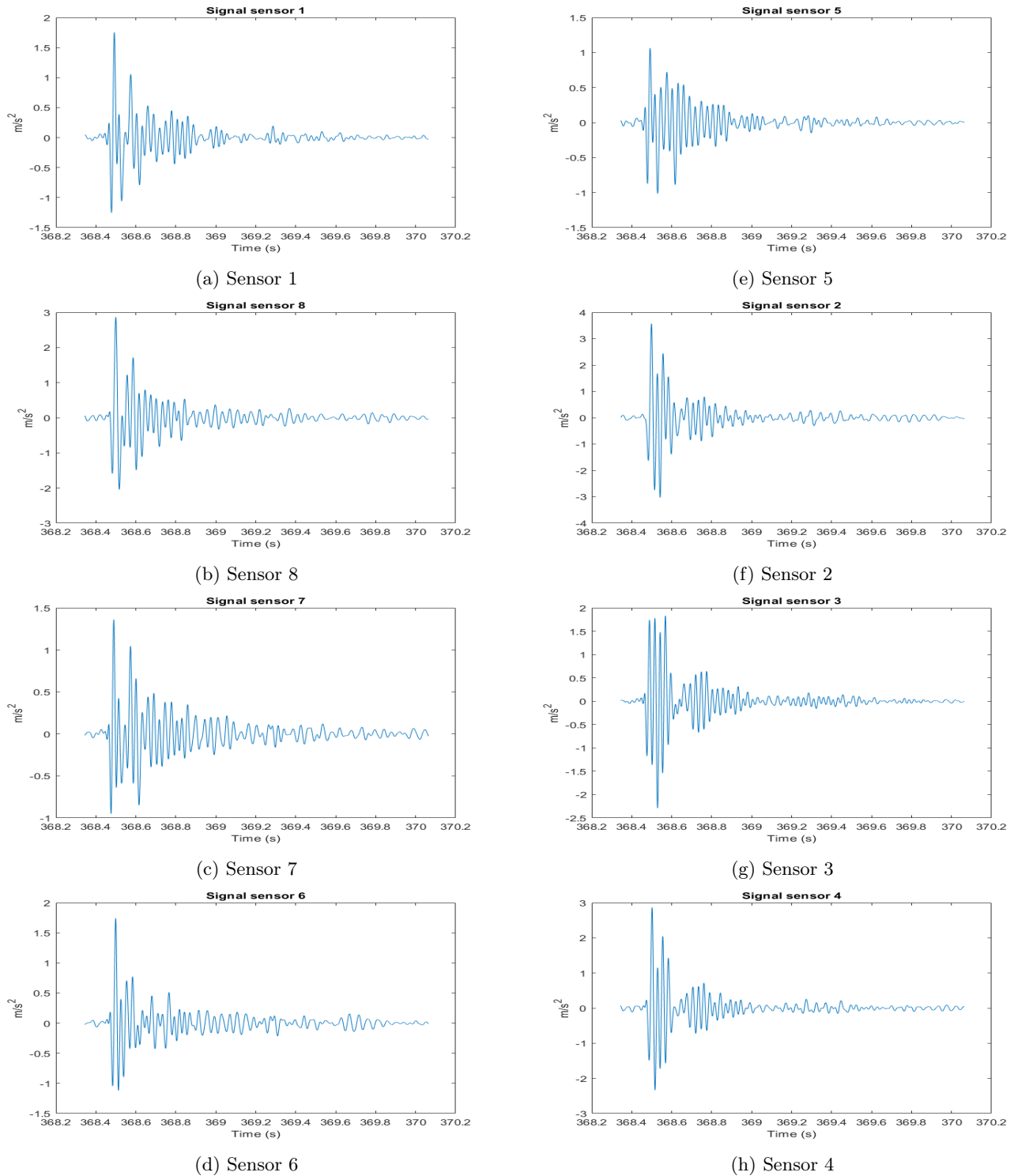


Figure 6.31: Band pass filtered signal for Hydroelastic frequency range 10-41Hz

The initial slamming event induces hydroelastic responses, while the slamming cluster that follows doesn't seem to influence the responses significantly. The side hulls follow different oscillation patterns. The overall oscillation amplitude seems larger for the starboard hull sensors, the pattern can be discerned into three beats. The port-side hull sensors on the other hand maintain a slightly lower amplitude along with a somewhat uniform pattern of oscillations. The responses seem to die out at 396,6 seconds, though it is hard to pinpoint a particular point where the responses have damped out completely. The total time duration of the global hydroelastic responses is found to be approximately 1.2 seconds, though the significant responses seem to last for about 0.5 seconds.

Using the responses from the above slamming event, the responses of the model in the three natural frequencies as they were defined from the modal analysis are calculated.

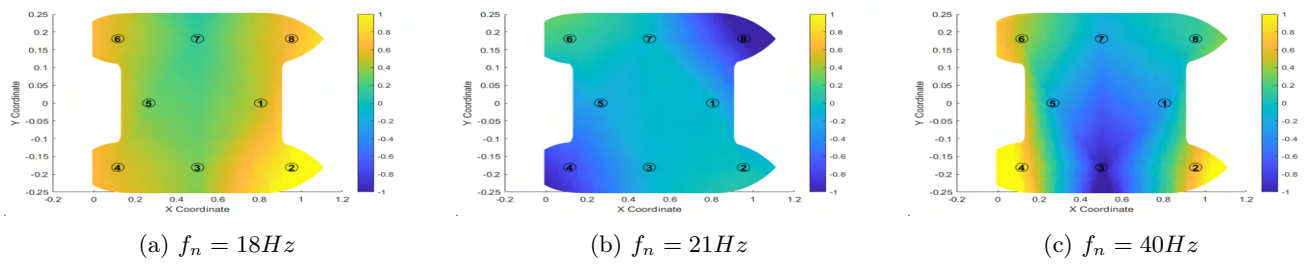


Figure 6.32: ODS for maximum hydroelastic response in run 5_76

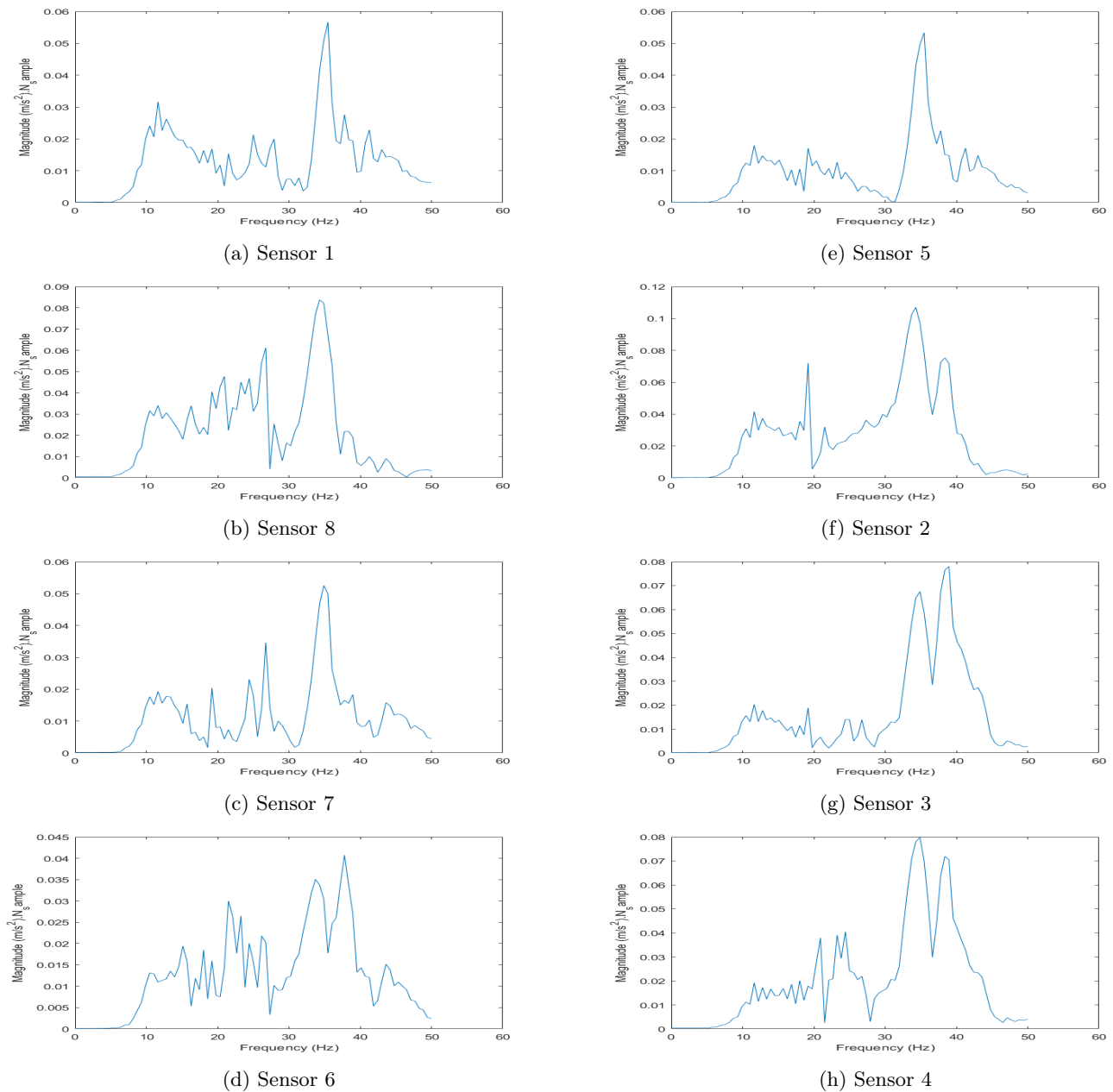


Figure 6.33: Fast Fourier Transform of investigated slam in run 5_76

6.3.5 Run 5_77

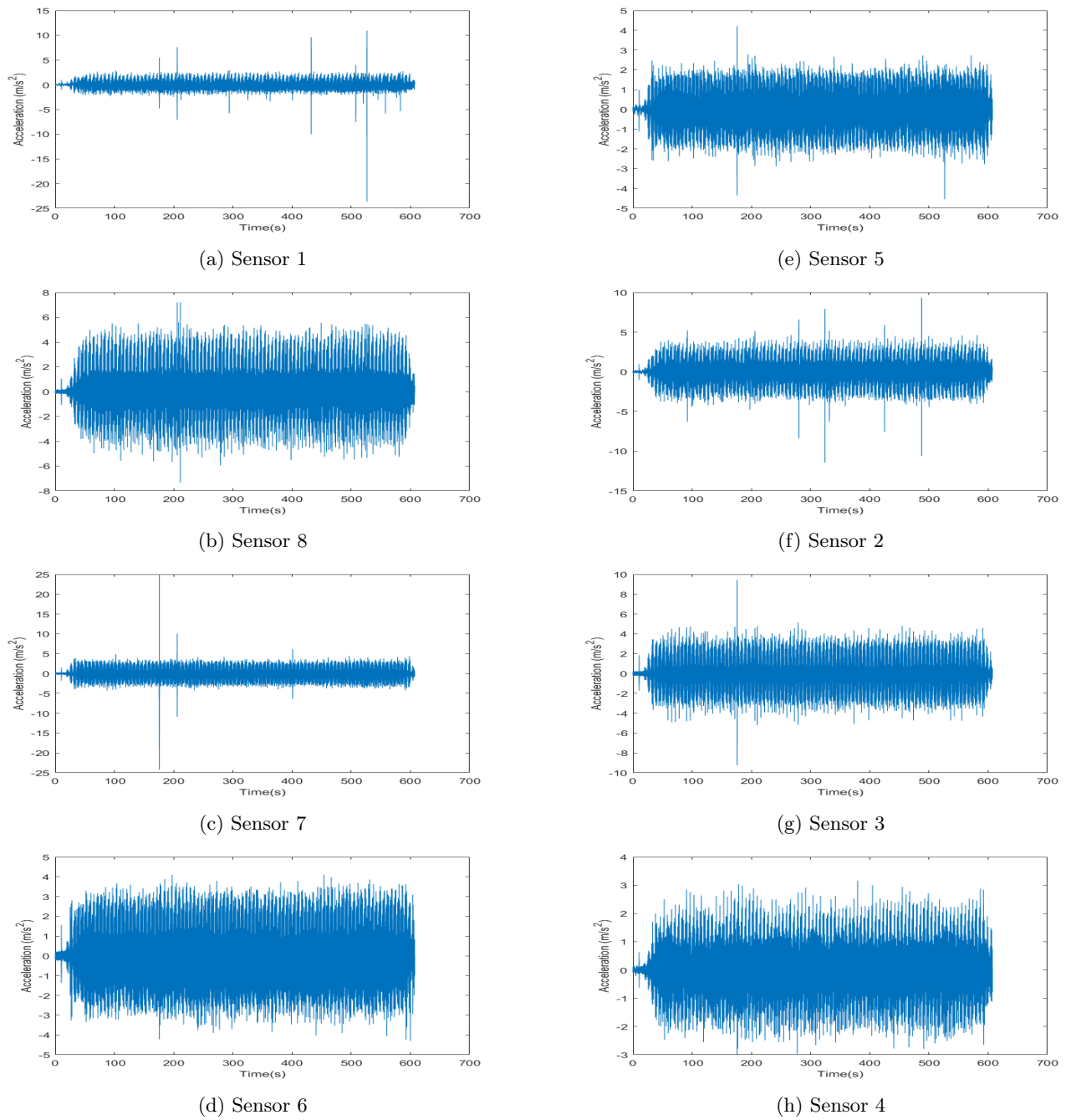
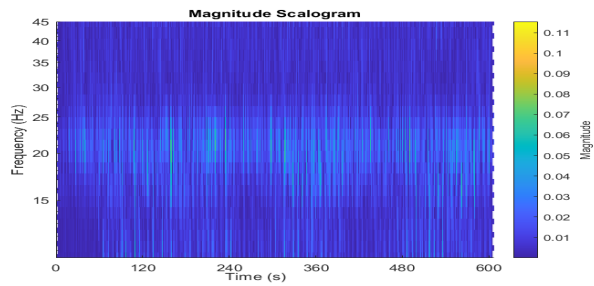
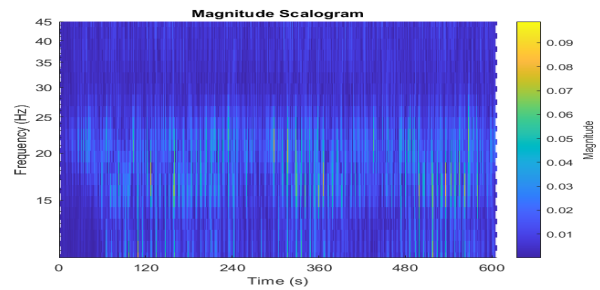


Figure 6.34: Acceleration recordings of run 5_77.

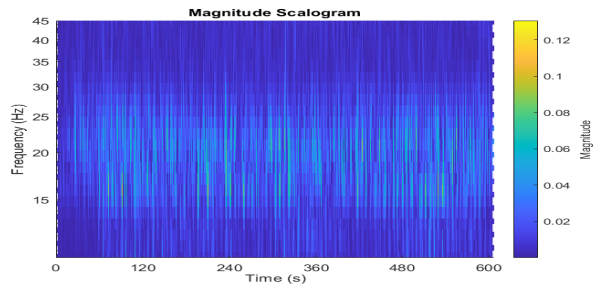
The test run is characterised by the fewest slams overall, with some sensors not measuring even a single impact 6.34c, 6.34g. As the whipping criterion did not identify slamming for this test run, CWT is applied to the whole recording to assess the frequency content of the responses.



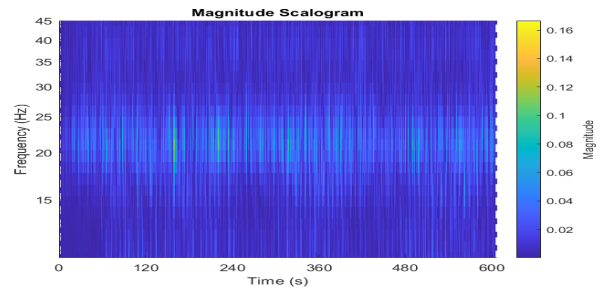
(a) Sensor 1



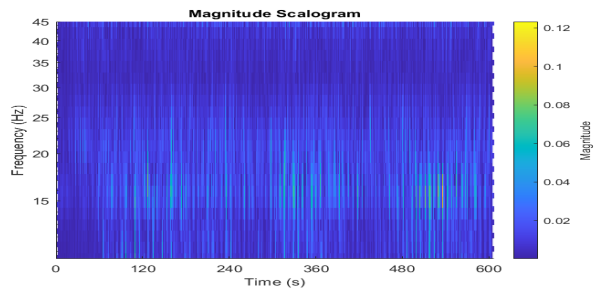
(e) Sensor 5



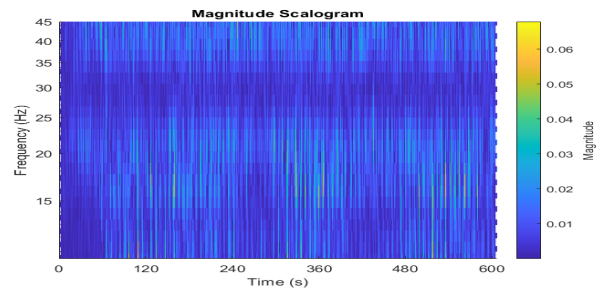
(b) Sensor 8



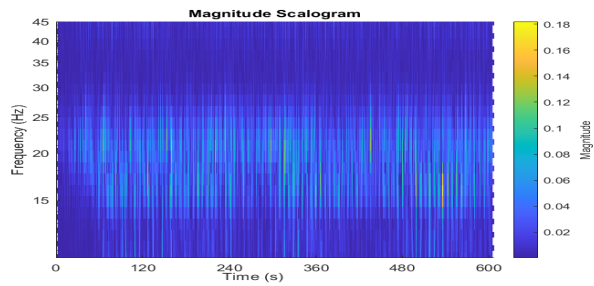
(f) Sensor 2



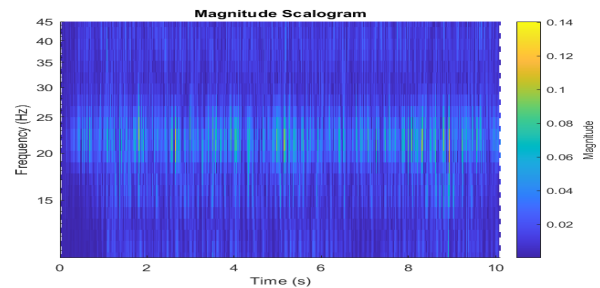
(c) Sensor 7



(g) Sensor 3



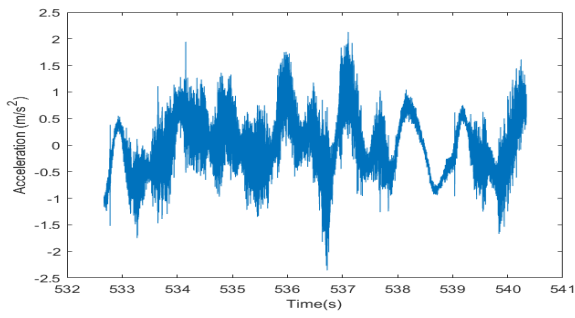
(d) Sensor 6



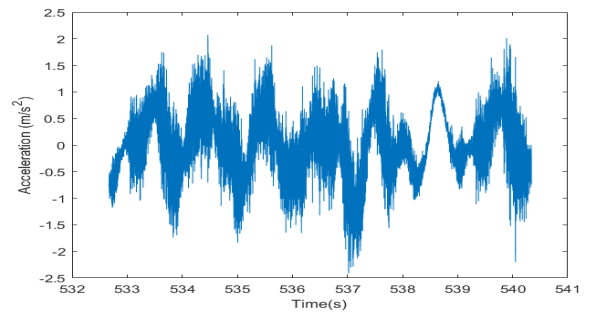
(h) Sensor 4

Figure 6.35: Scalogram of run5_77.

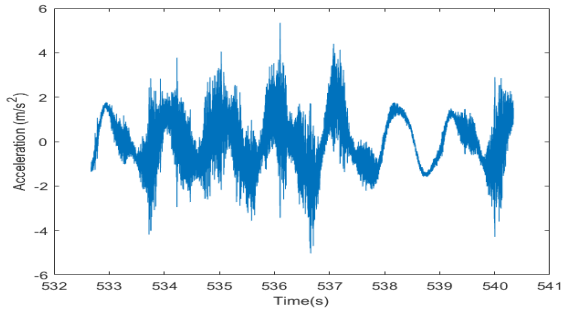
CWT does not identify any significant hydroelastic frequency response, the magnitude of the scalogram is also extremely low. This indicates that none of the slamming impulses produced hydroelastic responses, as indicated by the whipping identification criterion. As a somewhat increased content in hydroelastic frequencies is measured approximately at 530-540 seconds, that time interval is used for a more detailed investigation.



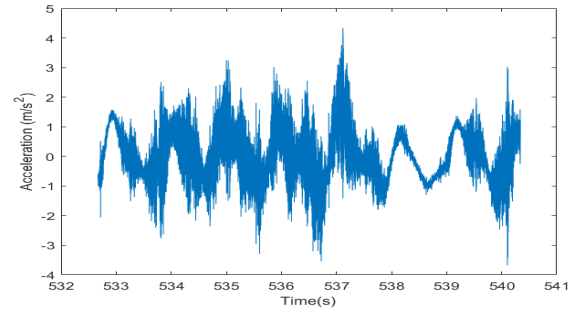
(a) Sensor 1



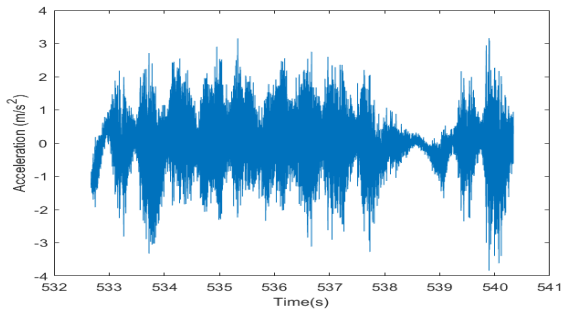
(e) Sensor 5



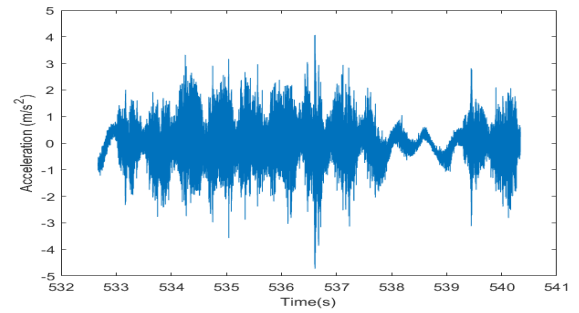
(b) Sensor 8



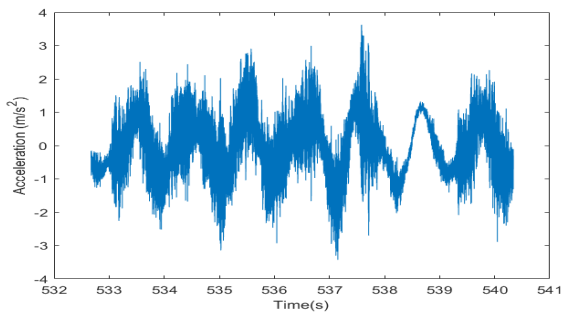
(f) Sensor 2



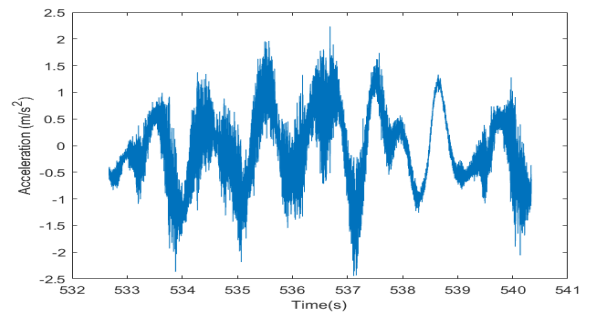
(c) Sensor 7



(g) Sensor 3

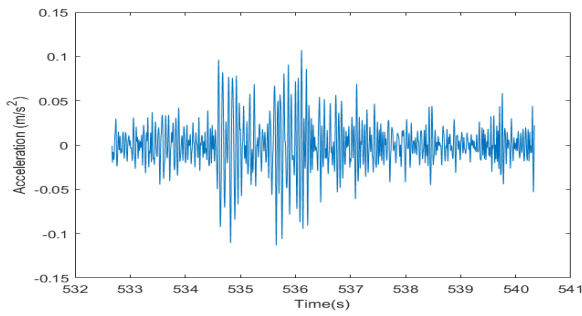


(d) Sensor 6

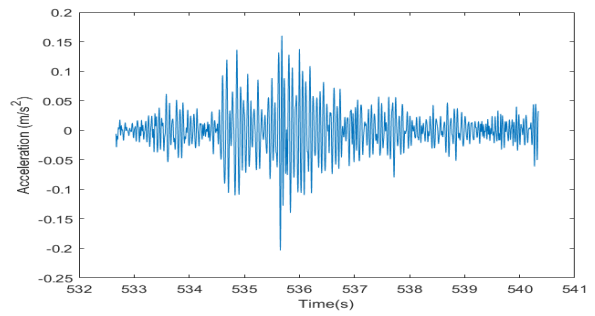


(h) Sensor 4

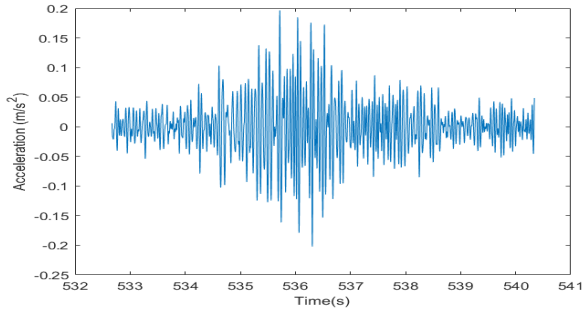
Figure 6.36: Zoomed in responses of slamming



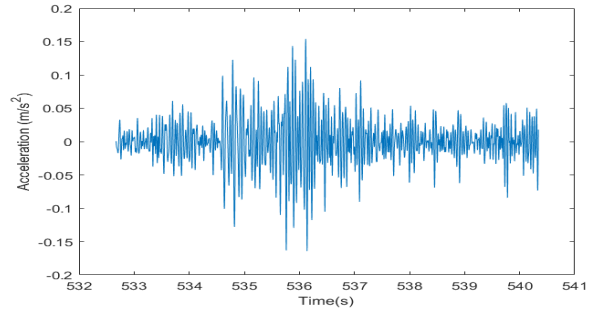
(a) Sensor 1



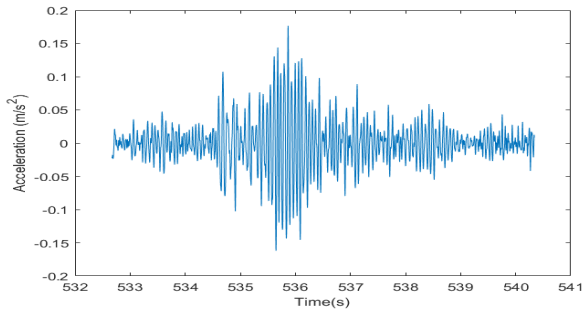
(e) Sensor 5



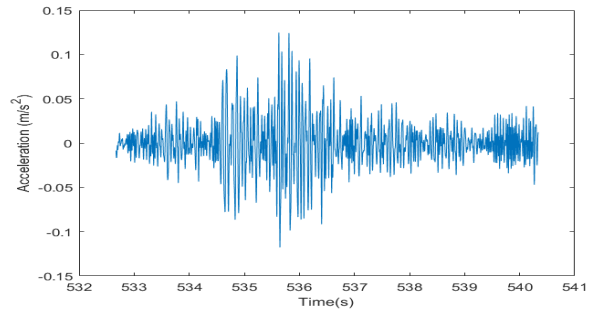
(b) Sensor 8



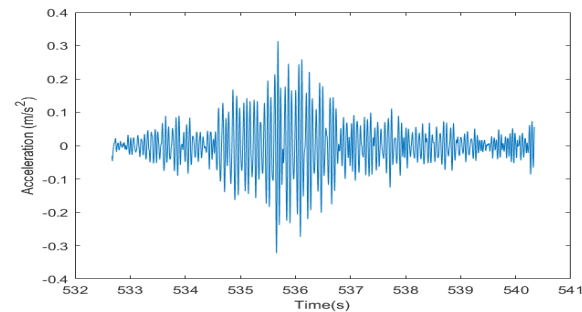
(f) Sensor 2



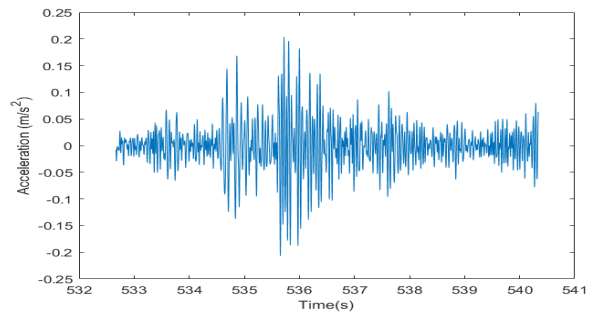
(c) Sensor 7



(g) Sensor 3



(d) Sensor 6



(h) Sensor 4

Figure 6.37: Zoomed in hydroelastic responses of slamming

Nosignificant slamming can be traced visually for the unfiltered signal, the responses are very low 6.37. The hydroelastic responses of the band pass filtered signals show some disturbance with characteristics similar to those of the previous test runs such as an increased response amplitude, a subsequent decay and a distinct oscillation pattern for the two hulls. The magnitude of the hydroelastic responses is extremely low, so much so that it is hard to discern the point where the oscillation has died out.

Using the responses from the above slamming event, the responses of the model in the three natural frequencies as they were defined from the modal analysis are calculated.

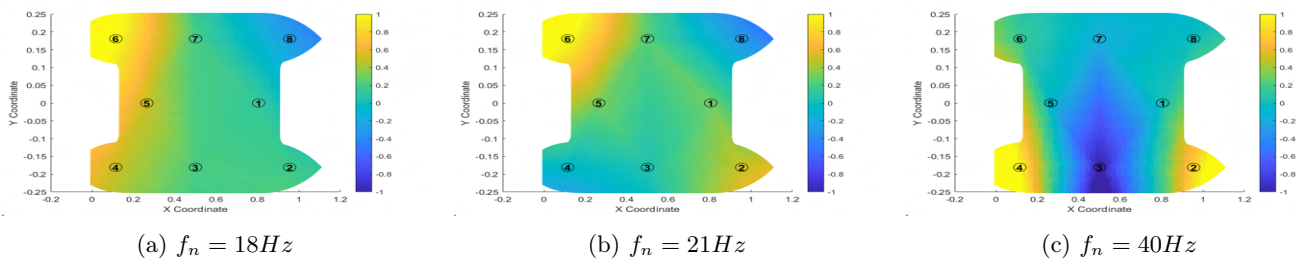


Figure 6.38: ODS for maximum hydroelastic response in run 5_77

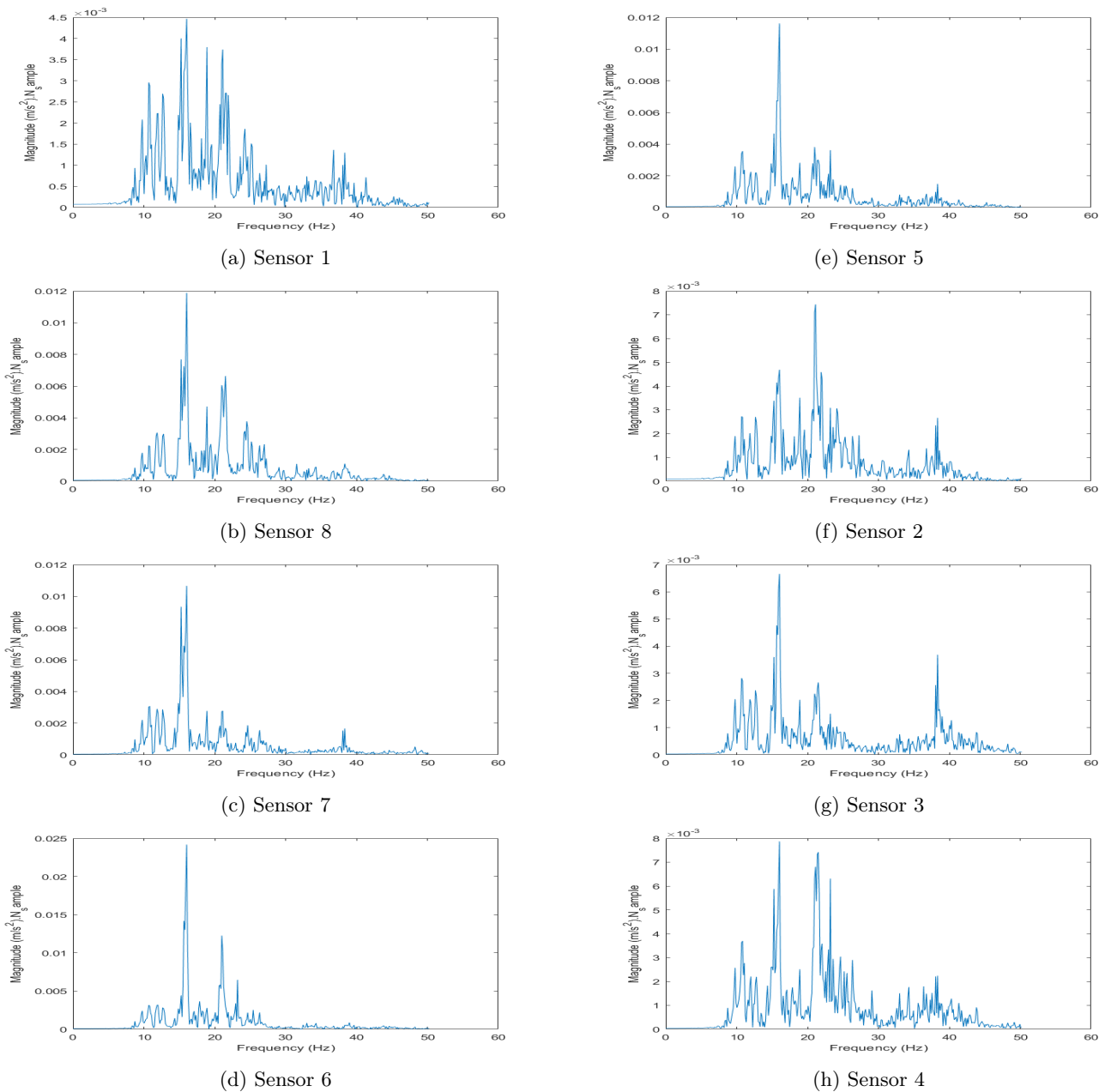


Figure 6.39: Fast Fourier Transform of investigated slam in run 5_77

6.3.6 Conclusions

This chapter addresses the identification and evaluation of hydroelasticity intensity by applying two criteria for slamming identification. Both criteria rely on model global flexible responses induced by wave impacts on the wet deck. While they share common points in identifying some events, they also exhibit differences. The main difference lies in how the slamming global responses are considered.

The filtering of the signal and the definition of thresholds for both methods are based on prior knowledge of the model's global deformation frequencies. For the whipping criterion, frequencies lower than 10 Hz and higher than 50 Hz are excluded by a band-pass filter. In contrast, EMD is more inclusive regarding the frequency range, as the IMF definition relies on both the desired frequency range and the magnitude of responses excited by the wave impact. This results in IMFs with a wider frequency range than 10.5-50 Hz, while at the same time some of the global hydroelastic frequency responses are omitted as they are part of a different IMF that does not fulfill the threshold requirements set by the user.

Green water is also appearing in test runs of specific wave conditions and particularly in the test run of the highest recorded hydroelastic responses. That fact shows how severe the sea conditions need to be for substantial hydroelastic responses to occur from wet deck slamming.

After further analysis of the test runs of the highest nominal wave height applied, the following conclusions were drawn. Hydroelasticity becomes more significant for the wave frequency combinations 4&5 rad/s and 4&7 rad/s. The most significant hydroelastic responses are often seen in slam clusters. The model exhibits asymmetric dynamic responses, each of the side hulls has followed a distinct oscillation behaviour with different pattern and magnitude.

From the calculated operational deflection shapes it can also be seen that the asymmetric mode shape is always the least distorted one, with the shapes corresponding to the other frequencies usually adopting a non-symmetric deformation pattern even though the dry modal shapes refer to symmetric modes. The wave impact dynamics of wet deck slamming are random with respect to amplitude and exact location of the impact. As such, it stands to reason that the first two modes would not in fact manifest as symmetric responses. The model has exhibited the capability to realise flexible deformations in accordance to numerical predictions, with some deviations that could be potentially mitigated with some changes in the design of the model. The merits of the use of a fully elastic model can be seen in the accurate representation of these asymmetric responses.

When applying FFT to the significant slamming events investigated, the frequencies participating in the global whipping response can be discerned. Natural frequencies show peaks, while each slamming case shows different patterns of the excited frequencies. Some of the highest frequency peaks do not correspond to the investigated natural modes. Mode masking becomes evident with multiple peaks concentrated in narrow bandwidths. The test runs with the most intense slamming events (5_74 & 5_76) show high peaks on the natural frequencies, even for the calculated third $f_n = 36.58 Hz$, even though the natural frequency is not detected in the modal tests. The most strong responses are seen for the frequencies 36 & 40 Hz. Test run 5_77 was established to not have significant wet deck slamming events occurring. Even so, high peaks are observed for frequencies 16 & 21 while frequencies 36 & 40 do not seem to be excited substantially. The level of excitation of frequency 16 Hz seems to maintain more or less the same amplitude in all test runs, even the ones with No significant global whipping, suggesting that it could be the result of a different dynamic response that is not identified. In any case the amplitude of the accelerations is much lower than the amplitude of the test runs with notable slamming and whipping. The response frequency content is much different for all 4 test runs examined, showing how the difference in wave frequency can affect the responses of the model as the global modes are excited in a different manner in each case.

Chapter 7

Conclusions

This study examined wet deck slamming using a fully elastic model, with conclusions drawn from experimental test runs and analysis. Potential improvements for the experimental setup are discussed in this chapter, to refine the experimental process in future works.

Wet deck slamming was investigated using a fully elastic model. Floating modal characteristics were investigated numerically for the first four flexible modes. The hydrodynamic behavior was calculated with commercial 3D potential solver AQWA. Numerical results were validated experimentally in the recirculation flume tank. Wet deck slamming was investigated for head bi-chromatic waves under two different current speeds.

Instrumentation included measurement of acceleration of the model top deck. Additionally, DIC measurements at the top of the cross-deck surface of the twin-hull model captured deformations induced by hammer and wave impacts. The incident waves were measured via three wave probes capturing the wave elevation in front, on the side and at the wake of the model. Rigid body motions were also measured by means of motion tracking.

The hydrodynamic behavior converged for vertical motions, except for Roll. Roll deviations were likely due to limitations in the experimental setup. The model follows the expected behavior and should give realistic responses under wet deck slamming.

Numerical results for natural frequencies and mode shapes generally aligned with SIMO impact hammer test findings. Improvements in the experimental setup could increase the results quality. DIC was used to measure deformations on the deck. The limited field of view and ambiguous pattern quality led to issues with the measurements. The DIC identified natural frequencies did not agree with the other approaches. Clear mode shapes were not identified for most natural frequencies.

Wave impact tests showed effective camera trigger settings for slamming instance capturing. The trigger conditions relied purely on water impact amplitude rather than hydroelastic responses. High-speed camera recordings create large data files, so a limit to the number of recordings per run was set. Time instances were recorded correctly but did not contain hydroelastic responses. There is still room for improving the DIC for future experiments.

Slamming identification used two response based methods focusing on global whipping. No clear slamming criterion can be established universally as the criteria are subjective and differ for each case. Local responses were found to be fairly close to the global responses. The whipping criterion could clearly separate the two flexible responses.

"Wave impact experiments exhibited asymmetric responses consistent with the modal analysis, highlighting one of the major advantages of these models over segmented ones. The current model showcases all key functions of fully elastic models and follows the expected modal and hydrodynamic behavior. This proves the worth of such research and highlights the merits of such models being used more often to describe complex water entry phenomena.

7.1 Experimental Setup Possible Improvements

Based on the observations made during test runs, noting potential improvements for future research would be worthwhile. Building more on this research could lead to the constitution of a standard framework to building fully elastic models in a precise and efficient manner. Some measures that can improve the quality of results are presented below:

1. **Better quality of speckle pattern for DIC measurement:** A more accurate means of application should be used, possible solutions could be:
 - (a) A rubber stamp with a computer-generated pattern capable of applying it to a hard PETG material surface.
 - (b) A laser cut stencil to be used to spray the pattern over with the appropriate paint.
2. **Wider field of view:** Using cameras that can capture the desired field of view or purchase lenses of shorter focal length would improve the DIC results greatly.
3. **Use of Shaker:** The fragile model can be tested better using a shaker instead of hammer tests, mode masking would also be dealt with. Such a setup in the flume tank would require the construction of a large frame to support the shaker in a safe manner.
4. **Better kinematics measurement:** Slamming analysis uses quantities like relative vertical velocity, to be able to measure such a quantity improvements are necessary:
 - (a) Maximize the sampling frequency of the motion tracking system to obtain the motion data of the model as close as possible to the moment of impact.
 - (b) Develop a way to capture the free surface wave elevation in critical locations such as between the side-hulls of a twin-hull model.
5. **Measurements directly on wet deck:** The current project conducted measurements at the top deck, as installing instrumentation at the wet deck itself was impossible. The design of future models should be able to accommodate measurements directly on the wet deck without compromising structural integrity.
6. **Initially test simpler models:** Starting with simpler models could reduce uncertainties and streamline the development of new experimental methodologies before progressing to more complex twin-hull designs.
7. **Research on fabrication materials:** Researching material properties, such as structural damping and elasticity, enhances the model's accuracy and realism. This deeper understanding allows for improved dynamic analysis and helps translate the design more effectively to the reference vessel.

Bibliography

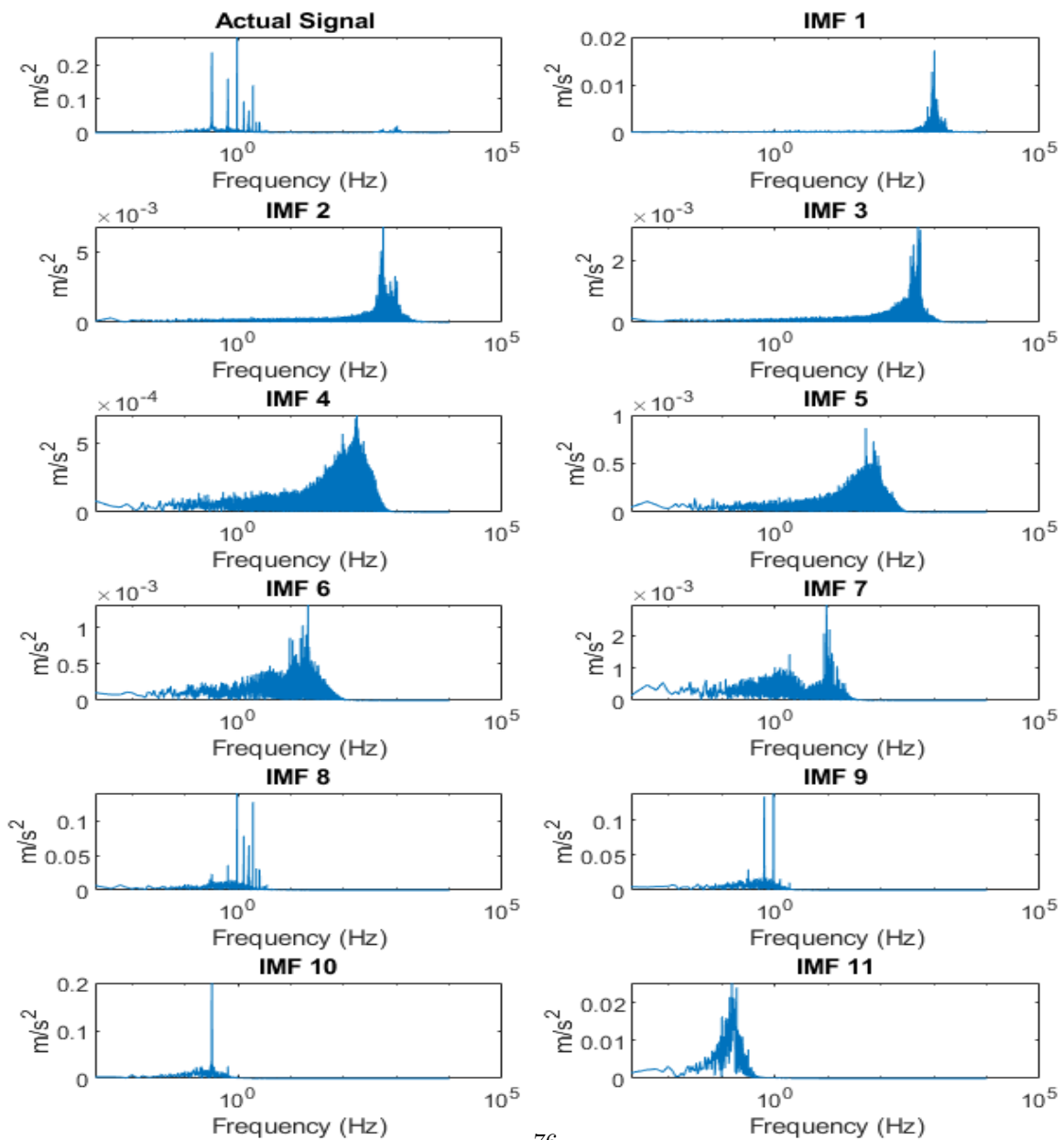
- [1] A. Keser, M. Verdult, H. Seyffert, and A. Grammatikopoulos, “The design, production, verification, and calibration of an elastic model of a catamaran for hydroelastic experiments,” English, in *HSMV 2023 - Proceedings of the 13th Symposium on High Speed Marine Vehicles*, E. Begovic, Ed., ser. Progress in Marine Science and Technology, 13th Symposium on High Speed Marine Vehicles, HSMV 2023 ; Conference date: 23-10-2023 Through 25-10-2023, Netherlands: IOS Press, 2023, pp. 139–148, ISBN: 978-1-64368-442-0. DOI: 10.3233/PMST230019.
- [2] J. Ramos, A. Incecik, and C. Soares, “Experimental study of slam-induced stresses in a containership,” *Marine Structures*, vol. 13, no. 1, pp. 25–51, 2000, ISSN: 0951-8339. DOI: [https://doi.org/10.1016/S0951-8339\(00\)00003-4](https://doi.org/10.1016/S0951-8339(00)00003-4). [Online]. Available: <https://www.sciencedirect.com/science/article/pii/S095183390000034>.
- [3] E. C. D. Dessi, “Slamming clustering on fast ships: From impact dynamics to global response analysis,” *Ocean engineering*, 2013. DOI: <http://dx.doi.org/10.1016/j.oceaneng.2012.12.051>.
- [4] D. Dessi, “Whipping-based criterion for the identification of slamming events,” *Int. J. Nav. Archit. Ocean Eng.*, 2014. DOI: <https://doi.org/10.2478/IJNAOE-2013-0232>.
- [5] A. Veer, “Behaviour of catamarans in waves,” Ph.D. dissertation, Delft University of Technology, 1998. DOI: <http://resolver.tudelft.nl/uuid:fc4c765a-3c7f-412d-9607-94fb9081ff36>.
- [6] G. A. Thomas, “Wave slam response of large high-speed catamarans,” May 2023. DOI: 10.25959/23242580.v1. [Online]. Available: https://figshare.utas.edu.au/articles/thesis/Wave_slam_response_of_large_high-speed_catamarans/23242580.
- [7] J. Ali-Lavroff, M. Davis, D. Holloway, and G. Thomas, “The whipping vibratory response of a hydroelastic segmented catamaran model,” *9th International Conference on Fast Sea Transportation, FAST 2007*, Jan. 2007.
- [8] G. Thomas, S. Winkler, M. Davis, *et al.*, “Slam events of high-speed catamarans in irregular waves,” *Journal of Marine Science and Technology*, vol. 16, pp. 8–21, Mar. 2011. DOI: 10.1007/s00773-010-0105-y.
- [9] G. Thomas, “Determination of wave slamming loads on high-speed catamarans by hydroelastic segmented model experiments,” *Transactions of the Royal Institution of Naval Architects Part A: International Journal of Maritime Engineering*, vol. 153, A185–A198, Jan. 2011. DOI: 10.3940/rina.ijme.2011.a3.211.
- [10] J. Lavroff, M. Davis, D. Holloway, and G. Thomas, “Wave slamming loads on wave-piercer catamarans operating at high-speed determined by hydro-elastic segmented model experiments,” *Marine Structures*, vol. 33, pp. 120–142, 2013, ISSN: 0951-8339. DOI: <https://doi.org/10.1016/j.marstruc.2013.05.001>. [Online]. Available: <https://www.sciencedirect.com/science/article/pii/S0951833913000439>.
- [11] G. T. M.R. Davis B.J. Frencha, “Wave slam on wave piercing catamarans in random head seas,” *Ocean engineering*, 2017. DOI: <https://doi.org/10.1016/j.oceaneng.2017.03.007>.
- [12] H. Hidetaka, K. Yusuke, M. Sadaoki, *et al.*, “Designing a hydro-structural ship model to experimentally measure its vertical bending and torsional vibrations,” *Journal of Advanced Research in Ocean Engineering*, vol. 4, no. 4, pp. 174–184, Dec. 2018.
- [13] A. Grammatikopoulos, J. Banks, and P. Temarel, “Prediction of the vibratory properties of ship models with realistic structural configurations produced using additive manufacturing,” *Marine Structures*, vol. 73, p. 102 801, 2020, ISSN: 0951-8339. DOI: <https://doi.org/10.1016/j.marstruc.2020.102801>. [Online]. Available: <https://www.sciencedirect.com/science/article/pii/S0951833920300952>.

- [14] A.M.E.Keser, *The design, production and verification of a fully elastic model of a catamaran for hydroelastic experiments*, 2023. [Online]. Available: <http://resolver.tudelft.nl/uuid:b5ca1efe-8c2f-4af4-82f8-beee4f3273ce>.
- [15] L. M. M.K. Ochi, "Prediction of slamming characteristics and hull responses for ship design," 1973.
- [16] "Prediction of occurrence and severity of ship slamming at sea," 1964. [Online]. Available: <http://resolver.tudelft.nl/uuid:d731b106-ce52-4181-b388-f0809322f053>.
- [17] A. Alsalah, D. Holloway, M. Mousavi, and J. Lavroff, "Identification of wave impacts and separation of responses using emd," *Mechanical Systems and Signal Processing*, vol. 151, p. 107385, 2021, ISSN: 0888-3270. DOI: <https://doi.org/10.1016/j.ymsp.2020.107385>. [Online]. Available: <https://www.sciencedirect.com/science/article/pii/S0888327020307718>.

Appendix A

Intrinsic Mode Functions

EMD Run5_75



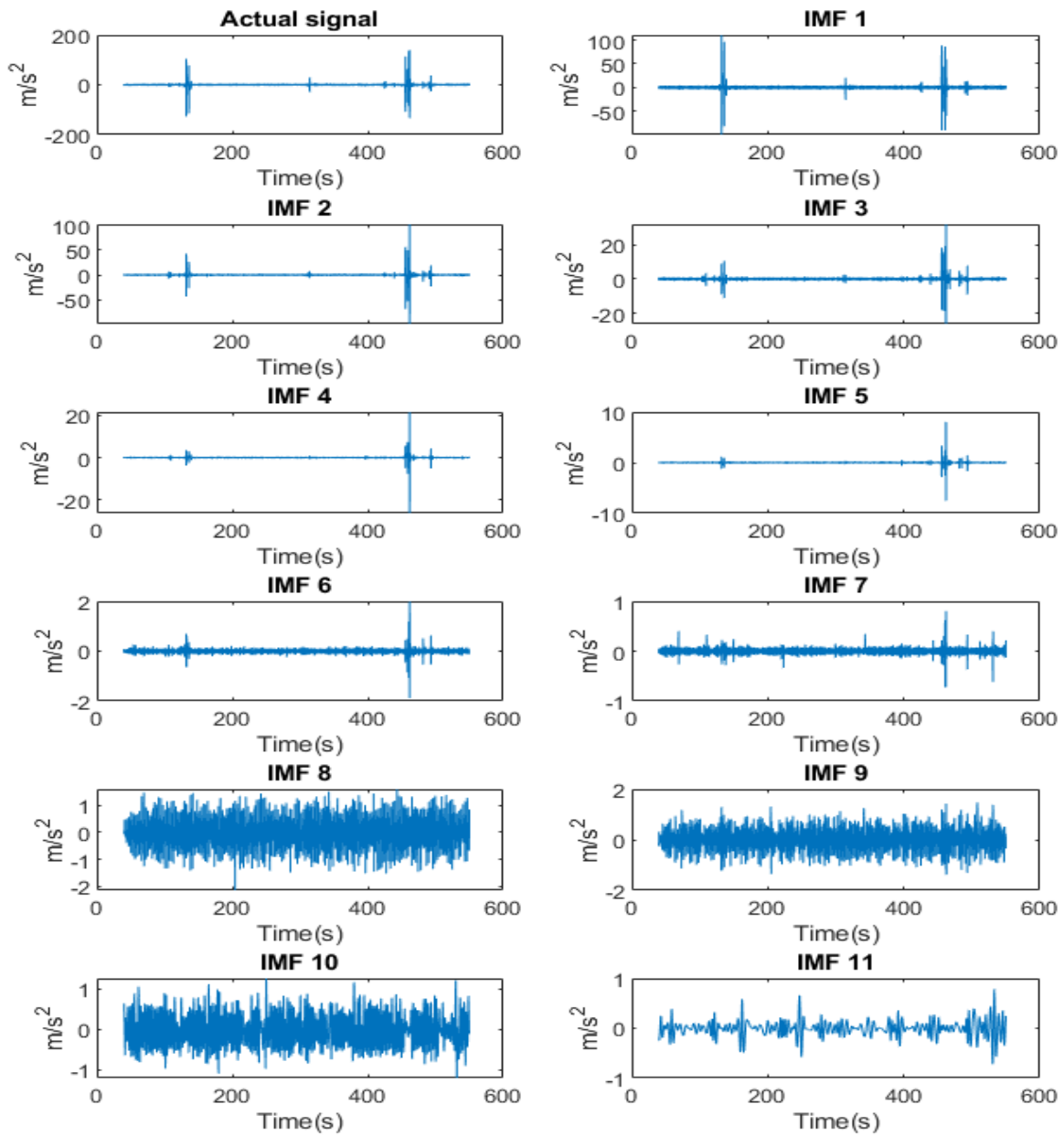


Figure A.2: Intrinsic Mode Functions in time domain of run 5_75

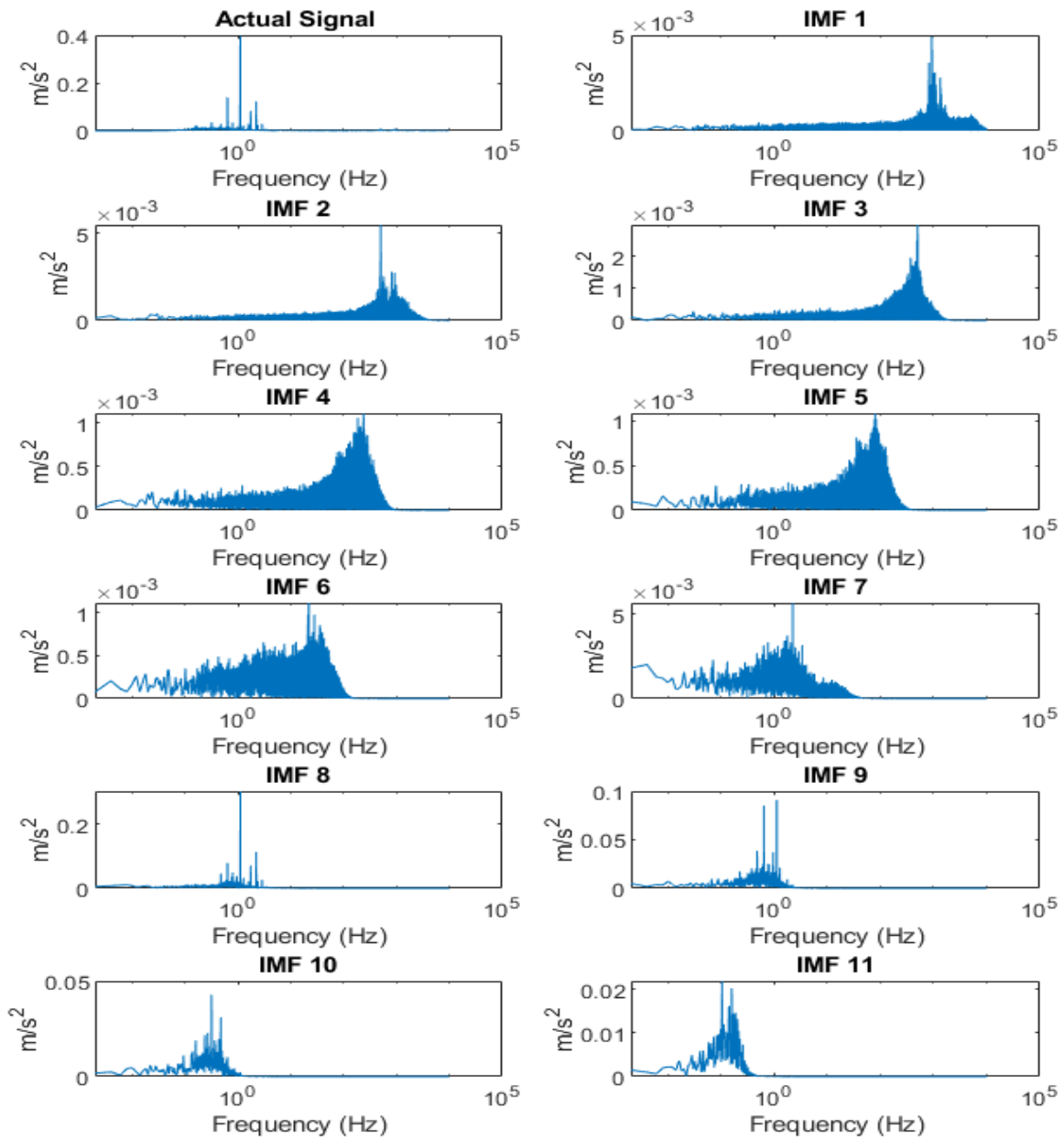


Figure A.3: Intrinsic Mode Functions in frequency domain of run 5_76

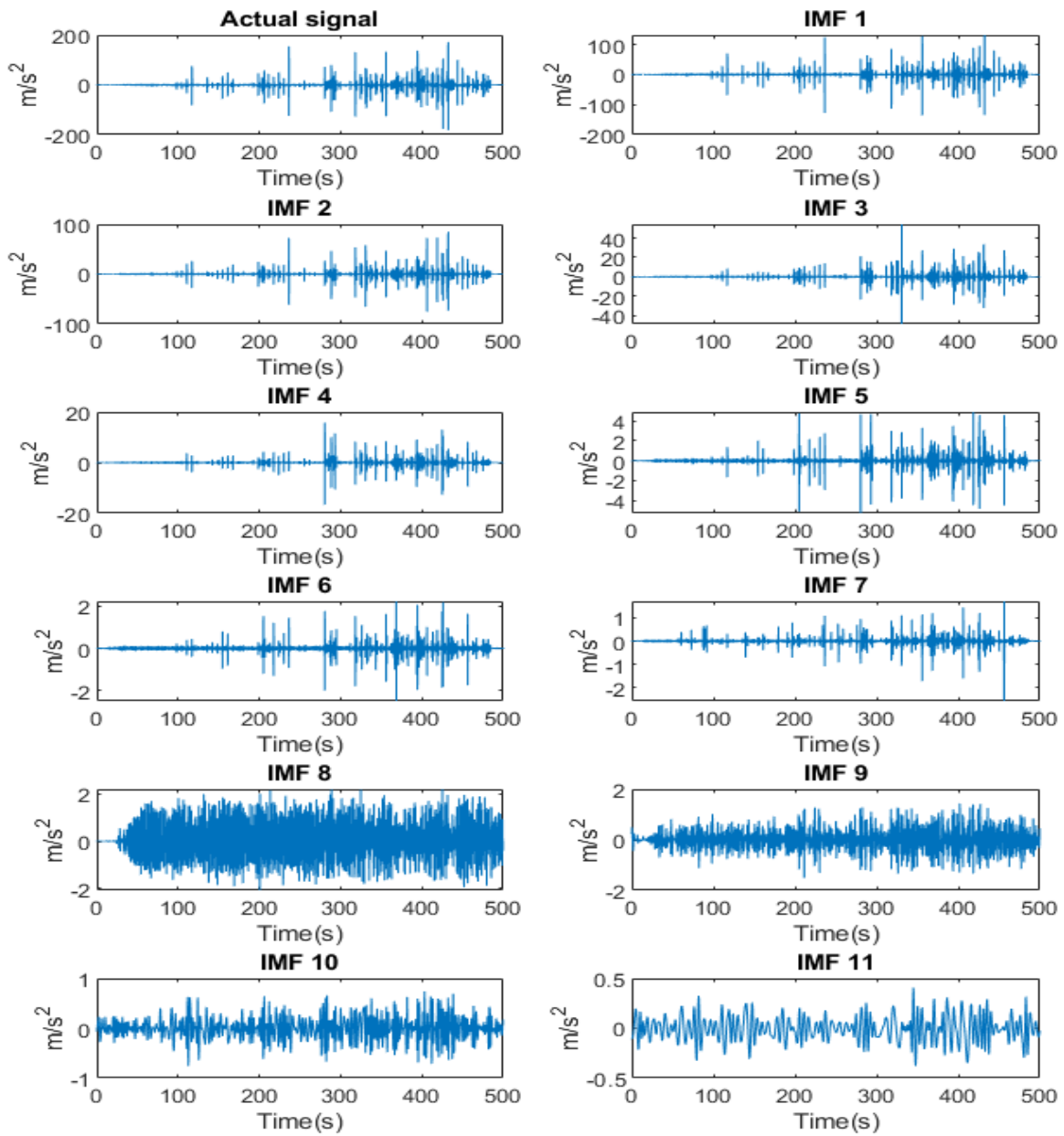


Figure A.4: Intrinsic Mode Functions in time domain of run 5_76

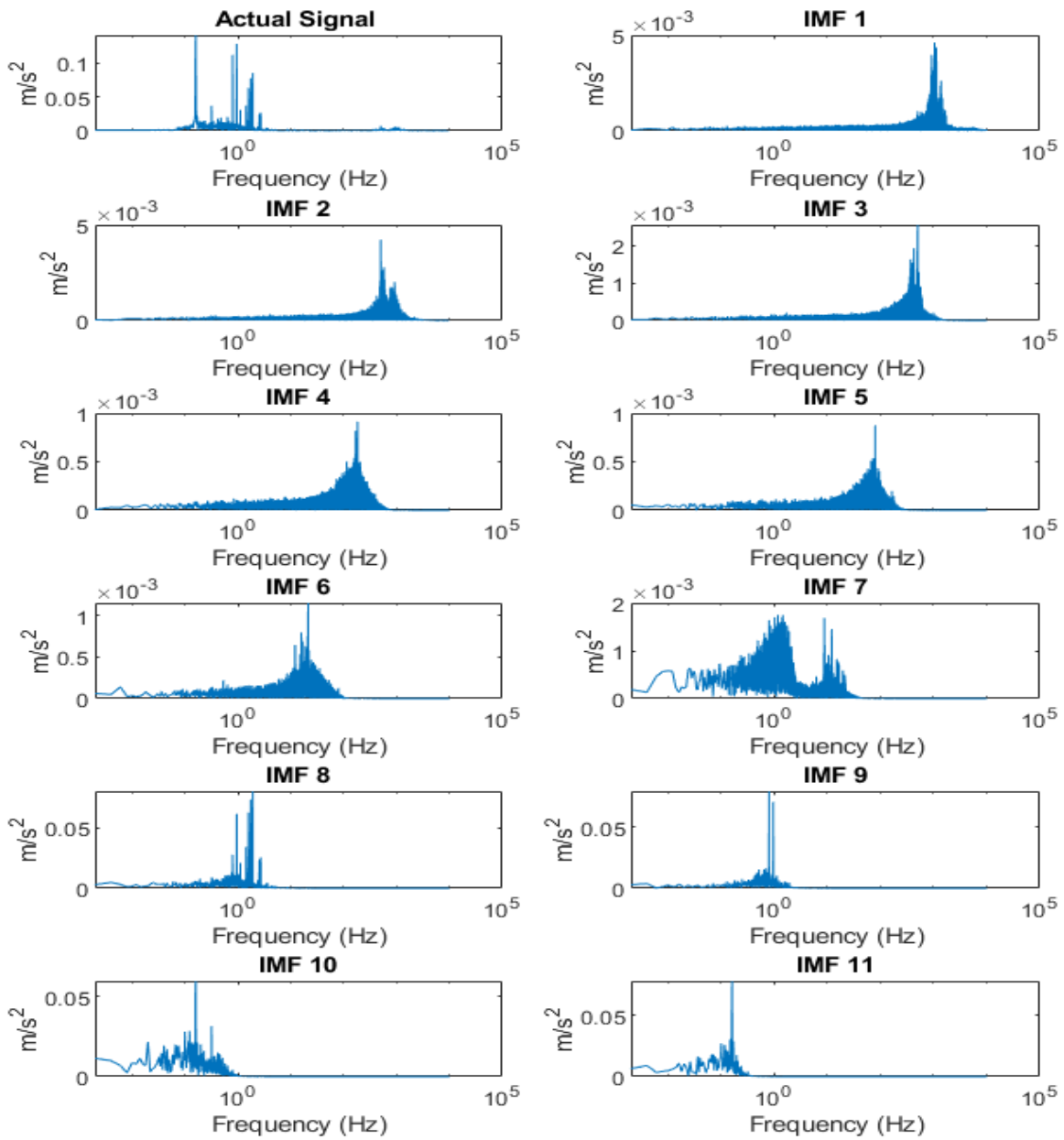


Figure A.5: Intrinsic Mode Functions in frequency domain of run 5_77

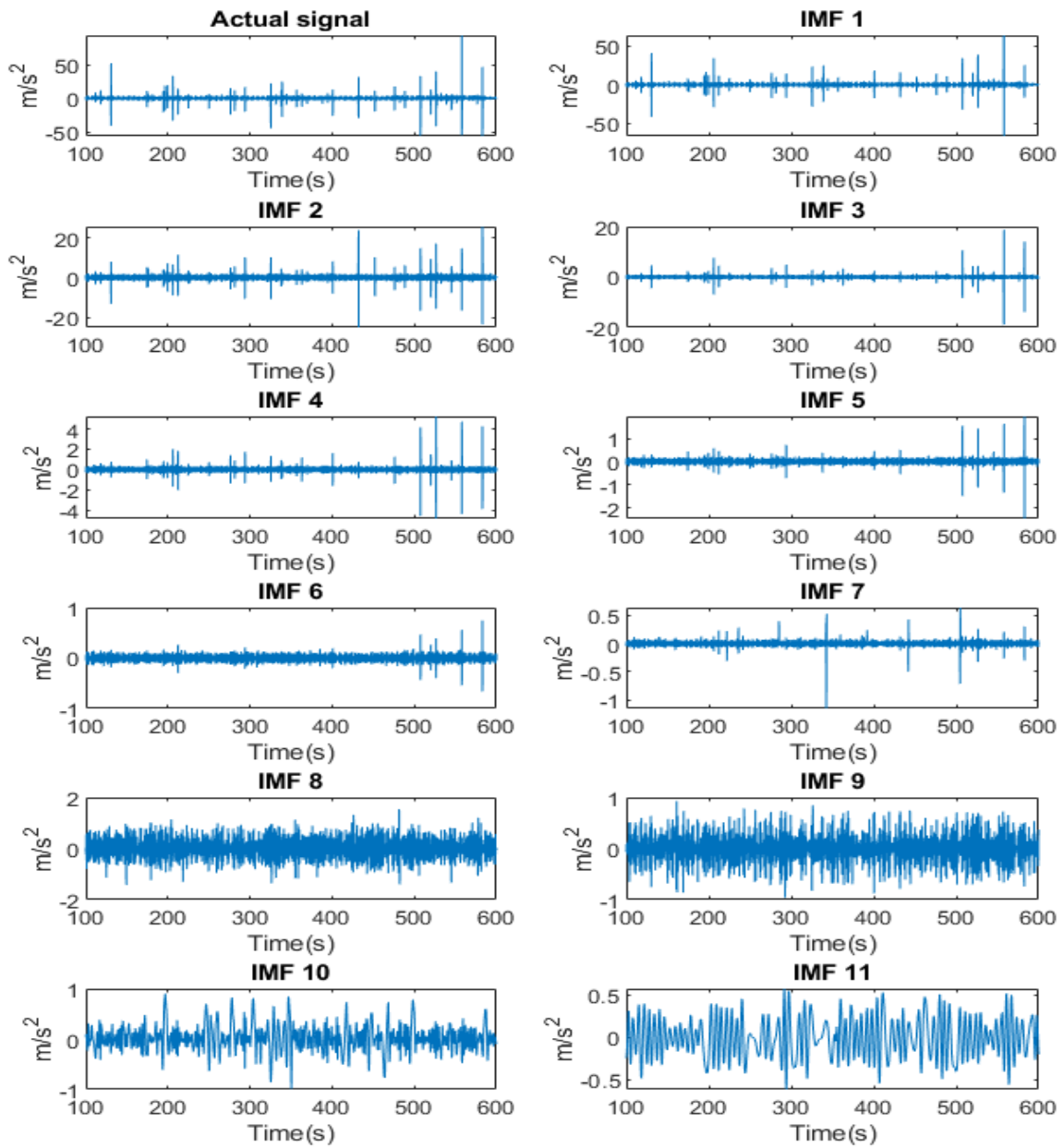


Figure A.6: Intrinsic Mode Functions in time domain of run 5_77

Appendix B

Slamming Identification Full Signals

5_74

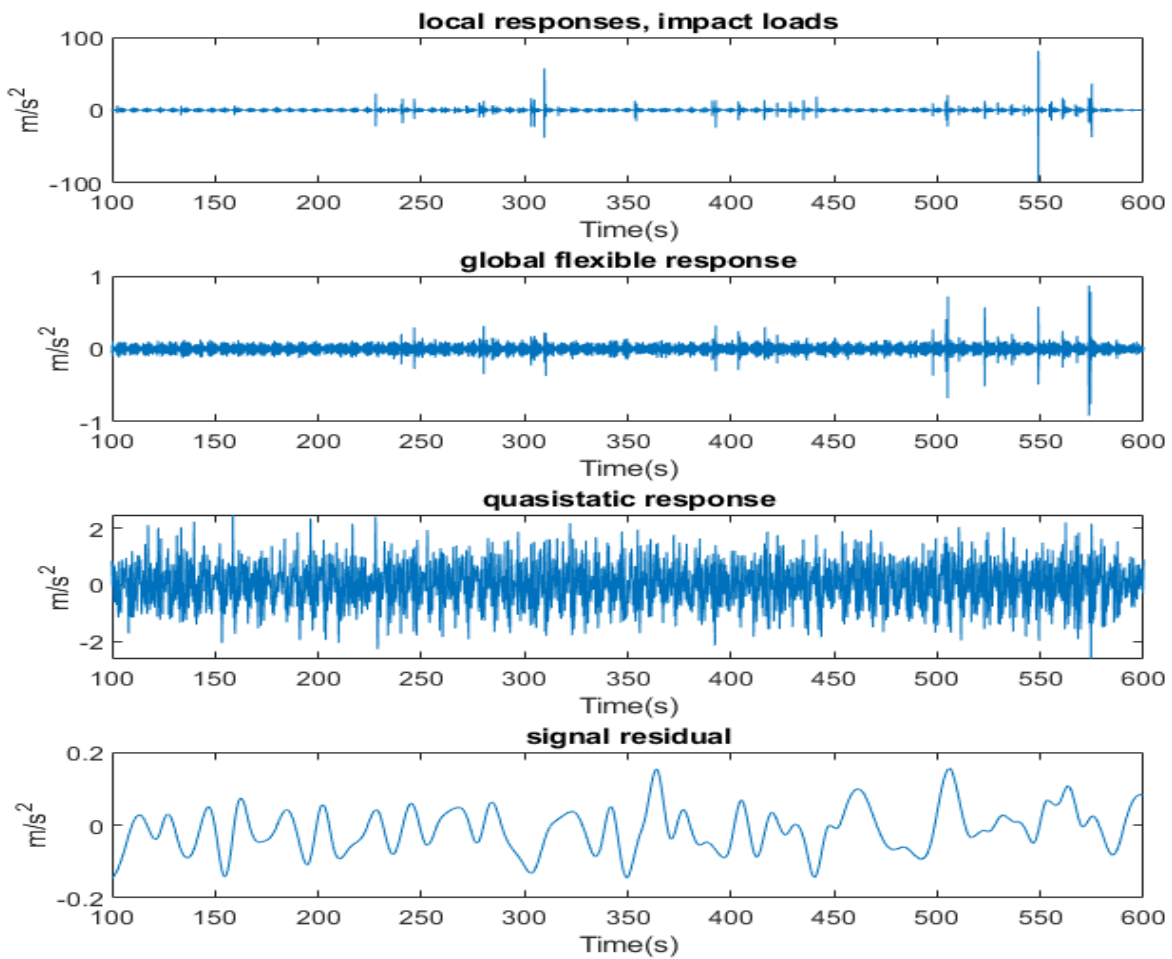


Figure B.1: Reconstructed signal of run 5_74

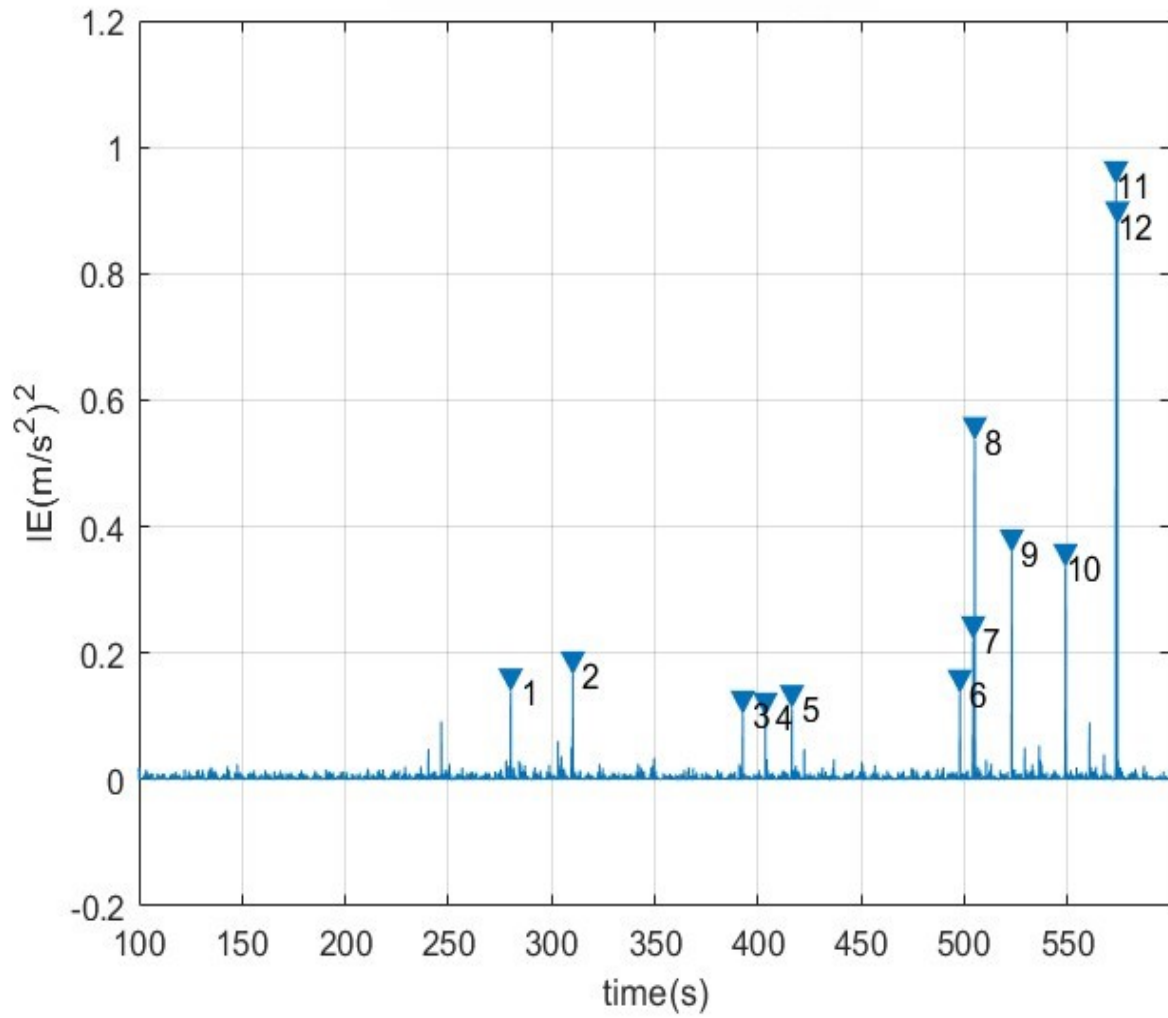


Figure B.2: Slamming identification EMD 5_74

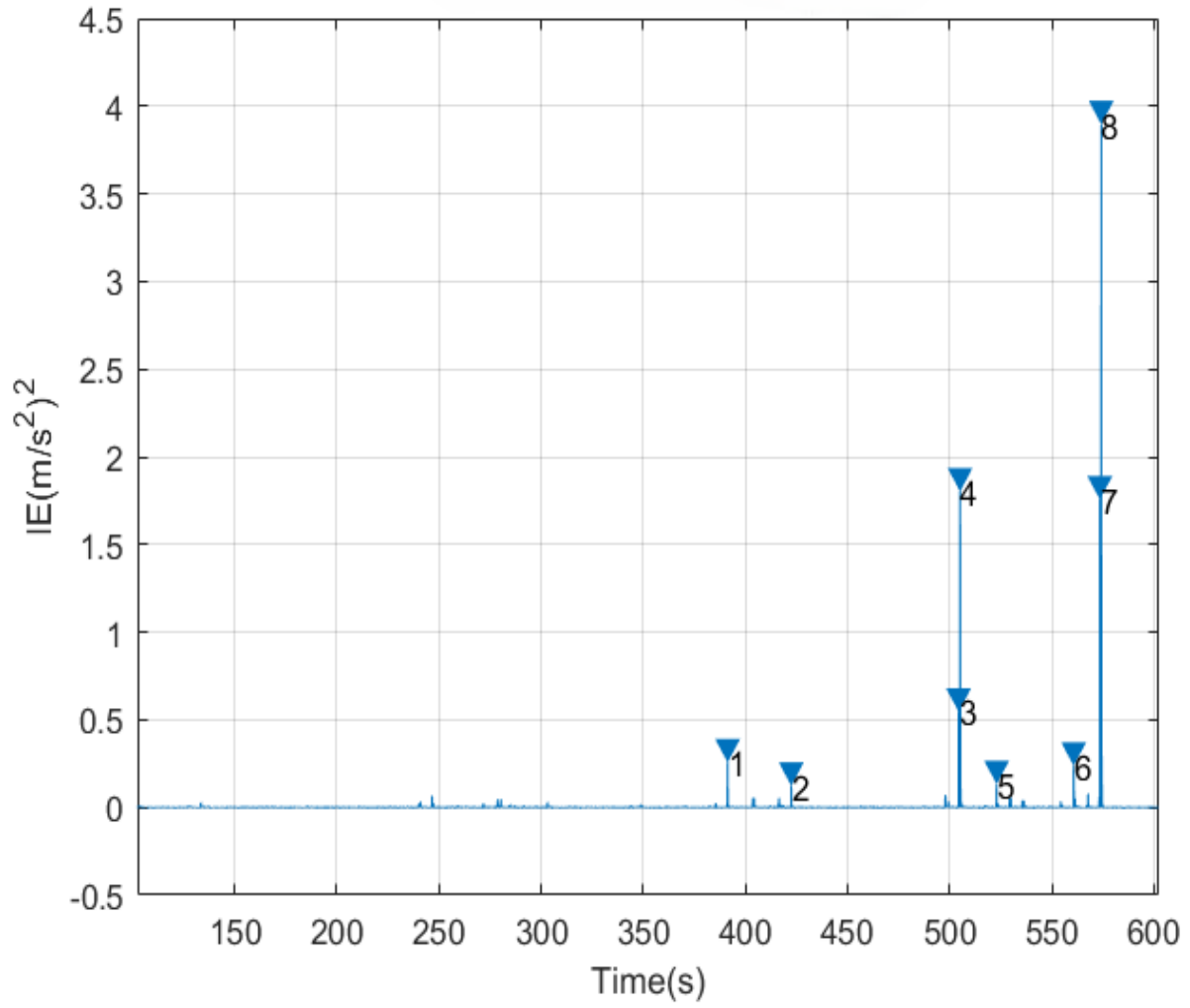


Figure B.3: Slamming identification Dessi 5_74

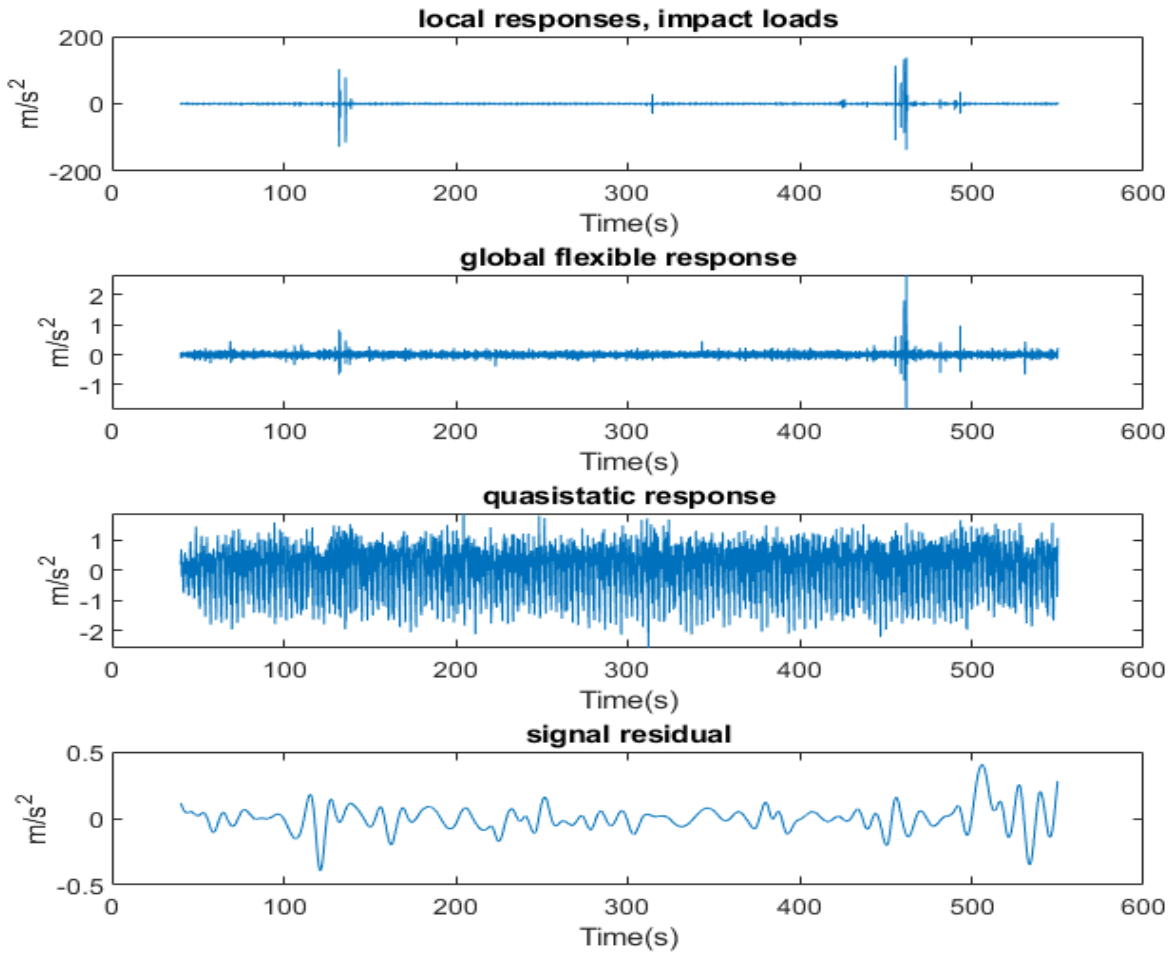


Figure B.4: Reconstructed signal of run 5_75

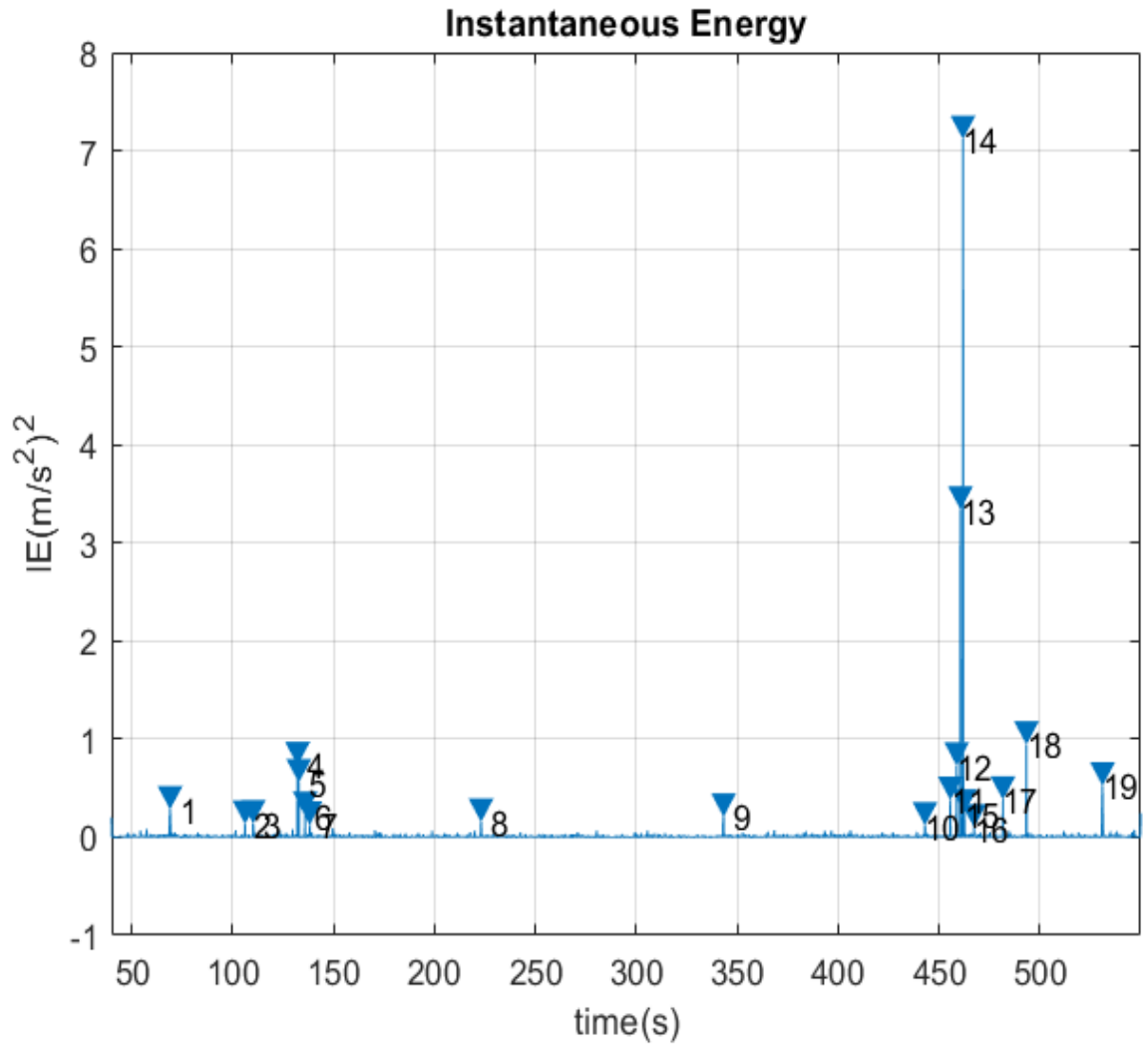


Figure B.5: Slamming identification EMD 5_75

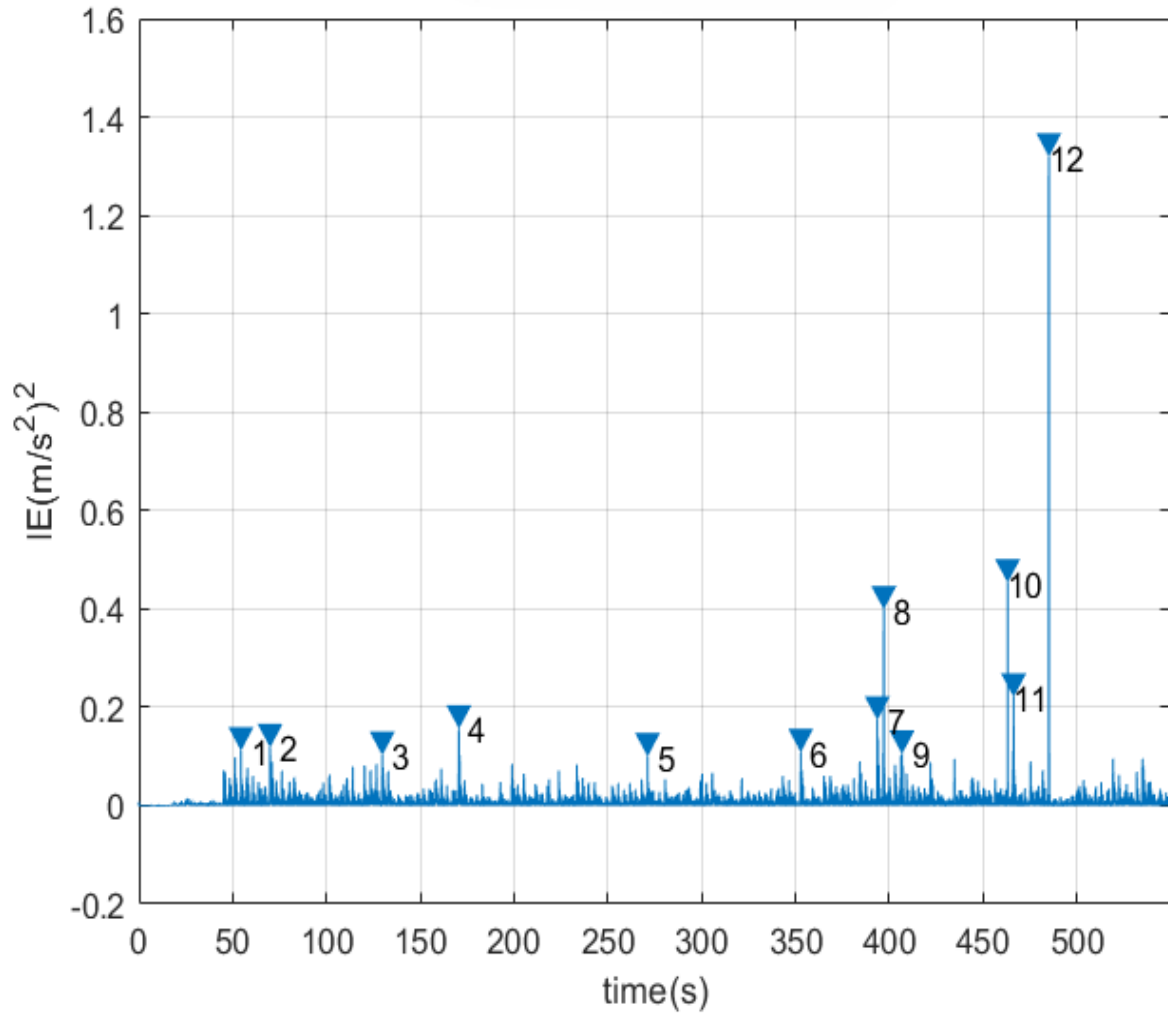


Figure B.6: Slamming identification Dessi 5_75

5_76

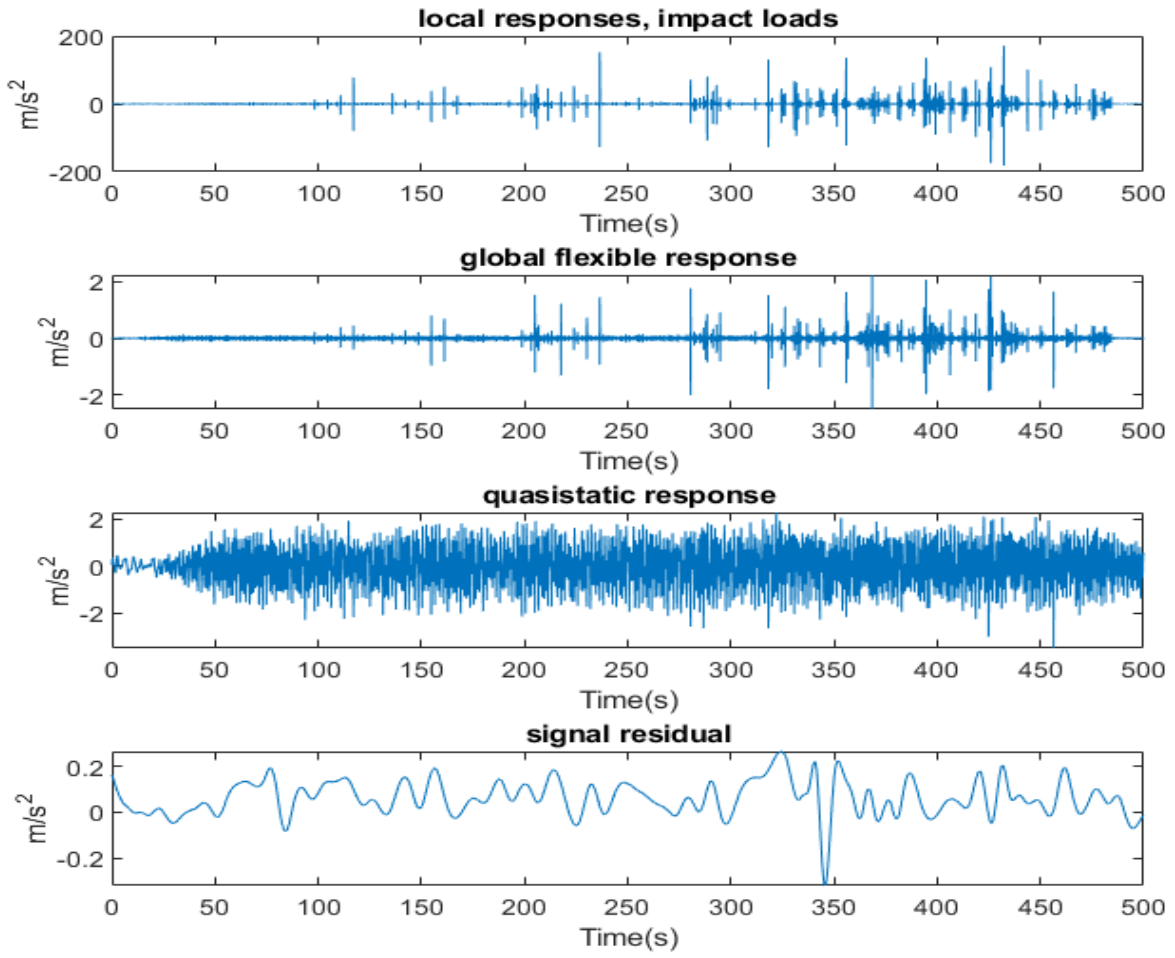


Figure B.7: Reconstructed signal of run 5_76

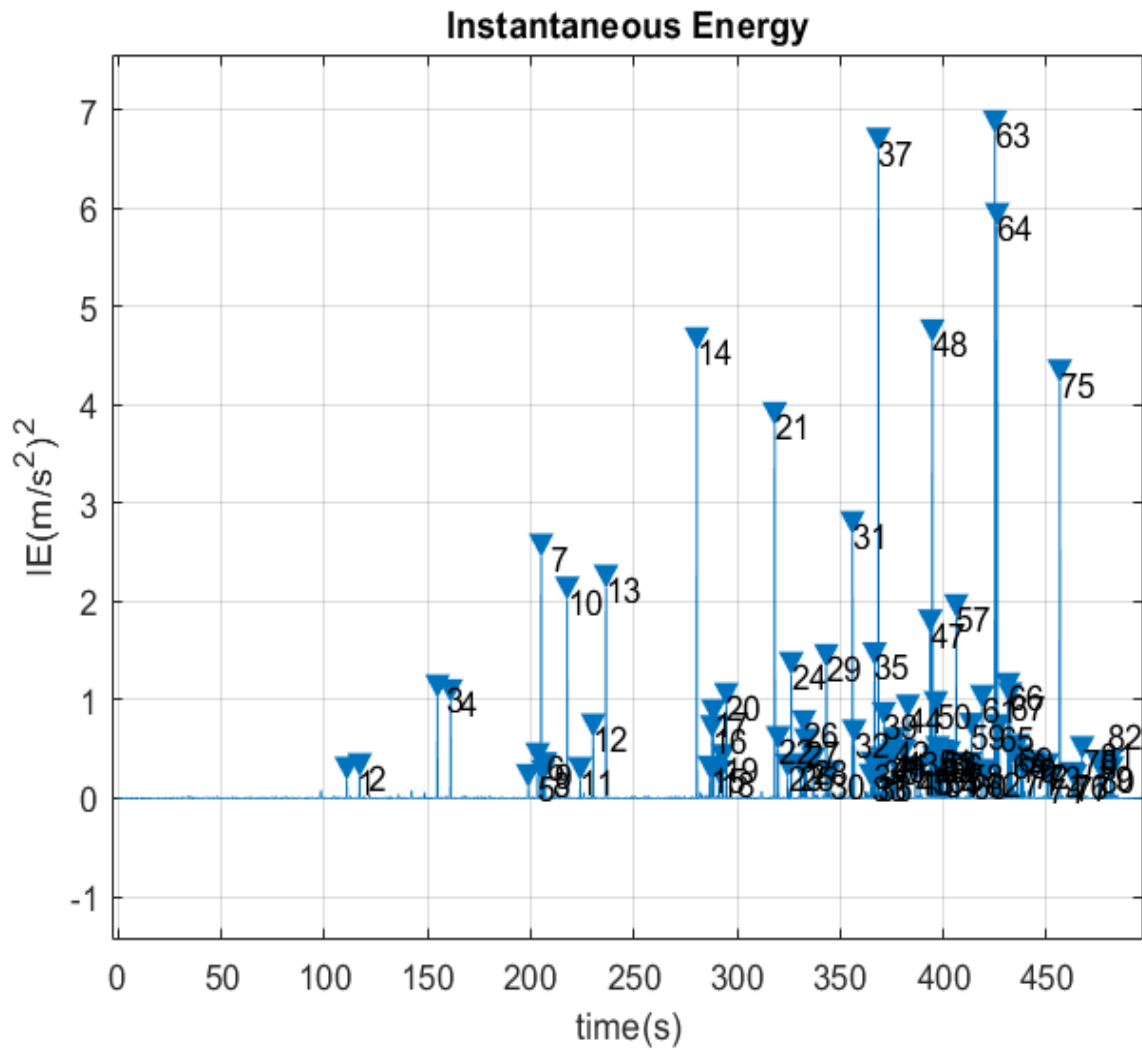


Figure B.8: Slamming identification EMD 5_76

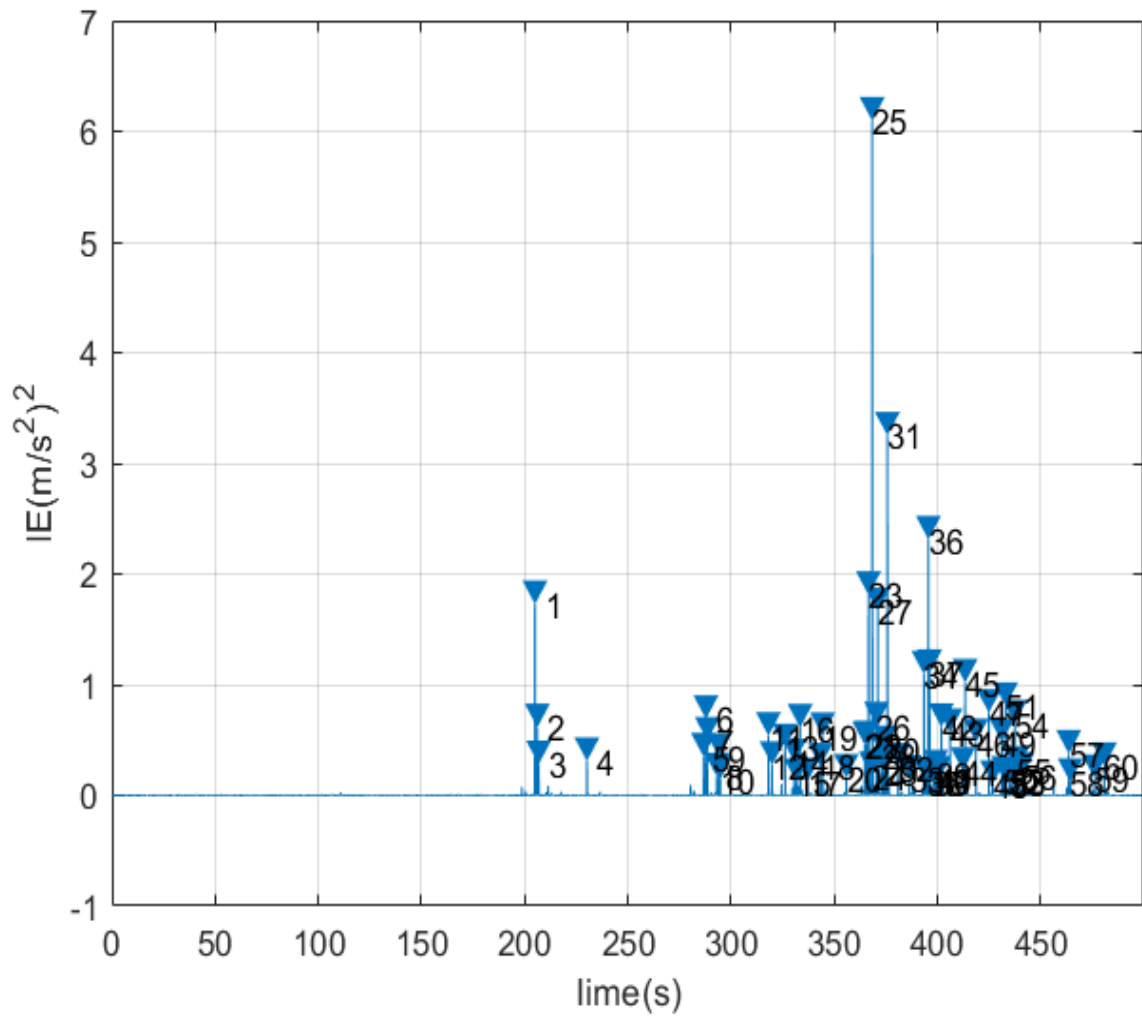


Figure B.9: Slamming identification Dessi 5_76

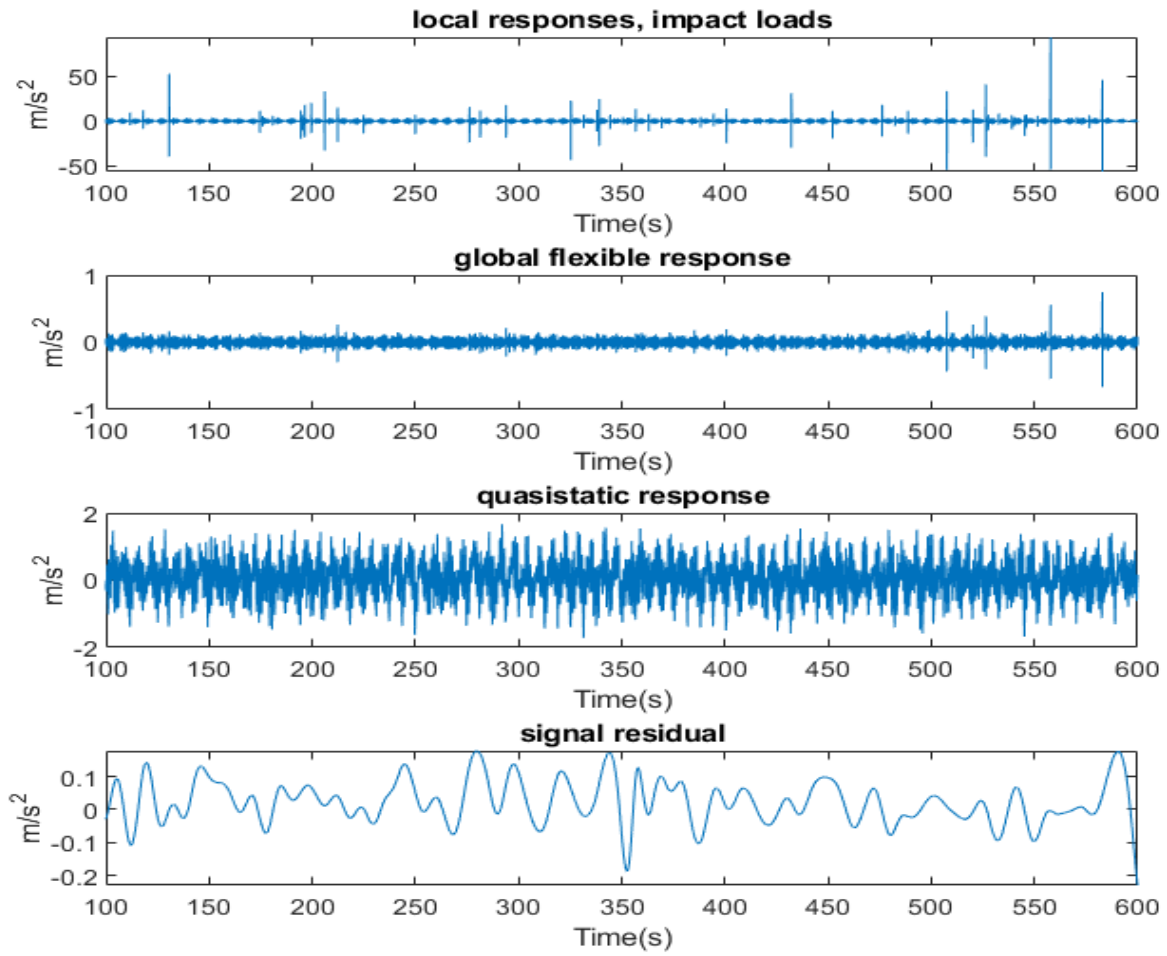


Figure B.10: Reconstructed signal of run 5_77

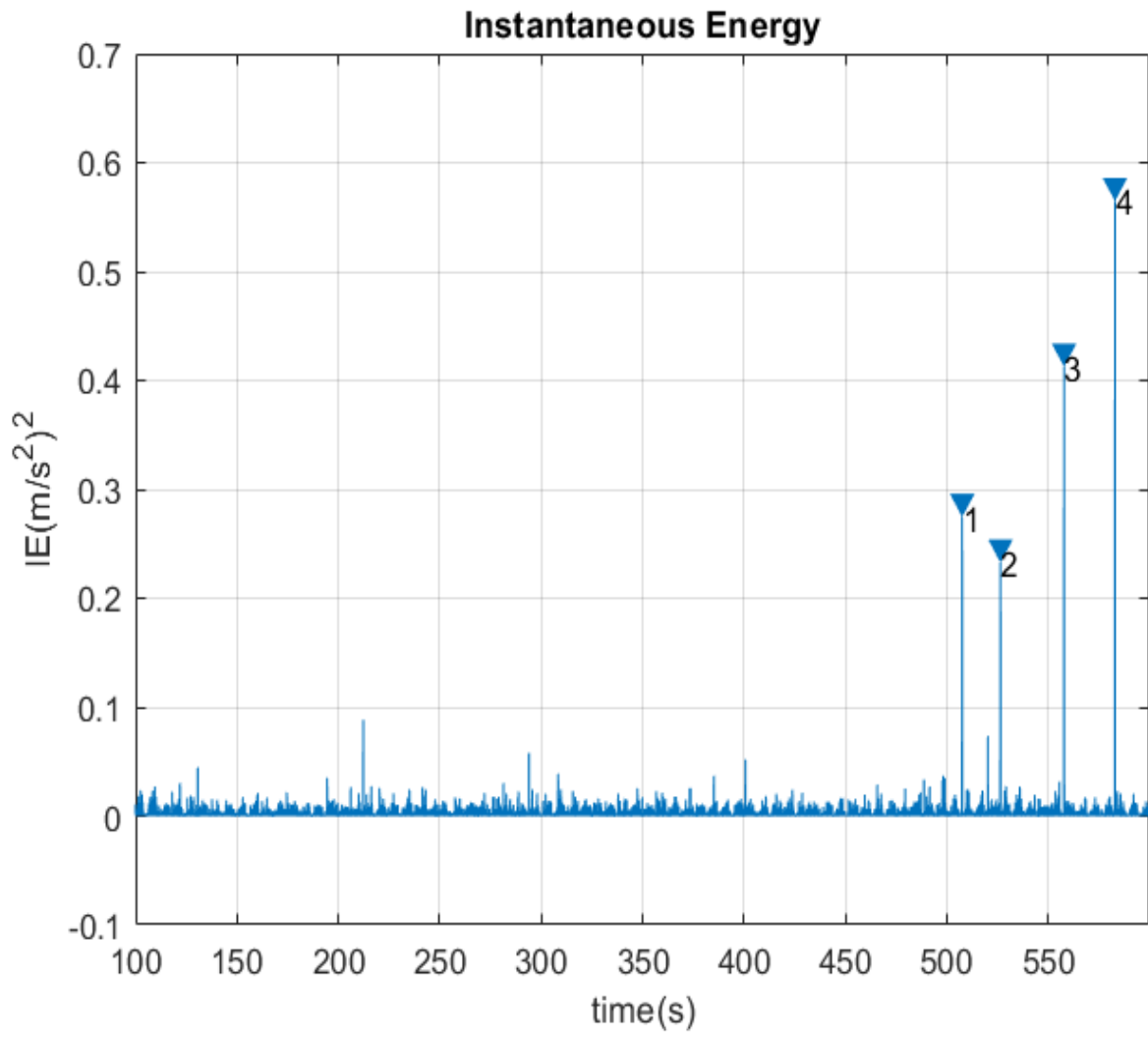


Figure B.11: Slamming identification EMD 5_77

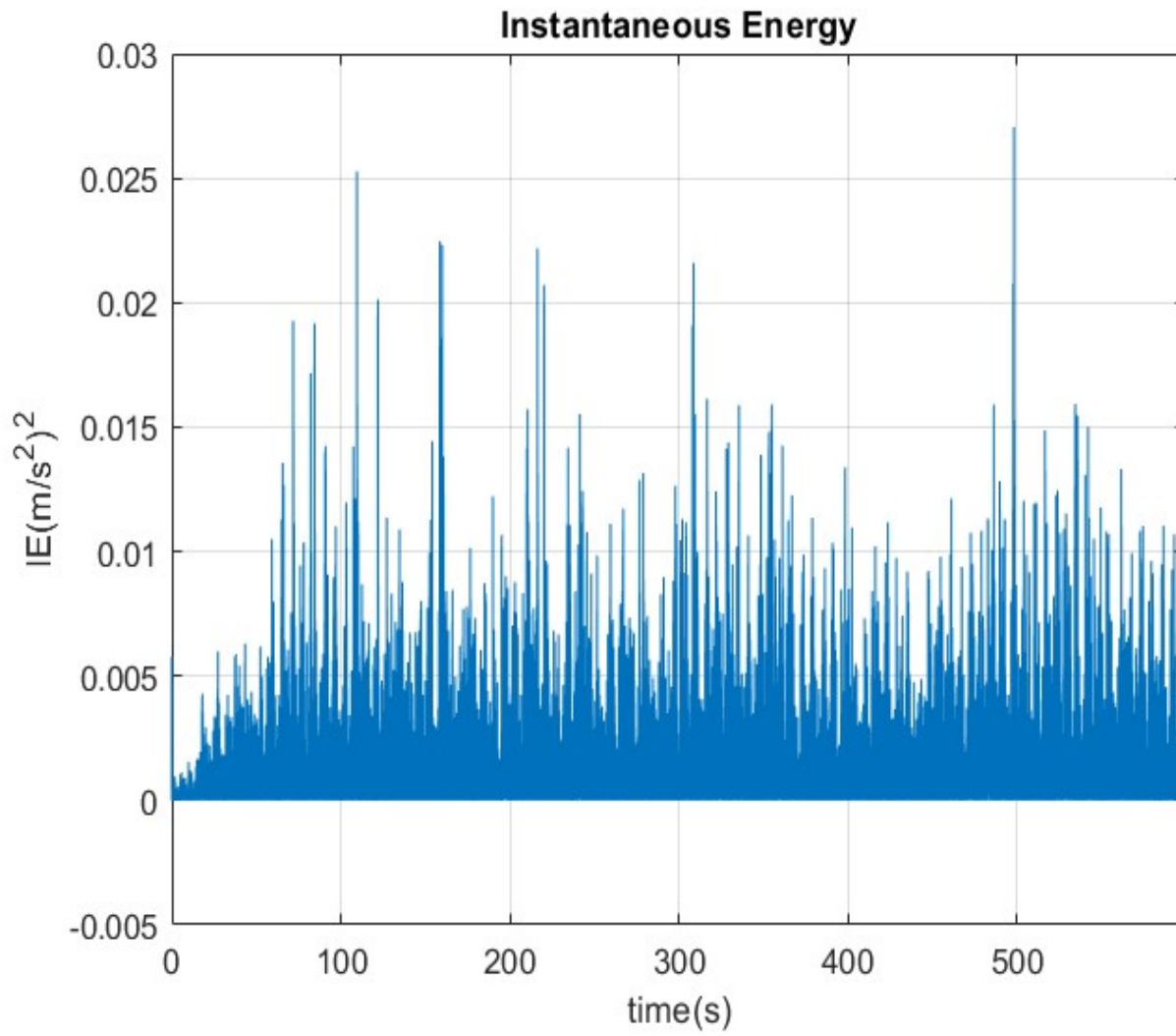


Figure B.12: Slamming identification Dessi 5_77